

**Design and Implementation of a Novel
Lightweight Soft Upper Limb Exoskeleton
Using Pneumatic Actuator Muscles**

Mae Irshaidat

School of Computing, Science & Engineering

University of Salford

Submitted in Partial Fulfilment of the Requirements of the
Degree of Doctor of Philosophy, June 2018

TABLE OF CONTENTS

TABLE OF CONTENTS	ii
LIST OF TABLES	vi
LIST OF FIGURES	vii
LIST OF ABBREVIATIONS	xii
ACKNOWLEDGEMENTS	xiii
ABSTRACT	xiv
1 Introduction.....	1
1.1 Motivation	1
1.2 Background on Rehabilitation Robotics	4
1.3 Challenges and Key Design Issues	6
1.4 Research Question	6
1.5 Research Aim and Objectives	7
1.6 Thesis Outline.....	7
2 Background to upper limb anatomy and clinical therapy.....	9
2.1 Introduction to Upper Limb Anatomy	9
2.2 Main Joints of Human Limbs	12
2.2.1 Muscles Acting at Joints	12
2.2.2 Human Upper Limb Joints	13
2.3 Stroke Rehabilitation for Upper Limb	16
3 Literature Review	21
3.1 Existing Devices for the Limb Rehabilitation.....	21
3.1.1 Actuators	23
3.1.2 Hard Robotic Devices for Upper limb Rehabilitation	26
3.1.3 Soft Robotic Devices for Upper Limb Rehabilitation	29
3.2 Pneumatic Muscle Actuator Modelling	33

3.3	Control Systems for Pneumatic Muscle Actuators.....	37
4	Mechanical design of the Soft Arm.....	40
4.1	Mechanical Design for Elbow Exoskeleton Robotic Device	40
4.1.1	Design Consideration.....	40
4.1.2	Design Advantages	42
4.2	Design Description of the Soft Arm	42
4.2.1	Mechanical Structure	42
4.2.2	Pneumatic Muscle Structure.....	43
4.2.3	Actuation System.....	43
4.3	The Contraction Pneumatic Muscle Actuator (pMA).....	44
4.3.1	Operation of the Contraction pMA.....	45
4.3.2	Geometrical Model of Contraction pMA.....	46
4.3.3	Experimental Inspection of Contraction pMA	49
4.3.4	Experimental Model vs. Mathematical Model.....	53
4.4	The Extension Pneumatic Muscle Actuator (pMA)	55
4.4.1	Operation of the Extension pMA.....	55
4.4.2	Geometrical Model of Extension pMA.....	56
4.4.3	Experimental Inspection of Extension pMA	57
4.4.4	Experimental Model vs. Mathematical Model.....	58
4.5	Bending Contractor and Extensor Pneumatic Muscle Actuator (pMA).....	60
4.5.1	Operation of the Bending Contractor and Extensor pMA	60
4.5.2	Experimental Inspection of Bending Contractor and Extensor pMA.....	61
4.5.3	Geometrical Model of Bending Contractor and Extensor pMA	64
4.5.4	Experimental Model vs. Mathematical Model.....	67
4.6	A Novel Elbow pMA Exoskeleton Arm (EpMAE).....	70
4.6.1	EpMAE Construction.....	70

4.6.2	Experimental Inspection for EpMAE	71
4.6.3	Enhancement to the Mathematical Model.....	74
4.6.4	Experimental Verification of Enhanced Model.....	74
4.7	Summary	75
5	Modelling Pneumatic Muscle Actuators	77
5.1	Numerical Model Consideration.....	77
5.1.1	Material Type Definition.....	78
5.1.2	Hyperplastic FEA Matrix Formulation Methodology	80
5.1.3	Nonlinearity of the Model.....	82
5.1.4	Contacts in FEA.....	84
5.1.5	Contact Modelling of Actuator.....	85
5.1.6	Braided Sleeve and Element Type Controls	86
5.1.7	Boundary Conditions	88
5.1.8	Convergence Criteria	89
5.1.9	Mathematical Formulation	89
5.2	Novel Model for contraction Muscle.....	91
5.2.1	Braided Sleeve Model.....	92
5.2.2	Thread Study	93
5.2.3	Contraction pMA: Displacement vs. Pressure	94
5.2.4	Contraction pMA: Force vs. Pressure.....	97
5.2.5	Stress Observations.....	98
5.3	Novel Model for Extension pMA	100
5.3.1	Thread study.....	102
5.3.2	Extensor displacement- data.....	104
5.4	Summary	105
6	Control of the soft arm	106

6.1	Pneumatic System Design.....	106
6.2	Simulink Simulation	110
6.3	Control System Design	110
6.4	Model Reference Adaptive Control (MRAC).....	112
6.4.1	Reference Model.....	113
6.4.2	Plant Model	114
6.4.3	Model Reference Adaptive controller.....	116
6.4.3.1	PID Controller	116
6.4.3.2	Figure 6.11. PID controlAdaptive Control	116
6.4.4	Control Structure	118
6.5	Adaptive Control Based on Neural Network	119
6.5.1	NN Main Configuration.....	119
6.6	Comparison.....	125
6.7	Summary	127
7	CONCLUSION AD FUTURE WORK.....	128
7.1	Summary of Contributions.....	128
7.2	Limitations.....	130
7.3	Future Work.....	130
	APPENDICES	132
	REFERENCES	146

LIST OF TABLES

Table 2.1. The Definition of Various Direction Used in Anatomical Descriptions (Aiello & Dean , 2002)	9
Table 2.2. Elbow Movements.....	13
Table 2.3. Normalised mass and length of body segments	14
Table 2.4. Comparison of traditional and robotic rehabilitation	20
Table 3.1. Some of existing upper limb robotic devices.....	32
Table 4.1. Specifications of contraction pMA.....	46
Table 4.2. Contraction pMA parameters.....	50
Table 4.3. Contraction Ratio of Contraction pMA at 2(bar), and L_0 , 30(cm).....	51
Table 4.4. A comparison between the observed results and the predicted results for the contraction pMA length in (m) at different pressure levels, to calculate the MFE	54
Table 4.5. Specifications of Extension pMA.....	56
Table 4.6. Extension pMA parameters.....	57
Table 4.7. Specification of bending pMAs.....	61
Table 5.1 Geometrical parameters description	78
Table 5.2 Materials properties	78
Table 5.3 Contact Properties	86
Table 5.4. Nodes and Element sets of pMA.....	87

LIST OF FIGURES

Figure 1.1. Stoke Survivors in the UK (2016/2017).....	2
Figure 1.2. Stroke Disabilities Percentage	2
Figure 2.1. Joints actions (Hall, 2003).....	11
Figure 2.2. The main muscles and joint for the human upper and lower Limbs.....	11
Figure 2.3. Schematic representation of the elbow joint shows the elbow kinematics. (Gaponov, Popov, Jun Lee, & Hwan Ryu, 2016).....	15
Figure 3.1. Rehabilitation robotics;	23
Figure 3.2. Different types of pMAs:.....	25
Figure 3.3. a) MIT-Manus; (b) MIME; (c) GENTLE/s.	27
Figure 3.4. (a) ARMin; (b) Armeo Spring; (c) REHAROB.....	28
Figure 3.5. Existing soft robotics for upper limb rehabilitation.....	31
Figure 3.6. Geometry of McKibben Muscle (middle section)	34
Figure 4.1. The Arm mechanical structure.....	42
Figure 4.2. PAM Build-up.....	43
Figure 4.3. McKibben pMA:	44
Figure 4.4. Experimental set-up pneumatic diagram.....	50
Figure 4.5. Contraction pMA at different pressures	50
Figure 4.6. Relationship between length (L), and the pressure (P)	51
Figure 4.7. Comparison between loaded and unloaded muscle: relationship between length (L), and pressure (P).....	52
Figure 4.8. The Experimental force of the contraction pMA vs. pressure at different pressures varies between 0-5 bar.....	53
Figure 4.9. A Comparison between the geometrical model and the experimental model, that shows the relationship between the length of the contractor pMA and the pressure level, where the Blue curve demonstrates the experimental result while the orange curve demonstrates the equation results.	53
Figure 4.10. An Experimental and Geometrical Force of the contraction pMA against different pressures.....	55
Figure 4.11. Illustrative length of inner tube and braided sleeve length in extension pMA ...	56
Figure 4.12. Relationship between the length and the pressure in the extension pMA.....	58

Figure 4.13. The relationship of the generated force at different pressure level varies from 0-5 bar	58
Figure 4.14. A Comparison between the geometrical model and the experimental model, that shows the relationship between the length of the extensor pMA and the pressure level, where the blue curve demonstrates the experimental result while the orange curve demonstrates the equation results	59
Figure 4.15. A comparison between the experimental results and the predicted results of the force generated at different pressure levels; the blue curve shows the observed results, the orange curve shows the predicted results	60
Figure 4.16. Illustrative construction of bending contractor pMA	61
Figure 4.17. Illustrative construction of bending extensor pMA	61
Figure 4.18. Bending pMA experimental setup to measure the bending angle and the force, fixed to a rig	62
Figure 4.19. The Relationship between the bending angle and pressure of bending extensor pMA.	62
Figure 4.20. Bending angle of extensor pMA more than 360° showing unpredicted behaviour	63
Figure 4.21. The Relationship between the bending Angle and the Pressure of the bending Contractor pMA	63
Figure 4.22 Bending Angle 180° of Contractor pMA and Extensor pMA, (a) extensor bending angle at 2.5 bar, (b) contractor bending angle at 1.5 bar	64
Figure 4.23. Relationship of the generated force at different pressure levels in an isometric configuration; the blue curve for the single extensor pMA and the grey curve for contractor pMA at, and the orange curve for double extensor pMA	64
Figure 4.24. Bending pMA geometry	65
Figure 4.25. A comparison between the mathematical model and the experimental model to demonstrate the relationship of the generated force at different pressure levels in an isometric configuration; (a) for the extensor pMA at 90°, (b) contractor pMA at 45°, and(c) for the double bending extensor pMA at 90°.	68
Figure 4.26. The observed and predicted bending angle for the bending contractor pMA; where the blue curve shows the experimental results and the orange one shows the calculated results	69

Figure 4.27. The observed and predicted bending angle for the bending extensor pMA; where the blue curve shows the experimental results and the orange one shows the calculated results	70
Figure 4.28. The proposed soft arm (EpMAE), the one on the left when it's unpressurised, and the one on the right when the soft arm is pressured	71
Figure 4.29. The prototype setup to find the force of the at different pressure level; e.g. the load is 4 kg at 4 bar	71
Figure 4.30 The observed and predicted bending angles for the bending prototype at different pressure levels; (a) shows the relationship between the angle and the pressure when it the prototype is unloaded, (b) when the prototype is loaded with 1.5 kg, the blue curve shows the experimental results and the orange curve demonstrates the calculated results.....	72
Figure 4.31. The proposed output force direction;	73
Figure 4.32. A Comparison between the mathematical model and experimental model for the prototype force vs. pressure level; the blue curve shows the experimental results, the orange curve shows the equation results	74
Figure 4.33 A Comparison among the new model, the mathematical model and experimental model for the prototype force vs. pressure level; the blue curve shows the experimental results, the orange curve shows the equation results, and the grey curve shows the enhanced results.	75
Figure 5.1. Contact compatibility	84
Figure 5.2 Contact Modelling of the pMAs, the left figure shows a gap between the inner tube and the braided sleeve, the right figure shows a bonded model	86
Figure 5.3. Braided sleeve modelling	87
Figure 5.4. Hexa-mapped mesh and tetra free mesh.....	88
Figure 5.5. Boundary conditions of the braid model	89
Figure 5.6. Force convergence with respect to number of iterations and number of sub steps	89
Figure 5.7. A comparison of threads number of the contraction pMA at 1 bar against the deformation and the stress; the blue curve shows the max. deformation, and the red curve shows the max. stress.....	93
Figure 5.8. Contraction pMA at 1 bar with different number of threads.....	94

Figure 5.9 A comparison between FEA and experimental results to show the displacement at different pressure levels; the red curve shows the FEA results; the blue curve shows the experimental results.	94
Figure 5.10 Curve fitting showing better approximation by quadratic representation over cubic, (a) quadratic, (b) cubic.....	95
Figure 5.11. FEA deformations of contraction pMA at 3 and 5 bars	96
Figure 5.12. The deformation with respect to the time.....	96
Figure 5.13. Iterations to enhance contact convergence	97
Figure 5.14. A comparison between the experimental results and the FEA results	98
Figure 5.15. Stress and strain plots, that shows the force convergence, force criterion, and substep converged.....	98
Figure 5.16. A close observation on the stresses provides insights on the probable failure regions	99
Figure 5.17. Gapping between the braided sleeve and the bladder	101
Figure 5.18. The deformations at each timestep.....	101
Figure 5.19. A comparison of threads number of the extension pMA at 1 bar against the deformation and the stress; the blue curve shows the max. deformation, and the red curve shows the max. stress.	102
Figure 5.20. Extension pMA at 1 bar with different number of threads.....	102
Figure 5.21. The deformation at different pressures for extension pMA.....	104
Figure 5.22. A comparison between the experimental results and the FEA results in the extensor change in length.....	105
Figure 6.1 A Schematic Representation of the Pneumatic System Setup.....	107
Figure 6.2. Pneumatic diagram of the experimental actuator.....	107
Figure 6.3 A MATRIX3/3 750 Series Solenoid Valve, (a) is a schematic MATRIS valve showing the 4 ports, (b) the solenoid valve.....	108
Figure 6.4 the driver's circuit, the first two figure shows the connection in the driver's circuit and last figure shows the schematic connection of the driver's circuit.....	109
Figure 6.5 The pressure sensor	110
Figure 6.6. MRAC scheme of the pMAs	111
Figure 6.7 Control System.....	112
Figure 6.8 Reference model in Simulink	113
Figure 6.9 Transfer Function.....	114

Figure 6.10 Plant model configuration.....	115
6.4.3.2 Figure 6.11. PID controlAdaptive Control	116
Figure 6.12 Adaptive control.....	116
Figure 6.13 Generator pulse diagram properties	117
Figure 6.14. Measured bending angle of the soft Arm	118
Figure 6.15. A comparison between Y_m vs Y_p values.....	118
Figure 6.16. General Block Diagram for Reference model adaptive control.....	119
Figure 6.17 NN Reference model adaptive control	119
Figure 6.18. Proposed configuration.....	120
Figure 6.19. Simulink model of the adaptive NN controller.....	120
Figure 6.20. Plant model resulting Network	121
Figure 6.21.MRAC NN View.....	121
Figure 6.22. Input Signal.....	121
Figure 6.23 Plant Neural Network identification	122
Figure 6.24 Validation results for model reference adaptive control	123
Figure 6.25 Mean Square Error curve for the NN for 6 epoches	124
Figure 6.26. Training Data	124
Figure 6.27. Y axis represent reference arm angle, and X axis represent time (s).....	125
Figure 6.28. Reference input vs plant model output.....	125
Figure 6.29.Bending angle theta output from NN	126
Figure 6.30. Bending angle theta output without NN	126

LIST OF ABBREVIATIONS

ADL	Activities of Daily Living
BCs	Boundary Conditions
DOF	Degree of Freedom
ESD	Early Supported Discharge
FEA	Finite Element Analysis
FEM	Finite Element Modelling
MPC	Multi Point Constraint
MRAC	Model Reference Adaptive Control
NN	Neural Network
PID	Proportional, Integral, and Derivative
pMA	Pneumatic Muscle Actuator
PWM	Pulse Width Modulation
ROM	Range of Motion

ACKNOWLEDGEMENTS

Completion of this thesis was possible with the support of several people. I would like to express my sincere gratitude to all of them. First of all, I would like to thank my supervisor, Prof. Samia Nefti-Meziani, the chairperson of the Robotics and Autonomous System Centre. The thesis would not have come to a successful completion, without the help I received from my colleagues at the department. I would also thank the lab technician Mr. Andrew Baker for his logistics services.

I owe a lot to my parents and brothers, who encouraged and helped me at every stage of my personal and academic life and longed to see this achievement come true. Especially to my father, who has advised me and put me across the right path during my study.

I am very grateful to my husband, who supported me in every possible way to see the completion of this work. Also, I would like to thank my sister from another mister Yara for her support and for being always there for me.

Saving the best for last, I am most grateful for the support and guidance of my co. supervisor Dr. Ipek Caliskanelli. You taught me the multiple, complex, and rewarding aspects of research.

ABSTRACT

Stroke is the leading cause of disability and weakness in the UK and around the world. Thus, stroke patients require an extensive rehabilitation therapy to regain some of the weaknesses. Many rehabilitation robotic devices have been designed and developed to assist the stroke patients to perform their activities of daily living and to perform repetitive movements. However, these devices remain unmanageable to use by the patients alone not only because they are cumbersome to use but also due to their weights, rigid, fix and non-portable characteristics. Thus there is a need to invent a novel exoskeleton soft arm that has a lightweight and a high power to rehab the elbow joint with lower cost and without the need to therapists. Here for elbow joint rehabilitation, we investigate and propose a novel exoskeleton soft robotic arm, which is wearable, lightweight and portable so that it would allow patients to perform repetitive motion therapy more often with a greater intensity in their homes and relevant to their Activities of Daily Living (ADL). The proposed arm consists of various bending pneumatic muscle actuators (pMA), where traditional pMA are not suitable.

Testing on various pMA (traditional and bending) revealed its behaviour and the relationship between pressure, length, force, and bending angle in different setups such as isotonic and isometric. Experiments are done to analyse its non-linear behaviour, moreover, geometrical and numerical models are compared to the experimental results to validate the results.

A developed control approach to control the soft arm is implemented to validate the design. Model reference adaptive control (MRAC) to control the arm using (Proportional, Integral, and Derivative) PID controller as an input for MRAC. Neural Network (NN) is also used in MRAC to improve the performance of MRAC.

1 INTRODUCTION

1.1 Motivation

Hemiparesis causes the majority of post-stroke patients to experience limited dexterity, sensitivity, strength, and coordination in their affected upper extremity. Due to this ensuing muscle weakness that severely affects their motor function, a great number of hemiparetic stroke survivors seek professional rehabilitative and/or assistive help. The conventional rehabilitation process for upper-limb impaired patients is greatly affected by time and money restrictions, which often results in patients not being able to achieve a maximum potential for recovery.

According to the World Health Organisation, the percentage of people over 65 years will increase by 73% in the industrialised countries and by 207% worldwide. The relative incidence of stroke increases every decade for people over 55 years old, therefore, an interdisciplinary rehabilitation programme is needed to provide therapies for people to survive stroke and to reduce the high cost of stroke rehabilitation. According to the Division of Health and Social Care Research at the University of London and NHS, the stroke rehabilitation in the UK costs around £1.7 billion yearly (Saka, MCGuire, & Wolfe 2009 and Stroke Association, 2017). Stroke is a major health problem as it is considered to be a leading cause of disability in the UK, leaving people with limited ability to perform activities of daily living (ADL), almost two thirds of stroke survivors are disabled (Department of Health, 2016). Age is a significant factor in increasing the chance of suffering a stroke as the probability of suffering a stroke increases proportionally with age (Huang , et al., 2016). Around 110,000 people have strokes in England yearly, and more than 900,000 people in England are living with the post-stroke complications as shown in Figure 1.1., the figure is generated based on data extracted from Stroke Association (2017) illustrates the number and percentage of stroke survivors in the UK between 2016 to 2017. Moreover, stroke is the fourth largest cause of death in the UK.

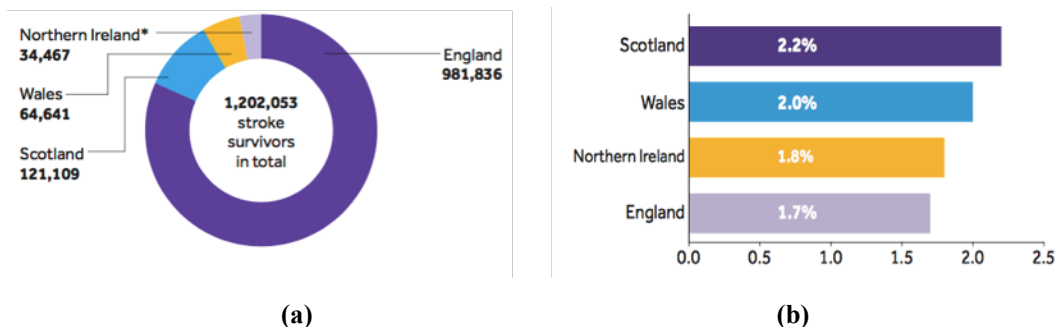


Figure 1.1. Stroke Survivors in the UK (2016/2017)

(a) The number of stroke survivors in the UK, (b) the percentage of stroke survivors in the UK

Stroke arises from a sudden interruption in blood flow to the brain or a rupture of blood vessels in the brain. Consequently, some parts of the brain do not receive sufficient oxygenated blood, causing the death of neurons in this region, and thus impairment of brain functions. The repercussions of this damage may come in the form of sensory, motor, cognitive and psychological symptoms, such as muscle weakness, sensory loss, and aphasia. Also, spasticity, attention and memory deficits, limited movement coordination, depression, and behavioural changes are caused by stroke (Dobkin & Dorsch, 2013). Motor deficits are one of the most remarkable complications in stroke survivors as illustrated in Figure 1.2 below as stroke can affect mobility, balance, speech and so on (Stroke Association, 2017). The most common complications that affect the mobility are muscle weakness, and hyperactive reflexes. Rehabilitation is the prominent intervention to deal with the limbs motor injuries (Wolf, Blanton, Baer H., Breshears J., & Butler, 2002).

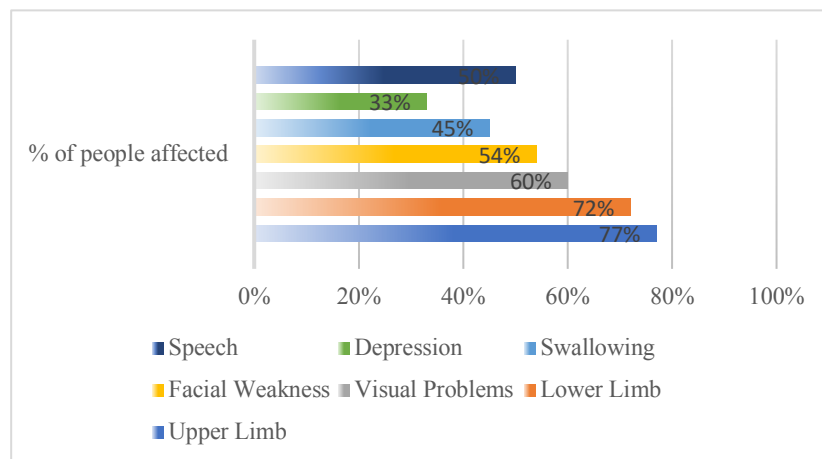


Figure 1.2. Stroke Disabilities Percentage

Concerning the upper and lower limbs, damaged arm and leg function may cause serious limitations in activities of daily living (ADL) for the majority of stroke patients (Hamed & Hayek, 2008). Directly after stroke, upper and lower limbs weakness is the most common

damage, occurring in 77% of patients. In a stroke longitudinal follow-up study, it is revealed that 60% of stroke patients regain very little dexterity after six months (Kwakkel, Kollen, Van Der Grond, & Prevo, 2003).

Providing stroke survivors with the required treatment that they need to recover and regain motor function is a remarkable challenge for physiotherapists. The process is not only physically difficult for the therapist, but it is also time-sensitive, and requires experts and expensive manpower that healthcare system struggles to provide. Stroke patients are discharged to Early Supported Discharge (ESD) in the UK, however, 19% of hospitals do not offer ESD (Intercollegiate Stroke , 2017). Unfortunately, this means that patients are usually not able to get as much therapy as needed and as fast as they need it. In order to recover from upper limb weaknesses that occur after stroke rehabilitation nurses, therapists, and physical therapists must carry out intensive rehabilitation. The demand for an effective alternative solution to rehab the upper limbs is needed to avoid the problems that patients face such as money, and time.

Stroke rehabilitation could include any traditional or robotic therapy; many approaches have been developed in last decades. Traditional motor rehabilitation depends on the patient and therapist (individual sessions), and it has many factors that can limit the rehabilitation process such as resources, poor insurance coverage, lack of potential and knowledge of rehabilitation, cost, and the number of therapists in comparison to stroke patients. According to (Hoenig, et al., 2006): *“One of the potential solutions could be providing the existing personnel with advanced tools that can reduce the monitoring time without any compromise on the impact of the treatment”*; therapists who offer rehabilitation to stroke patients have lack of sufficiently trained personnel.

Robotic technology is emerging as a tool to assist therapists with assessing stroke patients and providing the necessary therapy. One of the main goals of robotic therapy units is to increase the efficiency of the recovery process. Rehabilitation Robotic must be able to perform specific movements to stimulate motor plasticity (flexibility) in the patient’s limbs to provide therapy at the same level as a therapist, which will result in improving recovery and minimising functional restrictions in upper and lower limbs for the patient.

The use of robotic devices for rehabilitation to achieve motor recovery can be justified, considering its potential impact on better therapeutic treatment and motor learning. As these robotic devices become more cooperative and human friendly.

On the one hand, majority of existing rehabilitation robotic devices designed for upper limb therapy are rigid and actuated by electric drivers; because of its high mechanical structure, stiffness, and high bandwidth. However, it is not the most convenient selection for limb rehabilitation, due to its high weight, and complexity. On the other hand, soft robotics had risen to meet the requirement of convenient selection, lightweight, compliant, high strength, ease of use, human friendly, safe, high mechanical tolerance, and low impedance. Soft Robotics especially Pneumatic muscles have received more attention due to its high power to weight ratio, their wide range of capabilities including the range of motion (ROM), degrees of freedom (DOF), that are not achievable with hard (rigid) robotics (Rus & Tolley, 2015). However, they still have some disadvantages, including non-linearities in both force and air dynamics, and their dependency upon external source of air and their associated mechanical noise that can cause irritation during the rehabilitation.

The aim of robotic technology in a rehabilitation setting is to build a robotic device that can match the movement of upper limbs. Such robotic device will allow stroke patients to relearn the best possible use of their limbs, regain independence, and to perform the ADL.

The development of soft robotic devices has made a significant impact on rehabilitation, especially that rehabilitation process requires safe human-robot interaction. Hence, the need to provide an inexpensive, small, light-weight upper limb rehabilitation robotic device for stroke patients was suggested. This device will allow the patient to take it home and spend more time in training the injured limb to perform the ADL's with less money and time in therapy. Moreover, this device will help the therapist as well to take on more patients and monitor the patient's recovery.

1.2 Background on Rehabilitation Robotics

As the population of stroke patients continues to grow, providing sufficient rehabilitation treatment to patients can be expected to become more and more difficult due to its labour-intensive nature. Rehabilitation robotic devices have the potential to meet this growing demand that conventional manual therapy is struggling to cope with. These take advantage of a wearable design allowing them to be worn and fit to the patient's body due to having a similar kinematic structure to the human limbs.

Despite the technology revolution in the robotics field, and the many studies conducted to develop robotic rehabilitation devices for the upper limb, very few number of patients agreed

and appreciated these rehabilitation devices; due to several reasons such as cost, lack of necessary functions to observe and adapt to patient performance (as with a therapist), and safety (Maciejasz, Eschweiler, Gerlach-Hahn, Jansen-Troy, & Leonhardt, 2014).

Clinical acceptance of robotic rehabilitation devices will depend on its added value in offering features or functions difficult to achieve with traditional therapy (Scott & Dukelow, 2011). Offered features include exact repetitive movements, programmable resistance, high intensity, and objective evaluation. The design of an acceptable robotic rehabilitation system must address the needs of the patients and, therefore, requires the input of both therapists and stroke survivors.

Having a robotic system at home that could be utilised for therapeutic purposes may increase the contribution of care outside a primary health setting, and potentially enhance the patient's recovery.

With this in mind, the study aims to develop a soft wearable exoskeleton arm to rehab the elbow, so the patients would be able to devote more time to their therapy at lower cost while achieving a greater level of independence.

As stated by (Polygerinos, et al., 2017) a soft wearable robotic device could cause a better rehabilitation progress in home or at clinic by providing: (1) safe human-robotic interaction - human friendly; the materials used in the design are soft, (2) low component cost; the materials used in the design are inexpensive, (3) customised based on patients anatomy, (4) simple control mechanism; it has single actuation source, and (5) lightweight and portable to assist the patient to perform the activities of daily living (ADLs).

The literature review presents some existing robotic devices for rehabilitation that implemented pneumatic muscle actuators (pMAs). pMAs can play a significant role in upper limb rehabilitation due to its characteristics. However, the development of pMAs was slow compared to other systems that utilise different types of actuators such as electric motors, conventional pneumatic actuators, hydraulic actuators, and other linear actuators.

Recently, the demand of providing a safe assistive rehabilitation robotic device is growing rapidly, despite its obvious disadvantage of being non-linear in behaviour. This inherent disadvantage introduced a challenge on how pMAs are modelled and controlled, thus, the necessity of developing a novel model and control method has arisen.

The work described in the thesis sets out to determine if the soft arm design and control are suited to application in elbow rehabilitation. This was achieved through the model and

construction of a pneumatic Muscle Actuator (pMA) for elbow joint, and the adaptive controller. Experimentation using the platform to test whether the design and control were well suited to perform rehabilitation focusing on the shortcomings and trying to avoid them.

1.3 Challenges and Key Design Issues

This study introduces a development of a soft upper limb exoskeleton arm using various pneumatic Muscle Actuators (pMAs) to rehab the elbow joint. Using pMAs provides a motivation to design a novel model for the pMAs and control them to validate the results. Many researchers have modelled pMAs geometrically; however, their model implementation is not widely exposed. This study focuses on the design and implementation of pneumatic muscle actuator in upper limb exoskeleton and focuses on the modeling and control of pMAs. The challenges, issues and study contributions are formulated as follows:

- Develop a new exoskeleton arm to rehab the elbow joint without using rigid components to ensure safety as it is will be used by human at home.
- As the pMAs are nonlinear, a representative numerical model is required. The simulation model should be as real as possible to validate the experimental results.
- As the pMAs are nonlinear, a control should be provided in order to validate the results.

1.4 Research Question

The aim of this thesis was to build a new exoskeleton arm in order to formulate future challenges in this field. The thesis describes a literature review of the upper limb rehabilitation robotic devices, anatomy of the elbow joint, robotic devices classifications, patient acceptance of robotic devices, and different models and control method employed to pMAs. Based on the literature review, the upper limb exoskeleton robotic devices that used various pneumatic muscle actuators has yet to be widely investigated, modelled and controlled.

Is the Novel soft arm design and control are suited to application in elbow rehabilitation?

1.5 Research Aim and Objectives

This thesis aims to develop a soft wearable rehabilitation device that would allow patients suffering from post-stroke motor weakness to perform repetitive motion therapy in their homes. This therapy is commonly used in restoring lost motor skills by helping the brain rebuild neural pathways lost as a result of disease or trauma such as stroke. In removing the need for a physical therapist to conduct these exercises, the patients would be able to devote more time to their therapy at a lower cost while achieving a greater level of independence.

In detail, the research objectives of the experimental work in this thesis:

- RO1: Design a soft arm for elbow rehabilitation using pneumatic Muscle Actuators (pMA).
- RO2: Devise a novel model for various pneumatic muscle actuators. In addition, analyse the pMA's operation from a numerical modelling perspectives using ANSYS and other softwares.
- RO3: Conduct a systematic finite element analysis (FEA) to evaluate the actuators.
- RO4: Analyse the performance and behaviour of the pMA and compare it to the novel model.
- RO5: Develop an adaptive controller using Simulink/ Matlab to validate the results.

1.6 Thesis Outline

The following provides a project outline summary of each chapter in this study.

Chapter 2: Background to Upper Limb Anatomy and Clinical Therapy

This chapter reviews some of the background literature to demonstrate the motivation for this study. Topics included: a description of the anatomy of the human upper limbs, approaches used to rehab the injured limbs.

Chapter 3: Literature Review

This chapter reviews some of existing robotic devices, to build a clear picture of the areas in need of enhancement; a review of the actuators used for rehabilitation robotic devices was conducted. And finally, different pneumatic muscle actuators modelling, and control were summarised.

Chapter 4: Mechanical Design of the Soft Arm

This chapter introduces a new proposed design of the soft arm. The system used soft muscles (pneumatic Muscle Actuators) to provide motorise assistance of felxion and extension of the elbow joint. The custom made air muscle has been tested experimentally to examine the physical charecteristics of the muscle to help in controlling the muscle. In addition, various pMAs geometrical model were described and compared to the experimental results to validate the results.

Chapter 5: Modelling Pneumatic Muscle Actuators

This chapter discusses a novel non-linear Finite Element (FEA) numerical model of the proposed pMAs. Demonstrating the thread effect, Material, Boundary conditions, on the model, and compare it to the experimental model in order to validate the results.

Chapter 6: Control of the Soft Arm

This chapter introduces a new approach to control the air flow required to operate the proposed pMAs. Using PID as in input for the proposed Model Reference Adaptive Control, with and without NN and compare them to each other's to validate the experimental results.

Chapter 7:

Concludes with a summary of findings developed in this research. This chapter highlights the significant contributions to pMA and the novel design that is made within this body of work and discusses possible future work related to the pMA.

2 BACKGROUND TO UPPER LIMB ANATOMY AND CLINICAL THERAPY

This chapter summarises the anatomy and clinical therapy of the upper limb in human body especially the elbow joint. To ease the process of designing a proper soft arm to rehab the elbow joint.

2.1 Introduction to Upper Limb Anatomy

In order to understand the rehabilitation process and motions required to build a rehabilitation robotic, the anatomy of human upper limb was studied and discussed. The next section will focus on the main components of the human upper limbs and motions such as **joints**, **muscles** that control the joints, degree of freedom (**DOF**), range of motion (**ROM**), actions, position of muscles, and so on.

Standard terminologies are required to discuss anatomical structures. It is important to familiarise the reader with some of these terminologies as shown in Table 2.1 below. The following definitions will be used throughout this study (Bartlett, 2007).

Table 2.1. The Definition of Various Direction Used in Anatomical Descriptions (Aiello & Dean , 2002)

Term	Description
Anterior (Ventral)	The front
Posterior (Dorsal)	The back
Inferior (Caudal)	Below or away from the head
Medial	Toward the body's longitudinal axis or medial plane
Lateral	Away from the body's longitudinal axis or medial plane
Proximal	Toward an attached base
Distal	Away from an attached base

Moreover, it is also important to be familiar with the most common activities that joints perform. Joint actions (movements) can be described by its spatial movement pattern in relationship to the body in terms of the anatomical position. The joint type will decide how it can move and in what plane/s the movement occur/s (Hall, 2003) Figure 2.2 demonstrates the main joint actions.

- **Flexion and extension:** Flexion of a joint makes a body part move in a forwards direction from the anatomical position. However, an extension of a joint makes a body

part move in a backwards direction. The knee joint is the only exception to this rule where flexion moves the lower leg backwards, and extension moves the lower leg forwards

- ***Horizontal flexion and horizontal extension***: Horizontal flexion and horizontal extension are movements of ball and socket joints but tend only to be observable in the shoulder joint during sporting techniques. Horizontal flexion occurs when the joint shoulder moves toward the middle of the body and the shoulder are bent with the arms parallel to the ground. Horizontal extension occurs when the shoulder joint with the arms parallel to the ground moves away from the middle of the body.
- ***Abduction and adduction***: The abduction of a joint makes a body part move away from the midline of the body in the anatomical position. Adduction of a joint makes a body part move towards the midline of the body.
- ***Rotation***: Rotation of a joint is when a body part turns about its long axis from the anatomical position. For example, when using a screwdriver, rotation is occurring at the shoulder joint as the arm turns about an axis that travels straight through the arm from the shoulder to the wrist. Rotation does not have a separate opposite movement because it can be medial or lateral, which are opposite movements.
- ***Circumduction***: Circumduction of a joint makes a body part move from the anatomical position, describing a cone shape. The joint performing circumduction stays still while the furthest end of the body part moves in a circle.
- ***Pronation and supination***: Pronation and supination are anatomical terms unique to the radio-ulnar joint and are separate terms to describe the rotation of the forearm. In the anatomical position, the radio-ulnar joint is supinated. Pronation of the radio-ulnar joint makes the palm move to facing backwards or downwards. Supination of the radio-ulnar joint is with the palm facing forwards or upwards.
- ***Dorsiflexion and plantar flexion***: Dorsiflexion and plantar flexion are anatomical terms unique to the ankle joint. Dorsiflexion of the ankle joint makes the foot move towards the shin as walking on the heels. Plantar flexion of the ankle joint makes the foot move away from the shin as walking on the tiptoes.

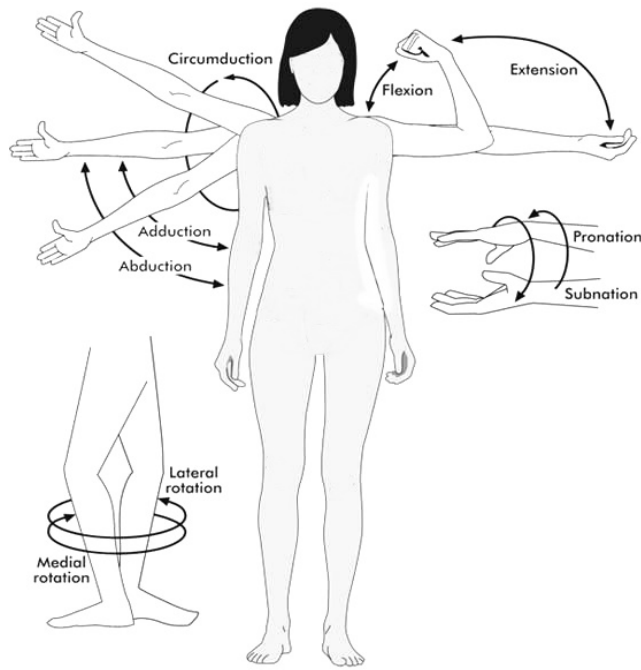


Figure 2.1. Joints actions (Hall, 2003)

The main components of the human upper limbs are **muscles**, **bones**, and the **joints** that connects the bones together in both upper and lower limbs. There is demand in studying human joints, and it has become extremely necessary in the area of orthopaedic and rehabilitation (Almurib, Al-Qrimli, & Kumar, 2011). The upper limb is divided into the shoulder (junction of the trunk with the arm), arm, **elbow**, forearm, wrist and hand. The lower limb consists of the upper leg (thigh), knee, lower leg, ankle, and foot as shown in Figure 2.2.

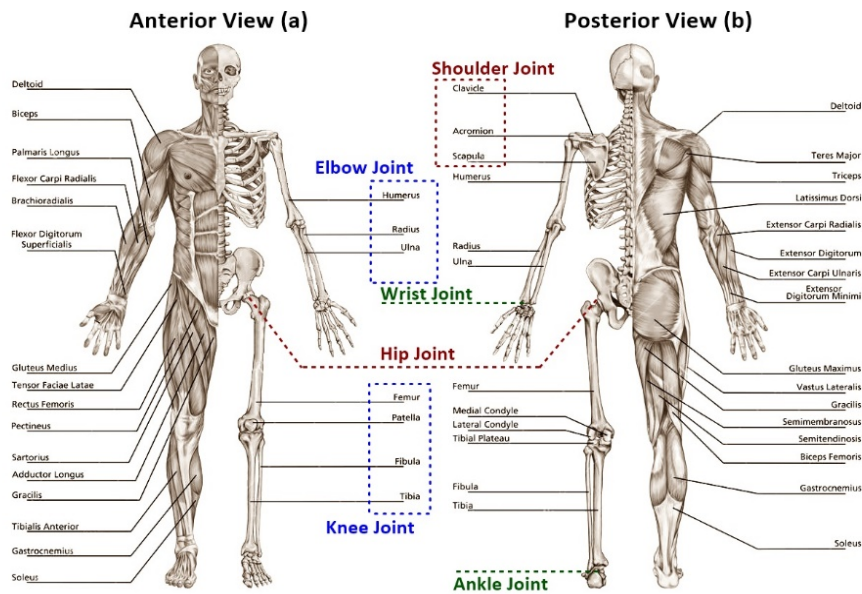


Figure 2.2. The main muscles and joint for the human upper and lower Limbs

2.2 Main Joints of Human Limbs

Joints allow a composite range of movements for the arm and leg and without these joints the human arm and leg would not be able to perform various movements as described in section 2.1.1. The tolerance and strength of material that will be used in the elbow, knee, shoulder joint, and hip joint require being significantly higher than the ones used for the wrist and ankle joints (Kong & Tomizuka, 2009).

2.2.1 Muscles Acting at Joints

The muscular system controls the human body movement. Attached to the bones of the skeletal system are about 700 named muscles that make up roughly 42% of a human's body weight (Starr, Evers, & Starr, 2010). Each of these muscles is a discrete organ constructed of skeletal muscle tissue, blood vessels, tendons, and nerves.

Muscles classification depends on either the movements (actions) they create: extensors, flexors, pronators, abductors, adductors, supinator and so on, or the number of muscle groups such as biceps (two groups), triceps (three group), and quadriceps (four groups) (Huston, 2009).

Muscles are divided into three groups according to the movement contribution (Zhiguo, Zhizhong, & Hongbo, 2008):

- Agonist Muscles: muscles that initiate the movement (generates most of the force)
- Synergist Muscles: assist the agonist's muscles. (less force is generated)
- Antagonist Muscles: resist the movement (provide a stabilising force during the movement).

Each movement in the limb has its antagonistic movement that moves the limb in the opposite direction such as extension and flexion, adduction and abduction, and so on.

The limbs motions are crucial for the daily human activities, such as eating, drinking, walking, and running. It is difficult for physically weak elderly, disabled or even injured people, suffering stroke or dementia, to perform the activities of daily living (ADL). Muscles play a major role supporting the movement of the human body and controlling the joints (Gopura, Kiguchi, & Horikawa, 2010). Upper limbs muscles power injuries are one of the most important causes of mobility limitations in older adults especially those who suffers a stroke.

2.2.2 Human Upper Limb Joints

The upper human limb consists of five main components: the shoulder joint, the **elbow**, the wrist, and the hand. The kinematics of these joints is a challenge due to the significant variations among people. Upper limb injuries can alter motion in substantial ways. There is relatively little data available for upper limb motion. Most available kinematic data for the upper limb was collected for specific purposes and measured using non-standardised approaches (Mizrahi, 2015).

For rehabilitation, functional range of motion is an important quantity that is often manifest as a minimum range of motion (ROM) required performing functional tasks. The following briefly discusses the **elbow** joint in terms of its structure. And for the purpose of this study, it discusses the joint movements and its range of motion (ROM). ROM for the joint is obtained as averages from some sources (Rosen, Pery, Manning N., & Burns, 2005) and is listed as a typical minimum (functional) and maximum degrees.

The Elbow

The elbow is a compound joint consisting of three bones and two articulations as listed in Figure 2.2. The humerus of the upper arm connects to the radius and ulna of the forearm through the humeroradial and humeroulnar joints. The humeroradial joint can be approximated by a ball-and-socket joint with 3 DOF while the humeroulnar joint is best described as a hinge joint with 1 DOF. The bones form a closed kinematic chain, restricting the elbow joint to 2DOF overall (Inagaki, 2013) as shown in Table 2.2.

Table 2.2. Elbow Movements

Joint	Joint Movement	Muscle Responsible	Location
Elbow	Flexion: The motion of the forearm toward the upper arm. ROM: ~ 110°; up to 150°.	Biceps Brachii	Anterior Upper arm
	Extension: The motion of the forearm away from the upper arm. ROM: ~ 110°; up to 150°.	Triceps Brachii	Posterior Upper arm
	Pronation: Rotation of the forearm in the palms downward, orienting the wrist. ROM: ~ 120°; up to 160°.	Pronator Teres Pronator Quadratus Brachioradialis	Superior Anterior Forearm
	Supination: Rotation of the forearm in the palms upward, orienting the wrist. ROM: ~ 120°; up to 160°.	Supinator Biceps Brachii Brachioradialis	Lateral Anterior Forearm

Upper Limbs Anthropometry

It is necessary to describe and study the anthropometry in order to build an arm to fit the human limbs. Anthropometry from the Greek: Anthropos (man), Metrein (to measure), Anthropometry is the study of the measurement of the human body in terms of the dimensions of bone, muscle, and adipose (fat) tissue (Nikolova, 2010). Anthropometric measurements must be considered when designing the robotic device intended for this study as it deals with the body shape, size, strength, and working capacity. Moreover, anthropometric measurements are usually classified as a particular population because the body dimensions differ among people. It might be most appropriate to use data that covers both genders and the patients suffering stroke, in addition, age must be factored into the choice of data as most incidents occur after the age of 65 (Delavande , Hurd , Martorell , & Langa , 2013). The average length or mass of a body segment can be estimated as a fraction of total standing height, H, or total mass, M, respectively. Table 2.3 lists the normalised mass and length of body segments for the standard human, see Appendix A (Winter, 2009).

Table 2.3. Normalised mass and length of body segments

Segment	Segment Mass/M	Centre of Mass/ Segment Length (Proximal)	Segment Density (Kg/m³)
Upper Arm	0.028	0.436	1070
Forearm	0.016	0.430	1130
Forearm and Hand	0.022	0.682	1140
Total Arm	0.050	0.530	1110
Lower Leg (Calf)	0.0465	0.433	1090
Upper Leg (Thigh)	0.100	0.433	1050
Foot and Lower Leg	0.061	0.606	1090
Total Leg	0.161	0.447	1060

Kinematic and dynamic analyses require data regarding mass distributions, the centre of mass, density, and segment length (Freivalds, 2011). Provided explanations to these required data as following:

Mass Density: Just like any other body segment, limbs have an exclusive combination of bones, muscles, fat, and other tissues, and so the segment density is not uniform. The higher proportion of bone leads to a greater density of distal segments in comparison with proximal

segments. The density of individual segments increases as the average body density increases.

Centre of mass (Segment length): The location of the centre of mass is presented as a percentage of the segment length from either the proximal or the distal end. To locate the centre of mass, the centre of balance of each segment has to be determined first.

Segment Mass: As the total body mass increases, the mass of each segment increases. Thus, it is possible to present the mass of each segment as a percentage of the total body mass. Segment mass is determined by segment density and volume.

To design a new device to rehab the elbow joint it's important to understand the elbow kinematics. Kinematics of the elbow joint occupies a considerable place in orthopaedic rehabilitation. Many devices have been constructed with this aim A schematic representation of elbow kinematics are shown in figure, Assuming elbow angle α to be zero when the elbow joint is fully extended, one can find it simply as:

$$\alpha = 180^\circ - \alpha_1 - \alpha_2 - \alpha_3 \quad (2.1)$$

where angles α_1 and α_3 are constant values which depend on position of cable insertion points at the arm, namely, upper and lower arm lengths u and l and respective offsets. Angle α_3 is uniquely determined by the tendon length c and can be found from the resulting triangle via the law of cosines;

$$e.g. \alpha_2 = \cos^{-1}((a^2 + b^2 + c^2) / 2ab) \quad (2.2)$$

where the quantities a and b are constant and can be calculated with the knowledge of the aforementioned cable connection point coordinates, and tendon length L_3 is assumed to be known (Gaponov, Popov, Jun Lee, & Hwan Ryu, 2016).

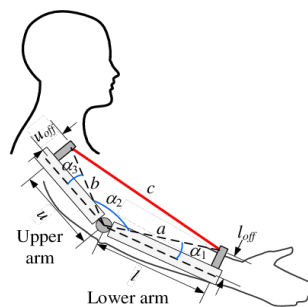


Figure 2.3. Schematic representation of the elbow joint shows the elbow kinematics. (Gaponov, Popov, Jun Lee, & Hwan Ryu, 2016)

2.3 Stroke Rehabilitation for Upper Limb

The widest range of damages caused by stroke is motor injuries that limit the function in muscles movements and actions (Langhorne, Coupar, & Pollock, 2009). Stroke-suffering patients have the chance to regain partial or full mobility after stroke through many rehabilitation therapy programmes for the limbs. Stroke rehabilitation normally involves assessment; to identify and quantify the patient's demands, setting goals and interventions; to determining what therapy to provide, to define realistic goals for improvement while monitoring the whole progress and detect how well the patient improves, and finally, the reassessment; to assess progress against the intended goals. In this section current assessment and therapy techniques are discussed and two types of rehabilitation: stroke rehabilitation therapy with a robotic device, traditional therapy that requires exercising with the therapist. There are several impacts that a stroke can leave on the upper and lower human limbs. As discussed before, stroke usually affects one side of the body causing one or more of the following symptoms (Stroke Association, 2013):

- *Weakness*: the shoulder, hip, and elbow, may become weaker, which means difficulty in picking, reaching, holding onto things, walking, running, jumping and so on. However, in severe cases the whole limb, upper or lower, may be paralysed.
- *Coordination problems*: being not able to move the limb, upper and lower, in a the way the patient wants due to the difficulties of planning and coordinating the movements of the limb.
- *Swelling*: as a result of limb disability fluids may build up in it causing swelling that also could be called as oedema.
- *Changes in muscle tone*: the muscle of the limb could be in either high or low tone. On one hand, the high tone makes the muscle stiff or tight. On the other hand, the low tone makes the muscle loose and floppy.
- *Subluxation*: the limb movements, in this case, are difficult and painful. The top of the limb drop out of the shoulder or hip socket slightly, because of the Weakness or Low tone.
- *Contracture*: weakness or high tone may shorten the arm muscles or reduces the flexibility of joints.
- *Changes in sensation*: losing the feeling in the limb and some other parts of the body gradually or abruptly. Moreover, sometimes feeling pins and needles, or increasing sensitivity.

Stroke has recently been named the leading cause of physical disability in adults over the age of 45 (Dobkin B. H., 2005). Reduced capabilities in upper and lower limbs are recognised as the most common impairments of stroke survivors.

The four main motor functions in the arm that are affected by stroke are flexion/extension of the elbow, pronation and supination of the wrist and other things related to finger movements. Wrist and finger extension are the hardest muscles movements to regain (Cauraugh, Light, Thigpen, & Behrman, 2000). The elbow joint on the human body experiences higher torque than that of the wrist or fingers due to the weight and anatomical position of the forearm and hand. In addition to that, an external load is placed on the elbow joint when an individual is carrying an object due to the lever arm nature of the forearm. Existing research has revealed that the muscles that actuate the elbow joint have selective weakness in post-stroke patients. In particular, the elbow flexors and extensors are weaker when the muscle fibres are in their shortened range that reduces the working range of the elbow joint (Ada, Canning, & Low, 2003).

Rehabilitation (Therapy)

The goal of a stroke rehabilitation programme is to help the patient to regain the ability to move their affected limbs. Stroke rehabilitation can help to regain independence and improve the patient's quality of life. There are numerous approaches to stroke rehabilitation such as traditional and robotic rehabilitation.

Traditional Rehabilitation: The aim of traditional rehabilitation is to improve the mobility using therapeutic exercises guided by the therapist, who moves the patient's limbs. Moreover, to restore the patient's ability to perform the activities of daily living (ADL). An early, high intensity and repetitive rehabilitation can substantially improve the long-term mobility of the limb (Bishop & Stein, 2013). In limb rehabilitation, therapy is often conducted by an individual or team of therapists, usually after a clinical assessment has been conducted. Traditional Rehabilitation totally depends on the therapist, therefore, the need to find a new and efficient rehabilitation approaches arise. Traditional rehabilitation has many limitations such as the shortage of therapists, and neither training duration nor training intensity can be guaranteed, so it is unable to gain an optimal therapeutic effect. Moreover, the therapist can implement rehabilitation treatment on one patient at the same time; the therapist has low efficiency and high work intensity. It is hard to evaluate the process of rehabilitation quantitatively because it is impossible to measure the physiological information of the patient

while training. Thus, it can be also considered as one of the traditional rehabilitation limitations (Patel, Park, Bonato, Chan, & Rodgers, 2012).

Traditional Therapy programmes focus on training with repeating the movements using different approaches in order to regain the ability to move. Some of these approaches can be counted and described as follows:

- **Restriction:** this approach can be used with minor injuries since the patient is likely to perform the activities of daily living (ADL) using the stroke-affected limb next to the unaffected limb. For example, Constraint-Induced Movement Therapy (CIMT) is one of the widely used methods for upper limb rehabilitation and mainly used as a part of clinical practices by the NHS (Bradshaw, 2012).
- **Manual Guidance:** One or more therapists help the patient by guiding the injured limb(s) through several activities. In this case the therapist assists the patient achieving the suitable and required response by tapping, stroking, and holding as needed, in other words the therapist passively moves the patients' injured limb(s) to provide the appropriate proprioceptive feedback, moreover, the frequency of assistance should be reduced as the patient's recovery progresses (Muratori, Lamberg, Quinn, & Duff, 2013).
- **Progressive- Resistive Exercise:** is the ability of muscle to generate force, in this approach the patient performs some activities against resistance, the therapist keeps increasing the resistance as the patient progresses (Taylor, Dodd, & Damiano, 2005).

Rehabilitation Robotics: The need for rehabilitation robotic devices increased and arose with the increment of aging population and people suffering a stroke. Improvements are required in order to offer a high quality of care that patients need. Rehabilitation robotic devices provide a potential solution to rehab the injured limbs by training, monitoring and reporting the movements precisely without getting tired or causing any mistakes (Rietman, Prange, Stienen, & Buurke, 2011). Moreover, robotic devices cannot be distracted and discouraged. The limb rehabilitation robotic devices system consists of a mechanical arm, PCs, sEMG signal tools, and control system. The robotic device can do the motion of 6DOF for the upper limb and other 6DOF for the lower limb (Minimum DOF). It is applicable for both active and passive training methods. The control system will include the motion control hardware; that consists of a controller, driver, and motor.

Considering the actual situation of patients, the ROM and DOF of the robotic device is smaller than the normal and can be adjustable, in addition to its ability to provide treatment repetitively without therapist fatigue.

On the one hand, out of the many advantages that rehabilitation robots have is providing feedback simultaneously during treatment. Also, using robot devices can reduce the need for moving patients among different equipment during the session. All of these advantages can be considered as a supportive tool in health care system. On the other hand, rehabilitation robots are costly and space consuming, most of the devices are limited to portions of injured and affected limbs.

Robots can be utilised to enhance the traditional approaches, as described before, where it can be used instead of the therapist to assist patients during the therapy session. Robots can be programmed to provide any level of assistance.

Despite all the advantages the robot has, also many limitations can show up when using it. Safety is one of the most important concerns that should be taken into consideration as there is an interaction between the human and machine. From design consideration robots are robust, however, it can be dangerous without implementing the suitable safety measures. The acceptance of robotic technology can be influenced by both patient and therapist due to the safety problems. Robots are not capable to provide qualitative feedback to patients. The cost can also play a major role in using robots (Sale, et al., 2014).

Studies conducted by Burgard *et al* (Burgard, Lum, Shor, & Loos, 2002) have demonstrated successful clinical outcomes of robotic rehabilitation in assisting patient's arm movements when compared to conventional therapy techniques, in these studies, the group of stroke patients exposed to robot-assisted therapy exhibited greater improvements in motor function and strength in comparison to the control group. The clinical outcomes of robot assisted therapy also suggest promising post treatment results, specifically in the patients' ability to voluntarily reach towards targets. All of the numerous motivations aforementioned have led to escalating advances in the field of robotic rehabilitation in recent years. Table 2.4 below summarise a comparison of traditional and robotic rehabilitation.

Table 2.4. Comparison of traditional and robotic rehabilitation

Principle	Traditional Rehabilitation	Robotic Rehabilitation
Intensity	Low, due to physical therapist limitation.	High, motorised system.
Effect	High, because it works actively.	Low, if it remains working passively during the training.
Independence	Low, the therapist, limits it due to safety.	High, a wide range of motion (ROM), and body weight supported.
Costs	High, paying manpower hours.	High, robot set-up and usage.
Duration	Short, limited to manpower.	High, repetitive training.
Assessment and Evaluation	Depends on the experience of the therapist, and less specific; the therapist cannot guide the motion properly.	High sensory, accurate biofeedback, and the robot can control the motion precisely.

As a result, using robotic devices in rehabilitation is not only able to improve the motor ability of the patients but also it reduces the requirements of therapeutic assistance and the time-consuming in the therapy process.

3 LITERATURE REVIEW

This chapter summarises the various aspects of rehabilitation devices and robotic devices, and the types of approaches utilised. It also summarises studies that have been carried out for testing different devices and techniques within rehabilitation robotics field. In recent years, new rehabilitation techniques are emerging to deal with upper limb injuries. Robotic devices are valuable tools for rehabilitation since they allow the repetitive application of controlled forces to the affected (injured) limb.

3.1 Existing Devices for the Limb Rehabilitation

These devices perform not only single simple movements and complex rehabilitation process, but also functional rehabilitation methods. All contribute to improving the efficiency and effectiveness of the rehabilitation process (Poli, Morone, Rosati, & Masiero, 2013).

Many assistive systems for limbs rehabilitation have been developed for several types of limb rehabilitation. These systems implement distinctive mechanical structures, designs, actuators, techniques, control systems and rehabilitation approaches, as well as various techniques to ensure the reliability and strength of the systems when compared to others. The fast development of rehabilitation robotics over the last ten years is working toward fully regaining or improving the movement of affected limb functions and helping patients achieve a better quality of life (Dzahir & Yamamoto, 2014).

Between the late 1980's and early 1990's engineers started exploring the opened opportunities to utilise robotic devices in rehabilitation therapy (Krebs, Hogan, Aisen, & Volpe, 1998). The first robotic devices for rehabilitation such as Lido and Biodex machines that considered active dynamometers robots were developed in late 1970's. These robotic devices aimed to provide activities that allow the patient to exercise and practice independently, moving the limb, and measuring the movement performance. Moreover, it is closely related to physical therapy. Robotic devices include a kit of bars and levers connected to the motor, the levers designed to assist the joint movements such as flexion, extension, adduction, abduction, rotation, and so on. Allowing the patient to train and move the joint, and then the dynamometers sense the mass (torque) and limb movement and display the information to both patient and therapist. Advances in the field of rehabilitation robotics have led to the development of many robotic systems used in physical assistance and rehabilitation in both clinical and domestic setting. Robotic devices improve the patients quality of life by

providing treatment and supporting the patient to perform the ADLs. Rehabilitation robotics have different DOF, which describes the total of independent movements that can be performed in all joints of the device. Moreover, it differs from each other in the number of actuators used depending on the weight of the device, number of supported movements, and number of joints.

The implication of robotic devices in movement rehabilitation has been increasing over the last few years. Many rehabilitation robotic devices have been developed in order to automate therapy for the upper limb (shoulder, elbow, and wrist), also, to strengthen the injured muscles and joints. Delving into different types of upper limb rehabilitation such as hard robotic devices and soft robotic devices. These systems implemented different mechanical structures, actuators, design, fabrication, and control methods.

There are several types of support devices for the upper limb rehabilitation. Devices for limbs rehabilitation may provide a different type of motion assistance such as active, passive, haptic, coaching, active exercise and passive exercise devices (Marchel-Crespo & Reinkensmeyer, 2009). **The active devices** contain a minimum of one actuator, which can be applied to patients who are too weak to perform a particular exercise as the device provides active motion assistance (**Active exercise**). This device can move limbs that also can be used in cases when the movement is not required from the patient (**Passive exercise**).

Passive devices are not designed to move limbs. However, they contain actuators that provide resistance to the limb movement. Such devices are used when the patient can move its limbs. The actuators used in passive devices are less expensive and consume less energy in comparison with the ones used for active devices (Basteris , et al., 2014).

Haptic devices interact with the patient through the tactile sensation such as vibration. Haptic devices can be either active or passive depending on the used actuators. **Coaching devices** are neither active nor passive devices as it used for monitoring and feedback related to the performance of the patient. Both of haptic and coaching devices are usually used in rehabilitation settings with a virtual environment (Maciejasz, Eschweiler, Gerlach-Hahn, Jansen-Troy, & Leonhardt, 2014).

Robotic devices for movements (actions) rehabilitation has two categories when classified according to the mechanical characteristics and design (structure) (Micera , et al., 2005): *end-effector-based*, and *exoskeleton-based*. The difference between the two categories is how the motion is transferred from the device to the patient's limb (Poli, Morone, Rosati, & Masiero,

2013). **End-effector-based** which can be also called operational robot applies mechanical force to the distal segment of the limb, however it limits the control of the proximal segment of the limb, it cannot target particular joint of the limb, which can be considered as a disadvantage, which will lead to abnormal movement pattern especially in the cases of multiple possible DOF. End-effector based has simple structure, thus, it needs easy algorithm and also easy to set-up because the patient should not make any precise alignments, where the patient grasps the handle of the robot as shown in Figure 3.1 (b) below while making movements in virtual environments.

Exoskeleton- based robot axes are aligned with the limb axes, which ease it to provide direct control of specific joints of the limb, exoskeleton-based robot is able to provide information on both cases kinematic and dynamic, However, the structure is very complicated and solid because the gear reducers that is used to decrease the weight of the motor as shown in Figure 3.1 (a). Moreover, due to the difference between limbs length among patients, and the difficulty to fit the patient's limb in the whole range of motion (ROM), misalignment and discomfort will be caused by the patient and robot joints (Cheng & Lai, 2013). Exoskeleton robots have actuators that generate force and power on the human joints to allow them to perform the necessary tasks. In addition to that exoskeleton robots control multi points and positions as in shoulder, elbow and wrist directly.



Figure 3.1. Rehabilitation robotics;

(a) exoskeleton-based robot, (b) end-effector based robot

3.1.1 Actuators

An actuator is a device that converts the stored energy into mechanical work; generally, actuators are powered by different energy source. In the rehabilitation robotic field, the actuators are considered to be one of the most essential components as it works as a muscle in the human body to perform motion. There are different types of actuators that are classified to three main types based on the source of energy such as electric actuators, hydraulic

actuators, and pneumatic actuators. Also, they are categorised based on the type of motion to linear and nonlinear, the traditional actuators are considered to be linear (conventional), however, the new actuators such as pneumatic muscle actuators are nonlinear (non-conventional).

The electric actuators are widely used because of their high power, precision control, and availability in different sizes. The electric actuators can be modified for any purpose, and they produce less noise than the hydraulic and pneumatic actuators. They are also safe to the environment as it does not leak fluids, in addition, they can be programmed and controlled easily due to its linearity feature. However, electric actuators are expensive, can be damaged easily because of the overheat that may damage the components, and can be exposed to many problems such as installation and portability because of the large size of some of them.

The hydraulic actuators energy source is fluid, generally, compressible oil. The nature of the hydraulic actuators allows it to produce an extremely high power-to-weight ratio compared to the electric and pneumatic actuators. However, they are heavy, and leak fluid that will result in reducing the system efficiency, the fluid leak can also damage the surrounded area. It is easy to control but it requires a control method that includes the pump control, valve control, and other components if needed.

The pneumatic actuators that are controlled by a piston and some supporting components such as valve are simple as they are easy to use and install, therefore they are lightweight and not expensive compared to other actuators. They are actuated by gas or air to create motion; moreover, they require low maintenance due to the component durability in the system. Pneumatic actuators are safe to the environment and human friendly; it is most use in rehabilitation field because it interacts with human. However, the pressure losses and air compressibility play a significant role in affecting its efficiency and precision; used in the industrial field where high precision is not required. To increase the efficiency of these actuators, the controller should be programmed to meet a specific purpose; thus, the cost will be increased relatively (Hollerbach, Hunter, & Ballantyne, 1992).

The conventional actuators have been widely used in conventional robotic devices. However, it was necessary to find new actuators (non-conventional actuators) taken into consideration their safety, lightweight, high power-to-weight ratio, portability, and others. Pneumatic artificial muscle is one the most important non-conventional actuators in the field of rehabilitation.

Pneumatic artificial muscles, or pneumatic muscle actuators (pMAs) was invented in 1950s by Joseph L. McKibben and was used for patients suffering polio (Nickel, Perry, & Garrett, 1963). They belong to the non-conventional actuators. They are widely used in biomechanical applications, medical, industrial, and specifically in rehabilitation as they are distinguished by their high power-to-weight ratio, simplicity in construction, lightweight, high stiffness, low material cost, ease of fabrication, and compliance. In addition, the most significant advantage of controlling PAMs in different applications is the need of controlling only one variable. When the muscle is provided with a pressurised air it either contract or expand radically resulting in generating force; this force is characterised by highly non-linear response (Tothava, Pitel, & Borzikova, 2013). pMAs are categorised into sets such as; braided pneumatic muscle, commonly referred to McKibben muscle, embedded muscle, netted muscle, pleated muscle, and others as shown in Figure 3.2, McKibben muscle/ braided pneumatic muscle is the most used one (Mizakova, Pitel, & Tothava, 2014).

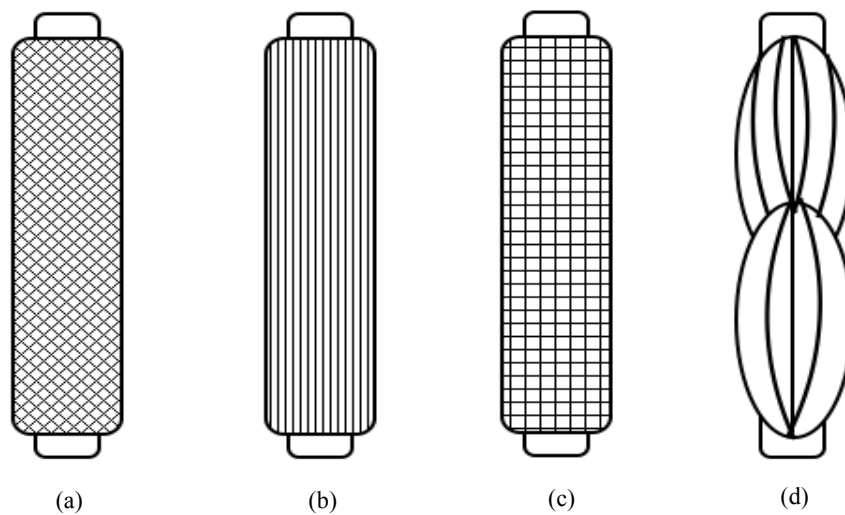


Figure 3.2. Different types of pMAs:

(a) McKibben muscle, (b) pleated muscle, (c) and (d) netted muscles, Rarlott, and ROMAC respectively

The pneumatic artificial muscles consist of the bladder (elastic inner tube) surrounded by a sleeve (non-extensible fiber). However, they differ in their mesh and bladder material, but rubber is commonly used for the inner tube. Bladder and sleeve are connected to terminals at both ends, one of the ends has an air inlet, and these end caps are made of metallic material such as aluminum and steel. They also differ in their mechanical construction, and the mathematical pMA model. It is necessary to derive and utilise the proper mathematical pMA model in order to control it.

3.1.2 Hard Robotic Devices for Upper limb Rehabilitation

Several robotic devices are able to support more than one joint at the same time, to assist both shoulder and elbow, such as MIT-Manus (Massachusetts Institute of Technology Manus), MIME (Mirror Image Movement Enabler) (Lum, et al., 2006), Assisted Rehabilitation and Measurement Guide (ARM) guide, and GENTLEs (Loureiro, Amirabdollahian, Topping, Driessen, & Harwin, 2003). The robotic therapy target for these robots is the same, active assist exercise. Where active refers to the patient's ability to be active and engaged. The assist refers to the therapist assistance provided to patients as needed (Curtin, Molineux, & Supky-Mellson, 2009). Moreover, these robots are easy to adjust with the human upper limb length, which make it simpler and easier to manufacture. However, determining the movement of the upper limb is not easy with only one interface (patients hand). End-effector based robots cannot control the torque at particular joint, in addition, the range of motion (ROM) is limited. as a result, a limited set of rehabilitation exercises can be generated by these rehabilitation robotics. MIT-Manus as shown in Figure 3.3 allows the movement only in one plane (Krebs, Hogan, Aisen, & Volpe, 1998), moreover it utilises massed practice and force feedback method to provide therapy that targets reaching motions towards an endpoint. The force feedback provided by the device consists of forces applied in the same direction as the reaching motion to assist muscle in the task completion. Studies conducted to evaluate the effectiveness of robot-assisted therapy with the MIT-Manus revealed that this system can improve the clinical outcomes for repetitive, goal directed therapy (Krebs, et al., 2004), as well as improve the motor and functional recovery gains in subject with acute and chronic hemiparesis. However, MIME and ARM guide, as shown in Figure 3.3, are both limited to linear movement, because the forearm is usually followed a straight-line trajectory, and both are designed for upper limb rehabilitation through massed practice methods (Lum, Reinkensmeyer, Mahoney, Rymer, & Burgar, 2002). On the one hand, Studies conducted by Kahn et al. regarding ARM guide devices did not reveal significant differences between results obtained with robotic assistive and resistive forces employed by this device and the free, unassisted methods used in conventional therapy for the training of reaching motions. On the other hand, MIME was the first robotic rehabilitation system that explored bilateral training for upper limb stroke rehabilitation, focusing specifically on the practice of reaching motion. The device is coupled to the user's unimpaired arm, allowing three dimensional motions that are assisted or resisted through force feedback (Lum, et al., 2006). Recently, rehabilitation robotics research has shifted to exoskeleton devices. Exoskeleton robots have

the potential to meet the growing of patience demands that traditional therapy is struggling to provide. Since it provides the patient with intensive rehabilitation systematically for a longer duration (Huang & Krakauer, 2009). The robotic devices are able to treat the patient without the presence of the therapist, and with more frequent therapy sessions, thus will result in a reduction of the cost of the rehabilitation process. Moreover, it can be attached at several locations in the upper limb. There are many of commercial robotic devices that has been used for the upper limb rehabilitation.

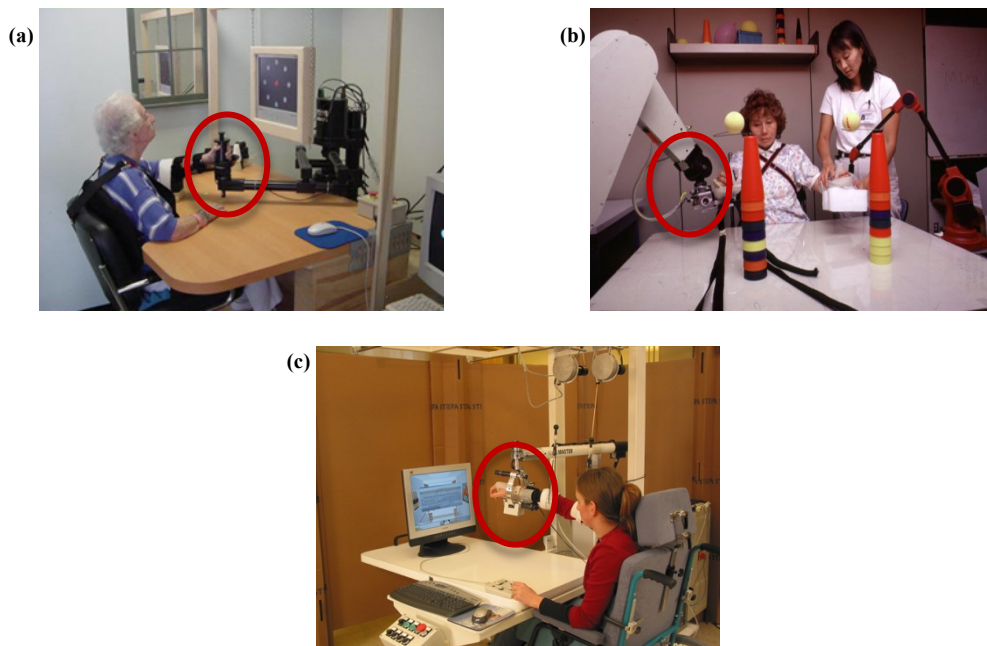


Figure 3.3. a) MIT-Manus; (b) MIME; (c) GENTLE/s.

One of the most popular devices is Armeo (ARMin) as shown in Figure 3.4/a below, which includes 7 DOF, active and passive; the active robot is called ArmeoPower (Nef, Guidali, Klamroth-Marganska, & Riener, 2009), and the passive is named ArmeoSpring as shown in Figure 3.4-b/c, respectively. (Sanchez, et al., 2004). Both of them used to assist shoulder, elbow, wrist, and fingers (whole upper limb) and the input signal is the joint angles and grasp force. InteliArm robot is used also to assist the whole upper limb with joint angles and torques input signals, the degree of freedom is fluctuates between 8-10 DOF (Ren, Park, & Zhang, 2009). The MGA robot assists shoulder and elbow with five degrees of freedom (5 DOF), the input signal joint torque and the actuator is electric motors (Carignan , Tang, & Roderick , 2009).

Robotic devices used for upper limb rehabilitation differ from each other by several factors such as: the DOF, joint movements they support, main control inputs, mechanical design and

structure, and type of assistance. Kiguchi (Kiguchi, Esaki, Tsuruta, Watanabe, & Fukuda T., 2003), MARIONET-Suzler (Suzler, Peshkin, & Patton, 2007), Rosen (Rosen, Brand, Fuchs, & Arcan, 2001), and Song (Song, Tong, Hu, & Li, 2008), all are robotic devices that assist elbow movements. However, some of them are classified to end-effector based such as MARIONET-Suzler and Song, and to exoskeleton-based as in Rosen and Kiguchi. The inputs signal vary from one device to another, in the mentioned devices above the input signal is sEMG except in MARIONET-Suzler as it is the joint angle. In addition, they all share the same degree of freedom: 1DOF. Kiguchi is utilised to support the shoulder joint with 2DOF (Kiguchi, Iwami, Makoto, & Watanabe, 2003).

REHAROB is an industrial rehabilitation robot that is used for the upper limb motion therapy for disabled, in other words, it is used for physical therapy. It was developed to support the upper limb joints, shoulder and elbow. REHAROB as shown in Figure 3.4/c consist of two arms supporting 6 DOF in each, in total 12 DOF. The input signal for this device is the end point torque, where the patients force causes movement of the device when it is in the passive state. REHAROB can also be used in the assessment, as it quantifies the patient's range of motion (ROM) (Fazekas, Hovath, Troznai, & Toth, 2007).

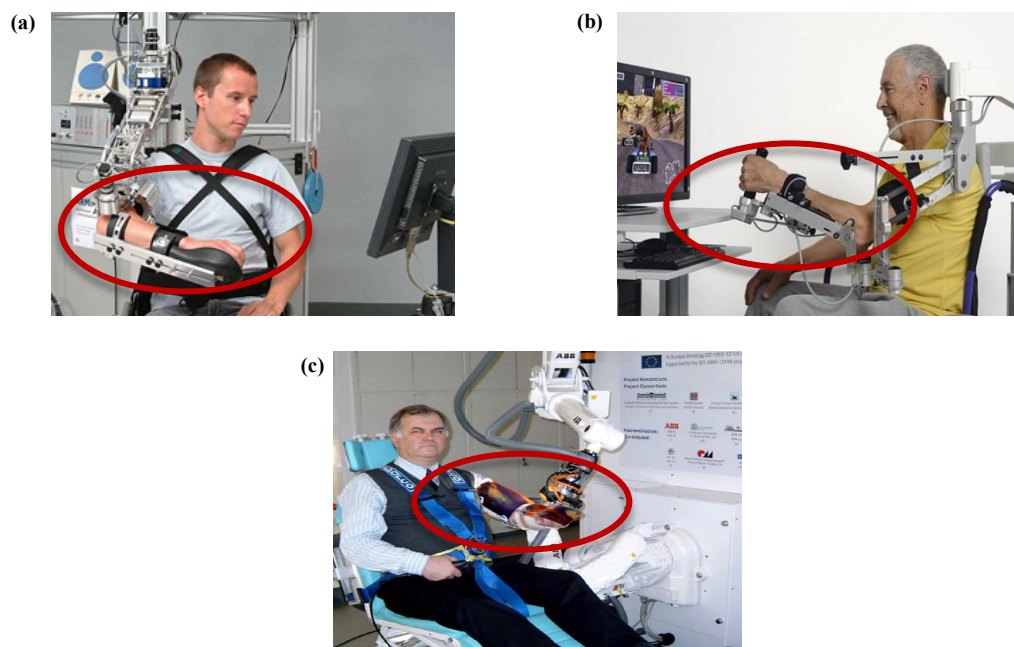


Figure 3.4. (a) ARMin; (b) Armeo Spring; (c) REHAROB.

3.1.3 Soft Robotic Devices for Upper Limb Rehabilitation

One of the most important factors that should be taken into consideration while designing a rehabilitation robotic device is the safety in the interaction with patients. To provide safety one of two possibilities can be implemented during the interaction with patients:

- Provide security by controlling the actuators.
- Use safe actuators to absorb unwanted forces produced by human-robot interaction tasks.

Pneumatic actuators are considered one of the safe actuators, where pressurised air is used as main energy source. The compressibility of air helps these actuators to absorb unwanted force. Moreover, pneumatic actuators have a high force/weight ratio, which make robots much lighter. However, the main drawbacks are the control because of the nonlinearity nature of the air compression. In addition to the high flow of the volume that is used to fulfil the cylinder. Pneumatic muscles can mimic the human muscles by applying air in the chambers.

There are several robotic devices for upper limb rehabilitation driven by pneumatic actuators such as SRE, RUPERT, PNEX-WERX, and iPam and others. The Salford rehabilitation exoskeleton (SRE) is an upper arm assistive exoskeleton, which was developed at the University of Salford. This device has an exoskeleton configuration with 7 DOF, almost covers the upper limb DOFs, and three operation modes. It is designed to work with elderly patients, and it is equipped with means of adjustment to fit the patient. This system has a 3D virtual environment; the virtual environment is complemented by a database to store information and progress of each patient. A prominent feature of the software is that it has pre-programmed routines for warming up the patient's arm thus avoiding possible injury. This robot is based on antagonist configuration of pneumatic muscles that are placed in the base of the robot and motion carried by wire transmission from base to each joint. The muscles in antagonist configuration work very similar to human arm muscles, contributing in this way, more realism and comfort in use. The control varies based on the type of operation mode, which can be positioned at each joint, torque control at each joint or impedance control. (Tsagarakis, Kousidou, & Caldwell, 2008). A deficiency expressed by the authors is that the mechanical design has a singularity when the arm is parallel to the horizontal. Another drawback of the system is that the torque exerted by the mechanism of antagonistic pneumatic muscle depends on the position of each joint, complicating the control loop. Another fault is that the pneumatic muscle system causes a delay between the desired signal

and the performed signal. Although, the delayed signal has the same form as the desired one, therefore, it does not influence the therapy results.

RUPERT; the main objective of this robot is to assist the therapist in the ADL. It can be classified as an exoskeleton robotic device with 4 active DOF and 3 passive DOF. Due to exoskeleton shape, this device only allows its use in the sitting position. The single or multiple targets to be reached and the real-time gesture of the arm are presented to the patient through a virtual reality presentation. The difficulty of therapy is determined by the targets location and the time required for achieving the objective. This robot, in its latest version, is driven by McKibben pneumatic muscles. These muscles are getting double compression effect by the action of compressed air and passive extension by a spring. The main control element is the gravity compensation that allows compensation of the weight of the patients arm. The control of each pneumatic muscles is via a PID controller with a process of self-tuning ILC (Iterative Learning Controller) for each patient. Therefore, it is necessary prior exercise for the regulator self-tuning to be adapted for the different symptoms of each patient, achieving an adaptive control loop and a feed-forward to increase the speed of system response. Fuzzy rules are used to solve the problem of nonlinearities. As result, it complicates the process of preparing the robot for each patient (Zhang , et al., 2010). The main advantages of RUPERT to be noted are: it is a lightweight robot, portable, inexpensive, safe, and easy to use. Another advantage is that it offers active safety by depressurising the pneumatic muscles and limiting the torque offering by the joints. A disadvantage of this robot is that it has only one degree of freedom in the shoulder, still insufficient for the entire workspace of the human arm.

PNEU-WREX; is a pneumatic-driven robotic device for upper limb rehabilitation and it is an evolution of a previous work called WREX (Rahman , Sample, & Seliktar, 2004). PNEU-WREX device is an orthosis for the rehabilitation of arm and hand. This system uses 5 DOF, 4 of them on the shoulder and 1 for the elbow. This robot is capable of therapies for arm and hand, the therapy for the hand is only for a full opening and closing, like an on-off system. The device is immersed in a virtual environment designed specifically for rehabilitation therapies based on the ADL. The system also provides information about the patients progress and, with this information, it is possible to evaluate the therapy progress. The active DOFs are driven by pneumatic cylinders. Each active DOF uses a pressure low control loop in each chamber of the cylinder to control the force exerted by each cylinder. One valve for each chamber is necessary to implement the loop pressure in each cylinder. To solve the

issues of friction in pneumatic cylinders, low-friction cylinders have been used. The force control of each chamber is based in nonlinear control techniques because of the nonlinear nature of the system (Xiang & Wikander, 2004). This system intended to be a low cost system, keeping the passive gravity compensation of the previous version, and add only the devices necessary to expand the workspace and make attendance at therapy. As drawback, it has not all natural movement of human arm.

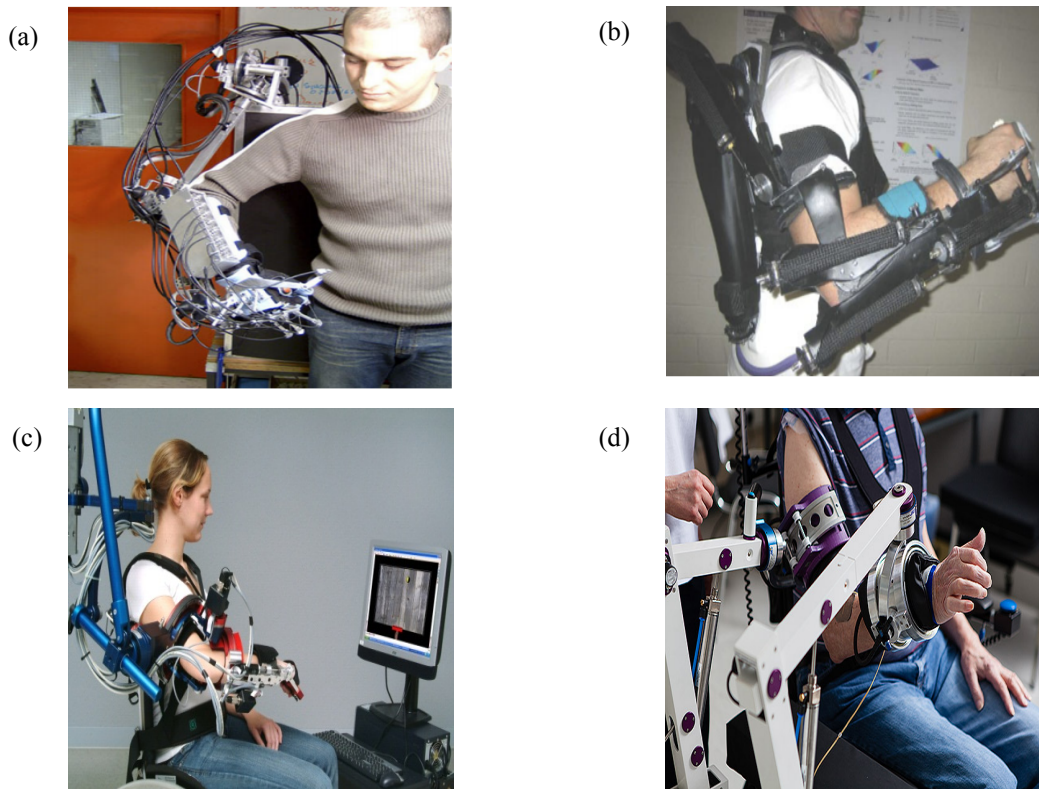


Figure 3.5. Existing soft robotics for upper limb rehabilitation

(a) SRE, (b) RUPERT, (c) PNEX-WERX, and (d) iPam

iPam, which was developed by the University of Leeds (Jackson, et al., 2007) .iPam is designed for sitting therapies where the patient is fixed in the chair with a handle. This system uses two symmetric arms with 3 DOF in each robotic arm. One of them grips the patient's wrist and the other one grips the patients arm. It also includes 3 passive DOF in each grip to the patient. Due to the similarity in both arms the robot can be used with left or right arm. The system provides the patient with feedback about the session, like the totals of targets and attempts. A comparison between the previous and the current session is displayed. This robot uses low-friction pneumatic cylinders to provide actuation at the active revolute joints which are controlled using 6 proportional control valves. Future work on this device include impedance control of each joint in order to control the dynamic behaviour of the

interaction with the patient. A key aspect to consider in the operation of this robot is that the position of the two robotic arms should be restricted to the kinematics of the human arm. If the requirements of the kinematics of human arm are not satisfied, the patient may suffer serious damage (Culmer, et al., 2005). For this reason, a cooperative control for both arms has been integrated. Furthermore, this robot is equipped with force sensors to measure the effort made by the therapist and to be replicate later during therapy. The iPam robot was installed in the local hospital of St Mary in Leeds PCT in the UK, within the rehabilitation unit in order to obtain clinical results in trials with patients with disabilities. The main advantages of this robot are: comfort, safety, and a simple system to attach to human arms. Moreover, the grip to the human arm is comfortable, safe, and easy to fix. Although, the whole workspace of the two robotic arms and the human arm is validated through the use of a motion capture software and infrared cameras. The main drawback of this iPam system is that the free space usually needed by the therapist to assist the patient during the rehabilitation task has not been taken into account in the design of this rehabilitation robotic system (Jackson, et al., 2007).

Table 3.1. Some of existing upper limb robotic devices

	Actuator	DOF	Type of Robot	Supported Movement
MIT-Manus	DC motor	2	End-effector based	Shoulder and elbow
MIME	Servomotor	6		
ARM-Guide	DC motor	1		
REHAROB	Electric	2-6		
GENTLE/s	DC motor	3		
MariBot	DC motor	5		
MEMOS	DC motor	2		
WREX	-	5	Exoskeleton based	Shoulder, elbow, and wrist
MGA	DC motor	5		
PNEU-WREX	PMA	5		
MULOS	Electric	5		
RUPRET	PMA	7		
ESTEC	-	9		
Li	Servomotor	5		
ARMin	DC motor	7	Hybrid	

Table 3.1 summarises some existing robotic devices that were designed particularly for the upper limb rehabilitation. Most of the mentioned robotic devices above cannot be used in rehabilitation process because of their low power, complex set-up as it takes too long time to

be configured, and poor interface between the patient and robotic devices. Also, most rehabilitation robotic devices are actuated by electrical actuators. So there is a need to build a new device that can be used for the upper limb rehabilitation with easier set-up and configuration. These are short-comes that motivated this research for design of new device that compensate above bottlenecks and at the same time to build an arm that can be used by the patient without the need of therapists.

3.2 Pneumatic Muscle Actuator Modelling

McKibben Muscles were introduced in the 1950s as stated by (Gaylord). It is important to derive the best mathematical model of pMA, and different approaches of modelling pMAs to ease the control process. The other important purpose of deriving the mathematical model of pMA is to understand and analyse the behaviour of pMAs and find the relationship between the pressure and length to the generated force along its longitudinal axis in the traditional pMAs, and the relationship between the pressure and bending angle in the bending PAMs to the generated force. In order to derive the mathematical model that describes the relationship between the length, pressure, angle, force its important define the length of the actuator, the diameter, the air pressure level, and the properties of the materials as these variables play a significant role in the dynamical behaviour of the pMAs. The relationship between the length of the pMA and the force is non-linear which pose an obstacle to control the pMA and achieve the required features (Caldwell, Medrano-Cerda, & Goodwin, 1995). Different approaches were employed to pMA models as follows:

Geometrical Model

It is difficult to measure the variables of the pMAs during operation, thus, different geometrical models were introduced. Tondo and Lopez model have been widely used due to its simplicity (Chou & Hannaford, 1996). The model was based on the assumptions of: (1) the material of the mesh is inextensible, (2) using the geometrical description as shown in Figure 3.6, and (3) the angle changes according to the change of pMA length.

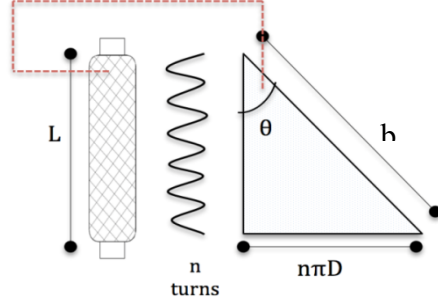


Figure 3.6. Geometry of McKibben Muscle (middle section)

Another widely used geometrical model that has been adopted is Chou and Hannaford model, as it is considered to be the simplest model of pMA for the static characteristics (Chou & Hannaford, 1996). The geometrical model was derived based on the assumptions of: (1) the pMA is a perfect cylinder, (2) the thread in the braided sleeve is inextensible and the inner tube and the braided sleeve are bonded, (3) there is no friction between the inner tube and the braided sleeve and between the thread of the braided sleeve, and finally, (4) the inner tube force is negligible. A model of a cylinder shape based on the geometry description in Figure 3.6, where L is the pMA length, D is the pMA diameter, n is the number of turn of the thread around the muscle, b is the thread length, and θ is the helix angle of the thread.

$$\cos \theta = \frac{L}{b} \quad (3.5)$$

$$\sin \theta = \frac{n\pi D}{b} \quad (3.6)$$

The volume of pMA is describes as:

$$V = \frac{b^3 \cos \theta \sin^2 \theta}{4n^2\pi} \quad (3.7)$$

Using the energy conservation theory, the force can be calculated as:

$$F = \frac{Pb^2 \left(3 \frac{L^2}{b^2} \right)}{4n^2\pi} \quad (3.8)$$

Chou and Hannaford model is not accurate as Tondo and Lopez as they rely on the experimental data. However, they both quantified an offset force experimentally to use it in the force calculation to enhance the model. The offset force is added to the force when it contracts and it's subtracted when it expands (Chou & Hannaford, 1996) and (Tondu & Lopez, 2000).

More realistic geometry model was introduced and utilised to model the real form of the pMA, by deriving the geometry model for both ends (conical frustum shape) and a cylindrical shape in the middle section.

Empirical Model

pMAs of various length and diameters can be also modelled by an empirical model. There is similarity between the pMA and the mechanical spring mechanism in producing force when it is attached to a load. Where the length of pMA with no load at zero pressure or at atmospheric pressure is the real length of the muscle L_0 . When the pressure changes from low pressure P_1 to high pressure P_2 the pMA either contracts or extends based on the type on the pMA to reach the new equilibrium length. As stated by (Wickramatunge & Leephakpreeda, 2010) the characteristics of pMA and mechanical spring are similar to some extent when operated with or without a force. In addition, they proposed a new parameter to be added to the model as a function of the operating gauge pressure inside the pMA. The new parameter increases when the air pressure inside the pMA is greater than the minimum pressure value.

Curved pMA Model

There are a lot of geometrical models for the traditional pMAs but there is a few that can be used for the curved pMAs. As proposed by (Zhang, Chen, Zhang, & Dong, 2008) two models were assumed based on physics for modelling the tube bending; the beam model, and the membrane model. The beam model assumes that the output power of the bending pMA is determined by the deformation with the same internal volume and it considers that the pressurised pMA is a long, slender member loaded in a single plane, and with a mechanical behaviour governed by the elasticity and pMA buckling. Whereas the membrane model assumes that the pMA does not stretch, although the cross-sectional shape deforms resulting in reducing the internal volume. These two models are used in the design and control of the proposed soft arm. The relationship between the curved angle and the force, internal radius, internal pressure is proportional. However, the curved angle increases when the curvature decreases (Zhang, Yang, Chen, Zhang, & Dong, 2008).

Phenomenological Biomechanical Model

The typical design of pMA consists of a combination of materials that is made from rubber, threads for the braided sleeve. When the pMA is pressurised it either extends or contracts based on its design characteristics creating an axial output force of the pMA based on the contraction or extension ratio. The phenomenological model that was proposed by (Serres,

Reynolds, Phillips, Rogers, & Repperger, 2010) describes the dynamics of the pMA using three elements; spring element, a damping element, and contractile element placed together in parallel.

Many approaches have been presented, however it is hard to control the pMA due to its non-linear behaviour, the next section is presenting some control strategies used in pMA. Modelling pMAs is a challenge because of its non-linear behaviour. In order to design the arm exoskeleton an accurate model that can predict the extension and contraction length is required. Models are generally categorised into:

- Dynamic models
- Quasi-static models

As stated by (Chou & Hannaford, 1996) the output work is equal to the input work is equal that is caused by the pressure pushing the inner surface of the bladder. However, this approach cannot predict the non-linear behaviour accurately because the geometrical model has a lot of parameters that cannot accurately be measured. Thus, the empirical quasi-static model is often used by introducing a correction factor taking into consideration the real shape of the muscle, the leakage, and the inner tube pressure. Table 3.2 summarises of pMAs models that are applicable and accurate to represent the relationship among force, length, and pressure. In the mechanical design chapter (4), the Tondo and Lopez model is utilised.

Table 3.2 Quasi-static model for PMA

RESEARCH	MODEL
(COLBRUNN, NELSON, & QUINN, 2001)	$F(P_g, L) = \frac{P_g(t)b^2}{4\pi n^2} \left[\frac{3L(t)^2}{b^2} - 1 \right] \cdot \text{Eff}(P_g(t) + F_{\text{maxlimit}} \text{ if } L(t) > L_{\text{min}}$ <p>F(P_g, L) is a function of Pressure P_g(t) and length of the PMA L(t). L_{min} is the minimum contraction length of the PMA, F_{maxlimit} is the maximum force the PMA generates given the pressure. Constants b and n indicate geometric constants related to the actuator. Eff(P_g(t)) is an empirical function to amend the theoretical model to practical performance.</p>
(TONDU & LOPEZ, 2000)	$F(\varepsilon, P) = (\pi r_0^2)P(t)[a(1 - \varepsilon(t))^2 - b]$ <p>F(ε, P) is a function of pressure P(t) and contraction ratio ε(t), r₀ is the radius of the PMA when it's at resting status. coefficients a and b are constants that are empirically determined to make the model applicable on particular PMAs.</p>
(PUJANA-ARRESE, MARTINEZ-ESNAOLA, & LAND, 2007)	$F = (P, q) = D_1 + D_2 \cdot q(t) + D_3 \cdot q(t)^2 P(t) + \varphi(t)$ <p>F(P, q) is a function of pressure P(t) and contraction ratio q(t); D₁, D₂ and D₃ are empirical coefficients. φ(q(t)) is an amendment function to cancel off the passive forces in the PMA.</p>
(WICKRAMATUNGE & LEEPHAKPREEDA, 2010).	$F_{\text{elastic}} = K(P, L_s)L_s; K = a_0P^2(t) + a_1P(t)L_s(t) + a_2L_s(t)^2 + a_3$ <p>F_{elastic} is a function of pressure P(t) and Stretched length L_s(t), a₀, a₁, a₂, a₃ are experimentally obtained coefficients.</p>

3.3 Control Systems for Pneumatic Muscle Actuators

Using the proper control technique to control robotic devices and how to interact with patients can be valuable. Control strategies are categorised into low level control such as PID and high level control, where a series of low level control approaches are used. A review of the main studies conducted on the control approaches of pMA is given in this section. As stated by (Qiang & Fang, 2006) some other difficulties in the control of pneumatic systems are the possible presence of unknown disturbances coming from leakage of valves, time-varying payloads, and external perturbations. Besides, uncertainties in system parameters make the controller design problem more challenging.

To solve the control challenges adaptive control systems are utilised to satisfy a certain degree of adaptivity and robustness. The Stefanovic & Safonov (2008) defined the adaptive control system models a class of controller that can adjust its own behaviours (input according to required output), in response to the dynamics of the process and the disturbances.

Open Loop Control of Pneumatic Systems

The open loop control is used when feedback signal is not available in order to produce a satisfactory result and at the same time the precision is not important. For example (Serres J. L., 2008) used the open loop control approach in order to demonstrate a resistance exercise task, where the pneumatic muscles were used for resistance

Proportional Valve Controlled Pneumatic Systems

Traditional control approaches such as Proportional, Integral, Derivative (PID) control or any combination of P, I, or D control are widely used due to its architecture simplicity, cost, ease of tuning, and high performance. However, the PID gains are difficult to determine in the case of non-linear systems. PID can still be used as a reference for other control approaches as proposed in this thesis. Many linear control approaches have been utilised proportional pneumatic systems, it was stated that velocity and acceleration/pressure feedback can improve the static and dynamic performance of the pneumatic systems; (Liu & Bobrow, 1998) used PD and PD+ pressure feedback. PD with gain tuning was utilised by (Fok & Ong, 1999), and PID with acceleration feedback by (Wang, Wang, Moore, & Pu, 2001).

Many studies have been conducted for non-linear systems, as stated by (Rao & Bone, 2008), and (Kaitwanidvilai & Parnichkun, 2005) the most important advantage of using servo

control is that they do not require a mathematical model. Fuzzy and neural network are used quite often to adapt and tune the gain of the conventional linear controller such as PID in order to identify the Controller parameter.

On/Off Valve Controlled Pneumatic Systems

Using On/Off solenoid valve-controlled system with Pulse System Modulation (PWM) technique to reduce the cost of the system. PWM can reduce the effect of the nonlinearities and improve the system performance and reliability. (Tsagarakis & Caldwell, 2003) developed a seven DOF upper arm rehabilitation system using PID control with on/off solenoid valve to improve the torque response, pair of agonist and antagonist pMA connected by a cable and pulley at each joint. Torque joint was implemented at each joint to calculate the amount of pressure required performing the movement, PID coefficients were obtained experimentally.

Adaptive Control

It is a control approach; the parameters of the controller are not static and change over time. The adaptive control approach has many advantages in rehabilitation robotics to suit any patient.

Many attempts have been made to improve the control techniques for the pMA (Caldwell, Medrano-Cerda, & Goodwi, 1995) proposed adaptive pole placement scheme to address the nonlinearity of pMA. (Repperger, Phillips, & Krier, 1999) used gain scheduling approach, and (Chan, Lilly, Repperger, & Berlin, 2003) used fuzzy PD+I controller and many others. Although different types of controlling approaches have been developed, most implemented control algorithm is still PID. Thus, the need to improve a traditional PID controller is needed to handle the non-linearity in pMA, a basic PID controller is advised as an input for the proposed control system for pMA.

Appropriate adaptive control techniques are used to replace traditional algorithms, NN can be used in different tasks such as recognise the motion of the patient performs during exercise, determine the optimal parameters during rehabilitation, and to build a model of controlled system.

(Ahn & TuDiep, 2004) proposed an intelligent switching control scheme by utilising a learning vector quantisation neural network and a nonlinear PID control to improve the control performance of pMA manipulator using NN. In 2008, (Aschemann & Schindele, 2008), developed the cascade sliding mode control scheme for a high speed linear axis

pneumatic muscle. Moreover, (Seung , 2009) proposed a trajectory tracking control using a neural network based on PID control. (Xing, et al., 2010) introduced the tracking control of pneumatic artificial muscle actuators based on the sliding-mode and non-linear disturbance observer in order to improve the robustness and performance of the trajectory tracking control. However, applying a complicated control algorithm does not always indicate the best solution used to control pneumatic muscles.

Overall System Response and Conclusion

From above investigation, it has been found that pMA has essentially distributed parameter, stochastic, non-linear and time varying nature, convoluted further with dead zone, time delay and saturation due to non-linear characteristics of electronic actuators and pipes. This requires extra efforts for designing a complex control system that can deal with pMA sophisticated nature and makes overall system response smooth. However motivations and several advantages that final suggested soft robotics arm offers justify required efforts. In next three chapters pMA behaviour, its distributed parameter nature of pMA and control development for final suggested soft robotics arm are investigated.

4 MECHANICAL DESIGN OF THE SOFT ARM

To ease the description of the new proposed soft arm, it is important to summarise some technical backgrounds. As mentioned in the previous chapter there are many devices utilised in upper limb rehabilitation. With rehabilitation robotic devices, many components affect outcomes. Often, the therapy is simultaneously made more intensive, supportive, and motivating for the patients than is possible with conventional therapy. As more repetitions per session, movements assistance via external actuators, and an involving and stimulating virtual environment all influence the process of rehabilitation.

4.1 Mechanical Design for Elbow Exoskeleton Robotic Device

Most rehabilitation devices for the upper limb use an external robot as a manipulator. However, these devices have many cons: expensive, non-compliant, large, and difficult to control. The structure of the proposed design has 1DOF at the elbow permitting flexion/extension. The soft arm is constructed primarily from different soft materials. This resulted in a lightweight, low material cost, high power to weight ratio, high stiffness, natural compliance, ease of fabrications, and comfortable structure providing a stable platform. The proposed design was developed to achieve these advantages by using McKibben pMA. These muscles are distinguished in being light-weight, cheap, compliant, easy to fabricate, fully soft, safe, and easy to wear.

4.1.1 Design Consideration

During the intensive therapies of the upper limb delivered to stroke patients by trained therapists; muscles are stretched, and the elbow joint is extended and flexed through its range of motion (ROM) in order to recover the smooth and elastic function of muscles. Hard robotics is designed to produce these movements. As they are based on rigid links connected by joints, they are heavy with expensive and complicated control. Moreover, they tend to be supported by a solid base on the ground. This kind of limitation restricts the possibility of assistive device. Furthermore, hard assistive devices require appropriate gravity compensation in proportion to the weight of the upper limb to offset gravity effects. All of these considerations lead to a set of design specifications required to be fulfilled by a soft wearable robotic assistive device in order to successfully assist in elbow motion.

- *Kinematics that allow patients to perform elbow movements:* kinematics of the rehabilitation robotic device must reflect the intended joint kinematics. The proposed arm is designed to train the elbow joint to flex and extend that requires kinematics with 1 DOF.
- *Structural transparency for active motion:* The structural transparency is such that the mass of the actuator is so small that a patient performing spontaneous motion does not feel resistance in interactions with the robotic arm.
- *Wearable assistive robotic device:* It should not require the base coordinate system of robotic device to be grounded so that it does not constrain the motion of the main body.
- *Safety:* As the system is in direct contact with the human operator the safety requirement is dominant for a rehabilitation device. The device must be designed not only to be safe but also to seem safe from the patient's viewpoint. Necessity of safe robotic device is important to prevent any body harm especially that it will be used by patients who are more prone to injuries.
- *Comfort of wearing:* As the extended use of such a device is certainly possible and probably necessary, the device must be comfortable, causing no fatigue to the patient even after long periods e.g. 1–2 hours of operation. This should include ease of fitting, adjustment and removal, and suitable for various patients regardless of gender, arm size and shape.
- *Extensive range of motion:* A generic specification for the display range of motion (ROM) can be defined as the workspace of the human arm motion.
- *Complexity:* As with most designs options that keep complexity to a minimum will tend to improve reliability and reduce cost and these should always be under consideration during the design process.
- *Reliability:* As with all systems, user acceptance is dependent to a large extent on the reliability and utility of the mechanism. It is therefore vital that appropriate design concerns are given to reliability in all operations and in environments where materials like water, dust or grease are presented.
- *Orthosis Mass:* Pneumatic muscle is bigger in size in comparison to the electrical drives with equivalent power (Liska, More, Janacova, & Charvatova, 2013). However, it has a lightweight that eases its use and portability.
- *Accuracy:* accurate automatic compensation for gravity forces.

- *Bending motion*: a bending motion is preferred at joint locations where low impedance is expected.

4.1.2 Design Advantages

Pneumatic muscle actuators (pMAs) have many features that make them special and up-to-date, starting with its light weight that makes it easily mobile and portable; also, another prominent feature is its feasible connectivity and replacement to different structures to be powered. In addition, it is safe and human friendly due to its adjustability and flexibility, and pMAs do not add any significant stress in assembly. pMAs lacks dynamic seals, making friction or air loss not an issue, and having a solitary chamber *i.e.* the air inlet, ease to control muscle. Moreover, pMAs provide lower of air consumption as it is pressurised and provide force changes with regard to length and diameter (Hannaford & Winters, 1990).

4.2 Design Description of the Soft Arm

4.2.1 Mechanical Structure

The mechanical arm structure has 1 DOF corresponding to the natural human limb for the elbow joint permitting flexion and extension. The arm structure is constructed from soft materials. This resulted in a light weight, low cost, comfortable structure. The wearable arm is constructed to suit many users due to its adjustability. The arm consists of (1) two extensor pMA (2) one contractor pMA, and (3) wearable elbow brace; as shown in Figure 4.1.



Figure 4.1. The Arm mechanical structure

4.2.2 Pneumatic Muscle Structure

Pneumatic Muscle Actuator (pMA) was used in the soft arm design that is also known as McKibben muscle. McKibben muscle is chosen over the other actuators that have been already mentioned in the literature review due to its capability to produce force required to actuate the muscle. PAM consists of stretchable inner tube (bladder); butyl rubber was used in the design, inserted into a braided mesh (sleeve) made of Polyethylene terephthalate (PET) that belongs to polyester family. In addition, other material such as nylon can be used for the braided sleeve. Plastic cable ties were devised to attach and seal the bladder and braided mesh onto stainless steel fittings (end caps). One of the end caps is fabricated so that air fitting can be attached to allow pressurised air inlet. The Figure 4.2 shows the PAM build up.



Figure 4.2. PAM Build-up

(a) PAM Components: 1. Braided mesh, 2. Inner tube, 3. Cable ties, 4. End caps, 5. Air inlet.

4.2.3 Actuation System

The physical model of McKibben muscle is highly nonlinear. The operation of the muscle is controlled via pressurised air supplied into the muscle. The muscle consists of two layered cylinder, the inner tube (bladder), surrounded by a braided sleeve; as shown in Figure 3.3. The sleeve consists of braided threads, the braided threads run helically about the muscle's long axis at an angle θ . Where θ is the angle between a single braided thread and the actuator's central axis as shown in Figure 4.3. The helix angle θ determines whether the muscle is contractor or extensor. For instance, if $\theta > 54.7^\circ$ the muscle acts as an extensor (Godage, Branson, Guglielmino, & Caldwell, 2012), whereas, $\theta < 54.7^\circ$ the muscle acts as a contractor (Liu & Rahn, 2004). The length (L), diameter (D) and braided angle (θ) change with the amount of the pressure supplied into the pneumatic artificial muscle until it reaches

54.7°. Experimentally, the construction of the pMA determines the type of actuator; by selecting the length of the inner tube and the braided sleeve in order to obtain the required angle to act either as a contractor or extensor accordingly.

In case the pMA acts as a contractor the length of the inner tube and the braided sleeve are equal. However, in the extensor case the length of the sleeve should be greater than the inner tube length. The extension is up to 50% based on the length and the diameter of the inner tube and the sleeve at 600kpa. (McMahan, et al., 2006). The ultimate pressure a typical muscle can withstand prior to failure is 7 bars (Tsagarakis & Caldwell, 2003), however, 5 bars is deemed to be a safe operating pressure that is adopted in the proposed design. Pneumatic muscle actuators can also act as a bending contractor or a bending extensor (Al-Fahaam, Davis , & Nefti-Meziani, 2018) based on the construction of the pMA. In order to develop the bending pMA the behaviour of traditional contractor and extensor is examined in the next sections. In addition, the whole prototype is examined experimentally and geometrically and will be described in detail in the following sections.

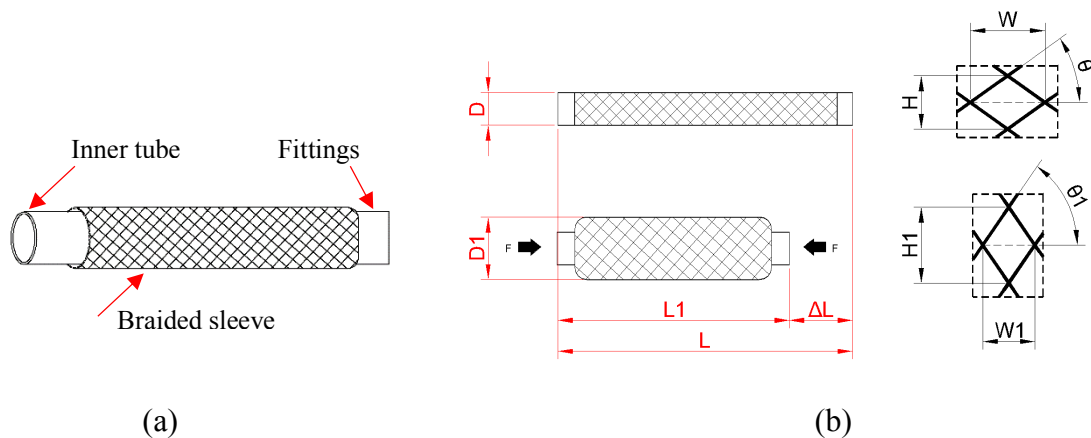


Figure 4.3. McKibben pMA:

(a) components of pMA, (b) the one in top is at rest, the one beneath is contracted; the right side is the scheme of a single braided structure demonstrating the helix angle θ

4.3 The Contraction Pneumatic Muscle Actuator (pMA)

The structure of the muscles gives the actuator a number of desirable characteristics (Caldwell et al., 1994):

- The magnitude of the contractile force generated from this muscle is proportional to the length and diameter of the muscle.
- Actuators are highly efficient due to force to weight ratio > 1 kW/kg.

- The contraction is dependent on the construction and loading but is typical 30%–35% of the dilated length this is comparable with the contraction achievable with natural muscle.
- High flexibility and soft contact distinguish pneumatic muscles as an excellent safe option comparable with natural muscles.
- The muscle can be controlled with high accuracy.
- Bandwidths for antagonistic pairs of muscles of up to 5 Hz can be achieved.
- Force control using antagonistic pairs for compliance regulation is possible again comparable with natural muscle action.
- For a given cross sectional area of actuator, contractile force can be over 300 N/cm² for the pMA compared to 20–40 N/cm² for natural muscle.
- The actuators can operate safely in aquatic, dusty environments.
- The actuators are highly tolerant of mechanical (rotational and translational) misalignment reducing the engineering complexity and cost.

4.3.1 Operation of the Contraction pMA

Operation of the contraction pMA could be demonstrated in two conditions; (*i.e.*): (a) isotonic; applying variable pressures and being loaded in one and unloaded in the other. (b) isobaric: where the pressure is constant, and the load is variable. Contraction pMA is potentiated when θ is less than 54.7°. By applying pressurised air onto the bladder through the inlet, inflating and increasing its diameter resulting in reinforcement of the bladder and the braided sleeve generating a contraction.

The following section contains detailed designed and analysed properties of the proposed contraction pMA. One of the most important components of the proposed model is the inner tube (bladder) and to comprehend its contribution to the design it is essential to clarify its properties.

- *firstly*, being made of butyl rubber that provides a seal preventing any air leakage.
- *Secondly*, the elastic property of the bladder creates a conservative resistant force at inflation.

The inner tube is 30 cm in length, 20 mm in diameter, and 1.1 mm in thickness. Another component is the braided sleeve; it is 30cm in length, 20mm in diameter, and 0.5mm in thickness. The braided sleeve consists of series of strands, each contains 3 threads. The

braided sleeve is made of Polyethylene terephthalate (PET); a material that offers an outstanding resistance, low coefficient of friction, minimal water absorption, high in Young Modulus, and high elastic modulus to resist permanent deformation (Doumit, Fahim, & Munro, 2009). The double layered structure terminates with fittings (caps) at each end; one is closed and the other has an air inlet to allow the pressurised air to inflow. Table 4.1 shows the specifications of the contraction pMA.

Table 4.1. Specifications of contraction pMA

Initial Length (m)	Rubber Thickness (m)	Braided sleeve Thickness (m)	Inner tube Diameter (m)	Braided sleeve Diameter (m)
0.3	1.1×10^{-3}	0.5×10^{-3}	20×10^{-3}	20×10^{-3}

Muscle action corresponds to two processes including inflation and deflation with compressed air. At time of inflation diameter drastically increases exceeding the end-fixture diameter forming an irregular shape at the ends of the muscle, in contrast to what occurs at time of deflation, where the muscle's shape is comparatively cylindrical.

4.3.2 Geometrical Model of Contraction pMA

Most of the previous work has been focused on modelling the force and the pMAs behaviour, however, there is no highly accurate model that can be utilised in different pMAs. The pMAs elasticity also plays a major role in affecting the model accuracy. Most of the conducted models were based on geometric aspects, to describe the relationship between the pressure and force, and pressure and length in both traditional contractor and extensor. Also, the relationship between force versus pressure and pressure versus bending angle in the bending contractor and extensor. The original approach for modelling the pMA was based on the geometry of the muscle, because it is difficult to realise the position control precisely, as the pMAs are non-linear in behaviour, compliance, and have large hysteresis. In the proposed model, geometry is used to device a model that mimics the real muscle. Two geometrical elements including:

- a cylinder; forming the cross-section at the middle of pMA, the pMA has length (L) with a diameter (D) and a helix angle θ . N is the number of turns around the length b ; where b is the length of the thread. In order to find θ experimentally the following equation was used.

Based on the geometry of McKibben muscle in Figure 3.6, Solving Equation (3.5) by substitution in chapter 3: Literature Review; θ equals to 22.87° , which is less than 54.7° . thus, the pMA acts as a contractor.

- (b) two conical frustoms forming the ends of pMA. However, the proposed design is considering that the pMA is a perfect cylinder, ignoring the effect of the conical frustoms (Chou & Hannaford, 1996) and (Tondu & Lopez, 2000).

Chou and Hanafford model is the simplest geometrical model for pMA, however, it is only valid under the following assumptions:

- The middle section of the pMA is perfectly cylindrical in shape.
- There is no friction force between the sleeve and the bladder and between the threads of the sleeve and there are not elastic forces within the bladder
- The thread in the braided sleeve is inextensible and is in contact with outside diameter of the inner tube (bladder).
- The bladder forces are negligible.

When the pMA inflates and deflates, L , D , and θ change, where the variables D and θ differ inversely with the increase in L , while n and b remain constant. The pMA length and diameter can be describes as follows:

$$L = b \cos \theta \quad (4.1)$$

$$D = b \frac{\sin \theta}{n\pi} \quad (4.2)$$

by combining equation (1) and (2), the thread length can be calculated as:

$$b = \sqrt{L^2 + D^2 n^2 \pi^2} \quad (4.3)$$

the volume of the cylindrical muscle is provided by:

$$V = \frac{D^2 \pi L}{4} = \frac{b^3 \cos \theta \sin^2 \theta}{4n^2 \pi} \quad (4.4)$$

It should be noted that the pMA is not a perfect cylinder in shape, resulting in an error for the anticipated volume calculation. Utilising the energy conservation theory, the force F can be calculated as pressure at each point multiplied by the change in volume with respect to length assuming that the pMAs is a perfect cylinder in shape, there is no stored energy, and it is lossless operation. The input work W_{in} is done in the pMAs when the pressurised air inflow

distributes across the tube inner surface area resulting in radial forces. This will equally result in a mechanical motion initiated by volume change and consequently contraction/ expansion with coreresponding force along the major axis of the pMA.; where P is the relative pressure, dv is the change in voulme, and dl is the change in the axial displacement.

$$W_{out} = W_{in} \quad (4.5)$$

$$-F dl = Pdv \quad (4.6)$$

$$F = P \frac{dv}{dl} = \frac{Pb^2(3 \cos^2 \theta - 1)}{4n^2\pi} = \frac{P\pi D^2(3 \cos^2 \theta - 1)}{4} \quad (4.7)$$

Due to the challenges imposed by measuring θ in practice, Tondo and Lopez proposed a simplified model assuming θ is 90° , the force generated form the muscle can be calculated in accordance with the theorem of virtual work as mentioned in chapter 2: Literature Review (Tondu & Lopez, 2000):

$$D_{max} = \frac{b}{n\pi} \quad (4.8)$$

$$F = \frac{\pi D_{max}^2}{4} P[a(1 - \varepsilon^-)^2 - b] \quad (4.9)$$

$$a = \frac{1}{\tan^2 \theta_0}, \quad b = \frac{1}{\sin^2 \theta_0}, \quad \varepsilon^- = \frac{\Delta L}{L_0} \quad (4.10)$$

Where θ_0 : is the initial measured helix angle at rest mode, ε is the contraction ratio. However, the force calculated by this model is generally larger than the actual force generated by the pMA, thus, it was addressed that the more the muscle contracts, the less cylinder geometry it forms.

In order to find the length of contraction or extension pMA when it is either contract or expand at different pressure level requires a geometrical formula to calculate it (Al-Ibadi, Nefti-Meziani, & Davis, Effecient Structure-Based Models for the Mckibben Contraction Pneumatic Muscle Actuator: The Full Description of the Behaviour of the Contraction PMA, 2017). the length decreases and increases in the contraction pMA, and extension pMA respectively, while the applied pressue level is incresed. The length is derived from the material stiffness matrix as:

$$L = x + \frac{y}{[1 + (\frac{p}{z})^m]^n} - 0.002L_{eo}\sqrt{p} \quad (4.11)$$

$$\text{where: } \begin{bmatrix} x \\ y \\ z \\ m \\ n \end{bmatrix} = \begin{bmatrix} 0.145 & 1 & 0.379 & 0.012 \\ 0.323 & 1 & 0.103 & -0.012 \\ 0.432 & 1 & -0.947 & -0.015 \\ -0.297 & 1 & 0.327 & -0.0032 \\ -0.297 & 1 & 0 & 0 \end{bmatrix} \begin{bmatrix} L_{eo} \\ L_{eo}^{0.9} \\ L_{eo}^2 \\ L_{eo}^3 \end{bmatrix}$$

where L_{eo} is the initial length and the parameters; x, y, z, m , and n are constants, and the definition of the coefficient in Equation 3.11. The initial length L_{eo} , initial diameter D_o and the stiffness of the butyl rubber S_r should be taken into consideration to find the length of the actuator, thus the following equation is used to avoid dividing by *zero*.

$$L = L_{eo} - \frac{x L_{eo}}{[1 + (n)^{-y D_o p / S_r}]^{2.543}} \quad (4.12)$$

$$\begin{bmatrix} x \\ y \end{bmatrix} = \begin{bmatrix} 0.5 & 2795 & -0.0000932 \\ 0.00043 & 0.5 & 19876 \end{bmatrix} \begin{bmatrix} 0.5 \\ \left(\frac{D_o}{S_r}\right) \\ \left(\frac{D_o^2}{S_r^2}\right) \end{bmatrix} \quad (4.13)$$

Where x , and y are constants depends on the initial diameter and the stiffness of the contraction pMA. To validate the equations of the length and force for the contraction pMA, a 30 cm contraction pMA has been built to the specifications explained in detail in the next section.

4.3.3 Experimental Inspection of Contraction pMA

The contraction pMA is operated by inflow of pressurised air via air regulator as shown in Figure 3.4, which results in radial forces acting on the inner wall of the muscle. This action will cause the diameter to increase and length to decrease and increase resulting in conversion of pneumatic force to contractile force longitudinally acting along the major axis of the muscle.

The purpose of the experiment is to determine contraction and corresponding force generated from the mechanical motion of the muscle, and also to investigate the relationship of both pressure vs. length and pressure vs. force. The experiment is set up as shown in Figure 4.4 - fixed at top and free at it end where load is attached- in two modes; the first mode utilised pressurised air gradually pumped into the muscle at different pressures varying from 0 to 5 bar with constant load attached to the end of the muscle; this mode is known as isotonic. The second mode used different loads varying from 0 to 5 Kg with constant pressure (2bar); this mode is known as isobaric (Takosoglu, Laski, Blasiak, Bracha, & Pietrala, 2016). The length

of the muscle was measured and recorded at each pressure step (0.5 bar), in order to find the difference between the initial length and the length at particular pressure ΔL . Table 4.2 shows the parameters of the contraction pMA that was used to set-up the experiment.

Figure 4.4. Experimental set-up pneumatic diagram

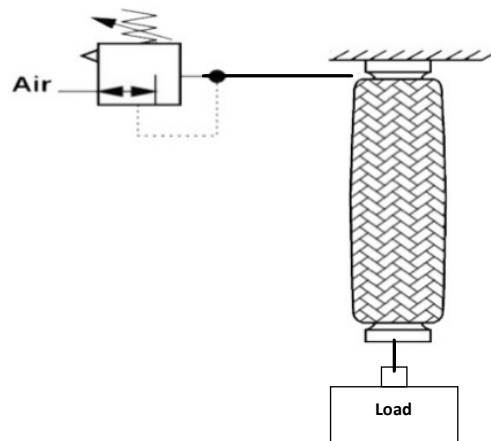


Table 4.2. Contraction pMA parameters

Initial Length L_0 (m)	Final length L_5 (m)	Muscle Diameter D_0 (m)	Muscle Diameter D_5 (m)	Load (1) (Kg)	Load (2) (Kg)
0.3	0.213	20×10^{-3}	20×10^{-3}	0	1.5

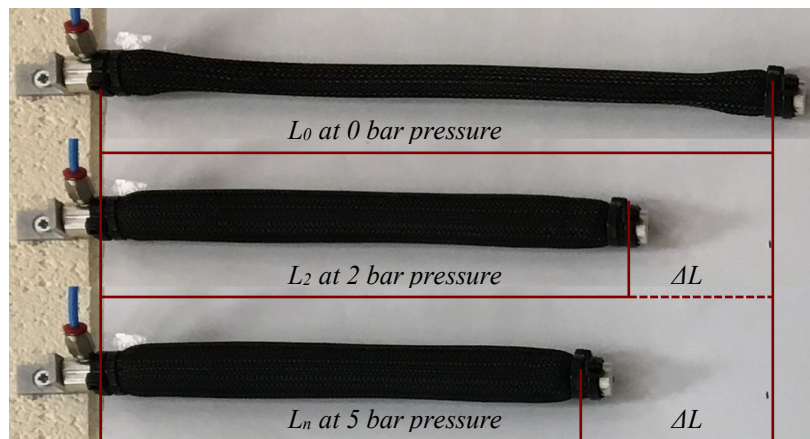


Figure 4.5. Contraction pMA at different pressures

Figure 4.5 shows the behaviour of unloaded contraction pMA at different pressures. Where L_0 is the length of the muscle at 0 bar, L_n is the length at different pressures, and ΔL is the decrease in length. Solving the Equation (4.10) by substitution; the contraction ϵ^- is equal to 29%. The contraction ratio changes according to the pressure value and the load attached to

the muscle, as shown in Table 4.3, the calculated contraction (ϵ) varies when the muscle is attached to different loads and applying constant pressure value (P).

Table 4.3. Contraction Ratio of Contraction pMA at 2(bar), and L_0 , 30(cm)

Load (kg)	length (cm) (L)	Displacement (cm) (ΔL)	Contraction (%) (ϵ)
0	22.8	7.2	0.24
0.5	22.9	7.1	0.24
1	23	7	0.23
1.5	23.1	6.9	0.23
2	23.3	6.7	0.22
2.5	23.5	6.5	0.22
3	23.7	6.3	0.21
3.5	23.9	6.1	0.20
4	24.1	5.9	0.20
4.5	24.3	5.7	0.19
5	24.5	5.5	0.18

The contraction ratio has an inverse relationship with the length of the muscle and the load. e.g. the maximum contraction at 2 bar was when the load was 0 kg. However, the relationship between the displacement (ΔL) and the contraction (ϵ) is proportional. Figure 4.6 shows the relationship between the length of the muscle and the pressure as it shows an inverse relationship; the length of the muscle decreases as more pressure is experienced. It can be noted that 87% of the maximum contraction occurs at 2.5 bar, the contraction range depends on the higher threshold angle limit. Thus, the contraction pMA above 2.5 bar decreases slightly due to its high stiffness.

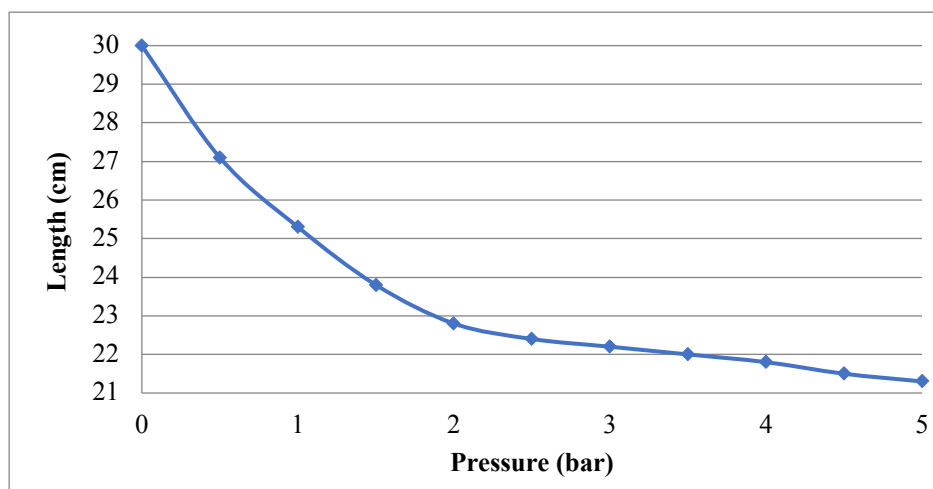


Figure 4.6. Relationship between length (L), and the pressure (P)

Figure 4.7 shows that the muscle behaviour when it is attached to 1.5 kg load, a slight change in length can be noticed. Where the blue curve shows the contractor length at different pressures when the contraction pMA is unloaded. While the orange curve shows the same relationship but when it is loaded. The experiment was conducted at 1.5 kg to match the weight of the forearm (approx. 1.5kg for both genders), it can be noted that the change in length with the attached 1.5 kg is almost comparable to that when the pMA is unloaded.

The contraction force produced by the muscle at a given pressure step can be measured experimentally by determining the mass in kg required to restore the contracted muscle to its initial length at 0 bar pressure. This is carried out by:

- Measure the length of the pMA at 0 bar pressure (initial length).
- Apply pressurised air gradually (0-5 bar); 0.5 bar per step.
- Attach load to the free end until the initial length of the muscle is restored.

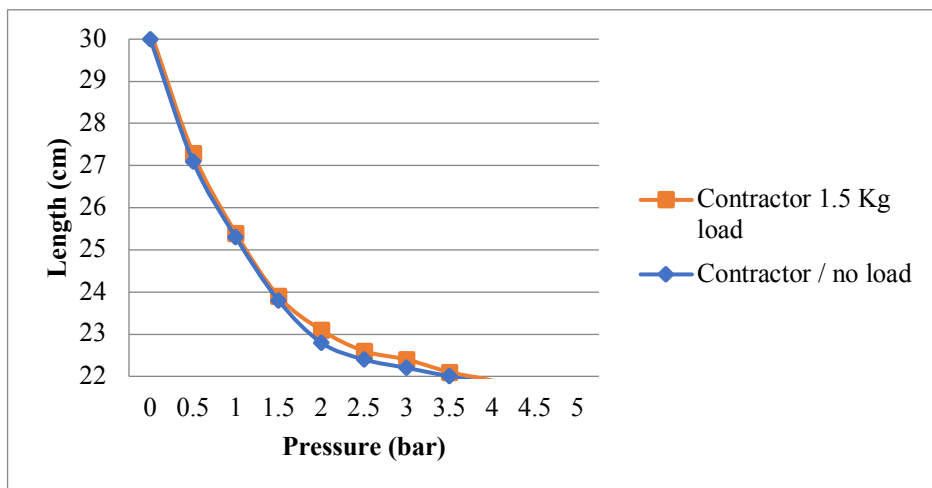


Figure 4.7. Comparison between loaded and unloaded muscle: relationship between length (L), and pressure (P)

the following Figure 4.8 illustrates the relationship between the force and pressure; the maximum force was measured experimentally by using a stationary spring scale, in an isometric configuration at a range of different pressures as mentioned above to be 450 N, where $F = M \cdot g$, the relationship between the contraction force and the pressure is linear, because the generated force depends on a constant area.

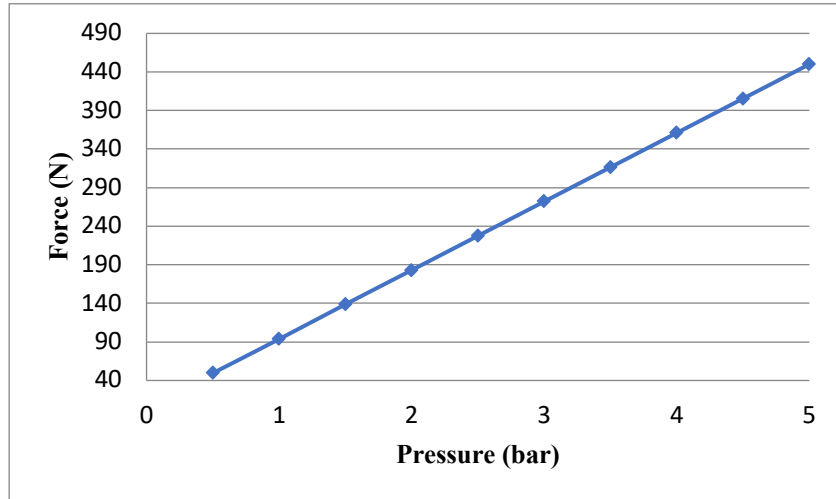


Figure 4.8. The Experimental force of the contraction pMA vs. pressure at different pressures varies between 0-5 bar.

4.3.4 Experimental Model vs. Mathematical Model

Figure 4.9 represents a plot of the length of the pMA versus the applied pressure using the experimental model and the geometrical model described in Equation y . Qualitatively, both models behave similarly in terms of their shapes. However, the results obtained from Equation y under predict the experimental model with a Mean Fold Error (MFE) = 1.01.

The relationship between both models, i.e., geometrical and experimental, a regression model was developed using the data in Table 3.4 and the resulting equation is:

$$y = 1.0247x - 0.6882$$

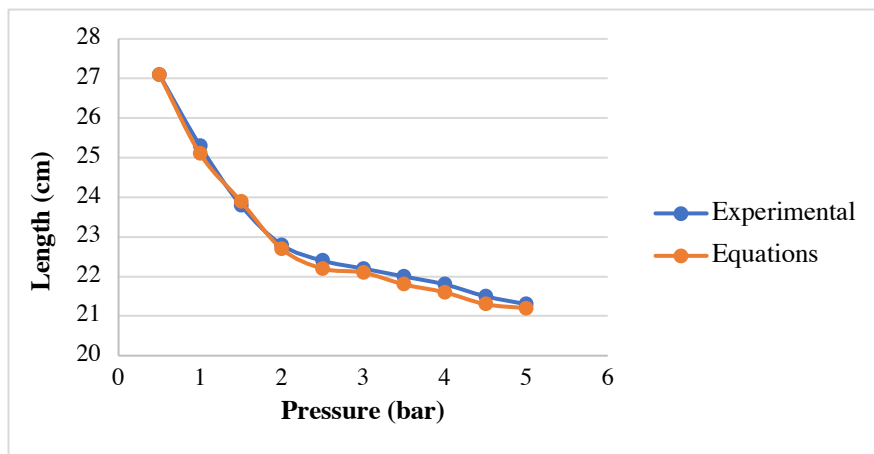


Figure 4.9. A Comparison between the geometrical model and the experimental model, that shows the relationship between the length of the contractor pMA and the pressure level, where the Blue curve demonstrates the experimental result while the orange curve demonstrates the equation results.

where x and y represent the lengths (m) obtained from the geometrical model results and observed data, respectively. The model has a relatively large R^2 of 0.9977 and the value of the gradient is approximately 1. The underprediction is a small percentage, between 2.7%-7.4% for the given range of pressure.

Table 4.4. A comparison between the observed results and the predicted results for the contraction pMA length in (m) at different pressure levels, to calculate the MFE

Length (m) Pressure (bar)	Length (m) Observed (O)	Length (m) Predicted (P)	Logarithmic Mean Fold Error
0.5	0.27	0.271	0.000
1	0.253	0.251	0.003
1.5	0.238	0.239	0.002
2	0.228	0.227	0.002
2.5	0.224	0.222	0.004
3	0.222	0.221	0.002
3.5	0.22	0.218	0.004
4	0.218	0.216	0.004
4.5	0.215	0.213	0.004
5	0.213	0.212	0.002
MFE			1.01

Figure 4.10 plots an experimental and geometrical force of the contraction pMA against different applied pressures. The relationship between the generated force and the pressure is linear; the generated force increases when more pressurised air is applied. However, the results obtained from Equation y overpredicts the experimental model with a $MFE = 1.07$.

$$y = 1.0239x - 0.1917$$

where x and y represent the lengths (m) obtained from the geometrical model results and observed data, respectively. The model has a relatively large R^2 of 0.99877. It can be noted that there is a slight difference in the force generated by the pMA and the theoretical force, the experimental force found to be less than the theoretical force approximately by 7%. This difference is expected and indicates the dissipated energy and simplification assuming the muscle is a perfect cylinder.

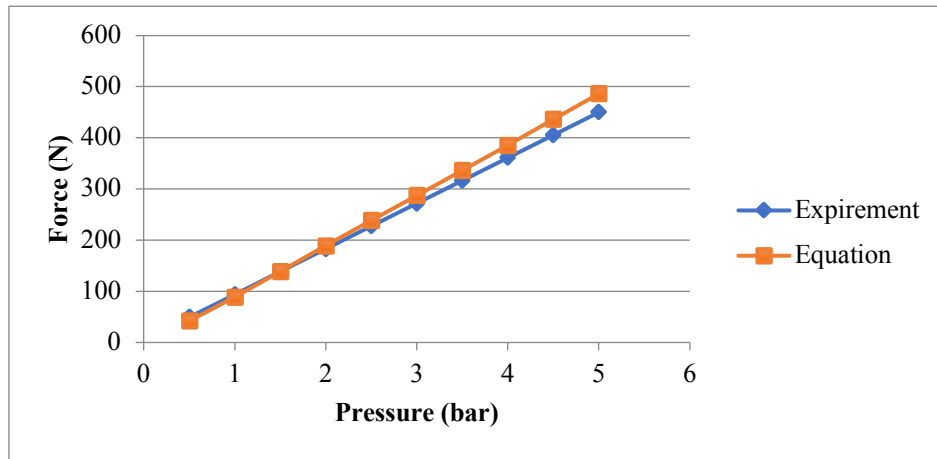


Figure 4.10. An Experimental and Geometrical Force of the contraction pMA against different pressures

4.4 The Extension Pneumatic Muscle Actuator (pMA)

4.4.1 Operation of the Extension pMA

The extension pMA has a reverse operation compared to the contraction pMA; the muscle is extended under inflow of pressurised air. The extension pMA is constructed of an inner tube (bladder), braided sleeve, fittings, and air inlet as described in detail in section 4.2.2. The braided sleeve restricts the lateral expansion of the pMA and allow for longitudinal expansion. In case of extensor θ should be more than 54.7° as mentioned previously, the value of θ is critical to the extension action. The braided sleeve used in the extension pMA is the same as the one used in the contraction pMA. Therefore, for experiment purpose the nominal length of braided sleeve should be greater than the inner tube length in adequate amount. This additional length is to ensure that θ in the initial mode is greater than the threshold angle, and to accommodate the anticipated increase in length when the muscle is operated. The force produced by the contraction pMA is pulling force, while the force produced by extension pMA is pushing force. In the proposed design the length of the braided sleeve is 2.5 times of the inner tube length as illustrated in Figure 4.11.

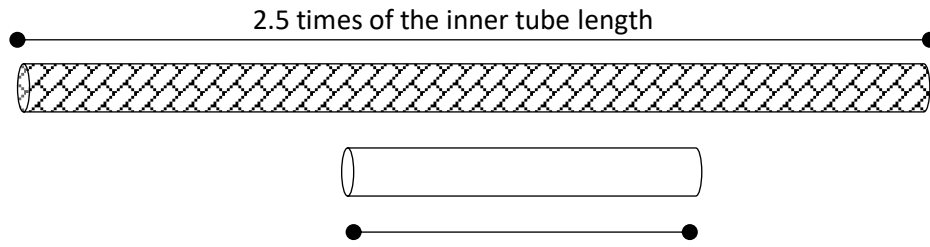


Figure 4.11. Illustrative length of inner tube and braided sleeve length in extension pMA

Table 4.5. Specifications of Extension pMA

Initial Length (m)	Rubber Thickness (m)	Braided sleeve Thickness (m)	Inner tube Diameter (m)	Braided sleeve Diameter (m)
0.34	1.1×10^{-3}	0.5×10^{-3}	20×10^{-3}	20×10^{-3}

In order to calculate θ in the extension case, refer to Figure 2.8 and Equation 2.5. Solving the equation by substitution; θ equals to 68.7° , which is greater than 54.7° . Thus, the pMA acts as an extensor.

4.4.2 Geometrical Model of Extension pMA

The geometrical model of the extension pMA is same as the contractor pMA, it was also assumed that the shape of the extension pMA is a perfect cylinder. Same expression L , D and θ are used, despite that both muscles appeared comparable, and there are significant differences between them. The direction of the force is opposite relative to each other; the direction of the force has the same direction of the change in length. Thus, the force generated by the extension pMA is a function of pressure and θ , the force is calculated as:

$$F = P \frac{dv}{dl} = \frac{Pb^2(1 - 3 \cos^2 \theta)}{4n^2\pi} \quad (4.14)$$

The maximum pulling force in the contraction pMA and the pushing force in the extension pMA is generated when both of them are at their minimum length. The force generated by any types of pMA depends on the value of helix angle θ of the braided sleeve; the expression of F can also be calculated by replacing the cosine θ with equation (1) as:

$$F = \frac{Pb^2}{4\pi n^2} \left(1 - 3 \frac{L^2}{b^2}\right) \quad (4.15)$$

This model can be easily used due to the challenges imposed by measuring θ in practice. In the next section an experimental model was built in order to validate the geometrical expressions.

4.4.3 Experimental Inspection of Extension pMA

The extension pMA is set up and operated same as contraction pMA, as shown in Figure 4.4 in section (4.3.3). Applying pressurised air into the extension pMA will cause increase in length and decrease in diameter, resulting in generating tensile force longitudinally acting along the major axis. The purpose of the experiment is to determine the elongation ratio, and associated force generated in the pMA. In addition, to investigate the relationship between the length versus pressure and force versus pressure. The pressure level of pMA was differed between 0 to 5 bar; 0.5 bar per step. The extension pMA was attached to stationary spring scale to determine the mass required - and subsequently the force- to extend the pMA to its maximum length. The initial length and the length at particular pressure level were measured and recorded in order to calculate the elongation ratio ε^+ ; the elongation is calculated as:

$$\varepsilon^+ = \frac{\Delta L}{L_0} \quad (4.16)$$

Where L_0 is the initial length, and ΔL is the displacement in length, solving equation 4.16 by substitution; elongation ratio is equal to 44%. Table 4.6 shows the parameters of extension pMA used experimentally to validate the geometrical model.

Table 4.6. Extension pMA parameters

Initial Length	Final length	Muscle Diameter
L_0 (m)	L_5 (m)	D_0 (m)
0.34	0.49	27×10^{-3}

Figure 4.12 shows the relationship between the length of the muscle and the applied pressure as it shows a proportional relationship; the length of the muscle increases as more pressure is experienced. It can be noted that 90% of the maximum expansion occurs at 2.5 bar, the range of elongation depends on the threshold angle limit, where its starts to change slightly above 2.5 bar. Thus, the extension pMA above 2.5 bar increases slightly due to its low stiffness.

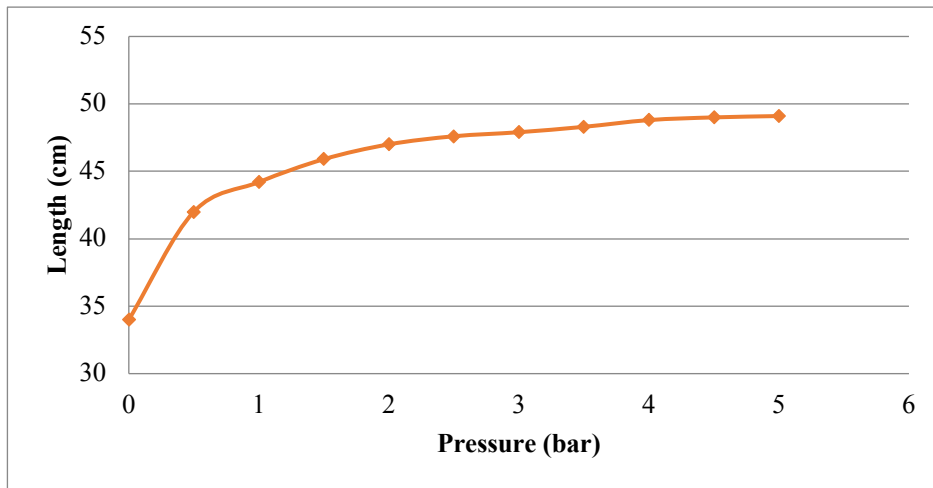


Figure 4.12. Relationship between the length and the pressure in the extension pMA

The following Figure 4.13 demonstrates the relationship between the force generated in the extensor pMA against pressure at different levels; the maximum force is measured experimentally by using a stationary spring scale, in an isometric configuration at a range of different pressures as mentioned above to be 15.9 N, where $F = M \cdot g$, the relationship between the extension force and the pressure is linear, because the generated force depends on a constant area.

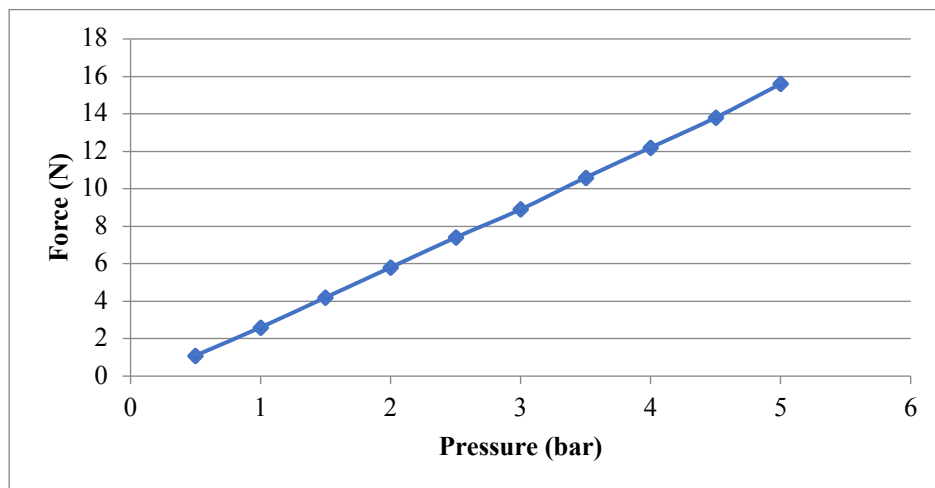


Figure 4.13. The relationship of the generated force at different pressure level varies from 0-5 bar

4.4.4 Experimental Model vs. Mathematical Model

Figure 4.14 represents a plot of the length of the extensor pMA versus the applied pressure using the experimental model and the geometrical model described in Equation y .

Qualitatively, both models behave similarly in terms of their shapes. However, the results obtained from Equation y overpredict the experimental model with $MFE = 1.01$.

The relationship between both models, i.e., geometrical and experimental, a regression model is developed using the data in Table () and the resulting equation is:

$$y = 1.0788x - 3.2299$$

where x and y represent the lengths (m) obtained from the geometrical model results and observed data, respectively. The model has a relatively large R^2 of 0.9989 and the value of the gradient is approximately 1. The overprediction is a small percentage, between 2.7%-7.4% for the given range of pressure.

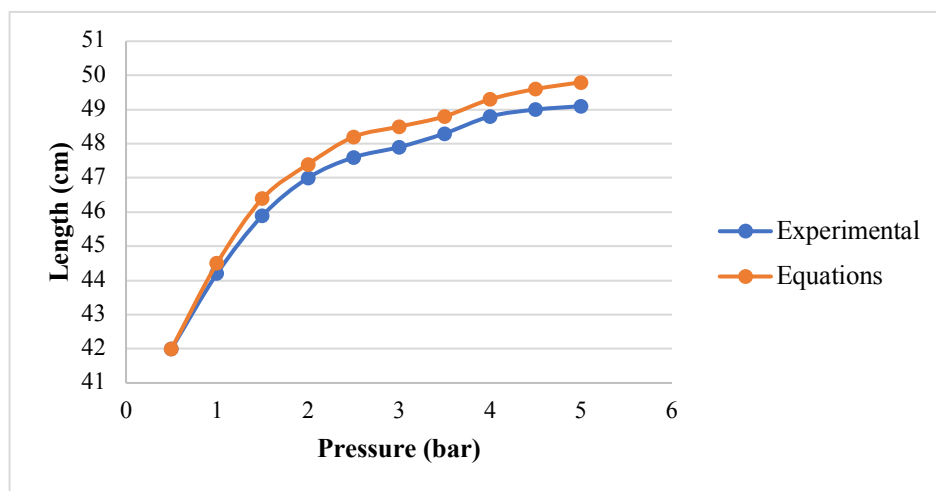


Figure 4.14. A Comparison between the geometrical model and the experimental model, that shows the relationship between the length of the extensor pMA and the pressure level, where the blue curve demonstrates the experimental result while the orange curve demonstrates the equation results

Figure 4.15 plots an experimental and geometrical force of the extension pMA against different pressure levels. The relationship between the generated force and the pressure is linear; and the generated force increases when more pressurised air is applied. However, the results obtained from Equation y overpredicts the experimental model with a $MFE = 1.07$.

$$y = 1.0239x - 0.1917$$

It can be noted that there is a slight difference in the force generated by the pMA and the theoretical force, the experimental force found to be less than the theoretical force approximately by 7%. This difference is expected and indicates the dissipated energy and simplification assuming the muscle is a perfect cylinder.

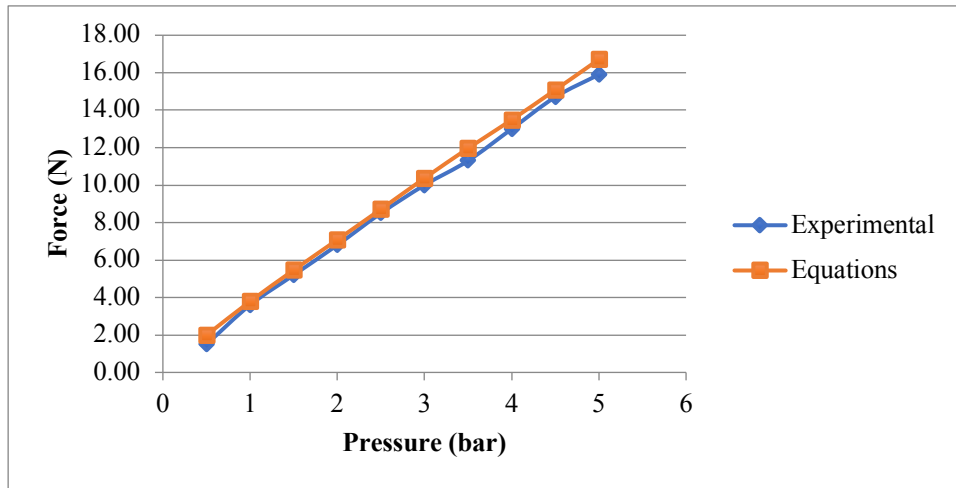


Figure 4.15. A comparison between the experimental results and the predicted results of the force generated at different pressure levels; the blue curve shows the observed results, the orange curve shows the predicted results

4.5 Bending Contractor and Extensor Pneumatic Muscle Actuator (pMA)

4.5.1 Operation of the Bending Contractor and Extensor pMA

The construction of bending contractor pMA and bending extensor pMA is very similar to that of contraction pMA and extensor pMA, respectively, in terms of constituting of an inner tube, a braided sleeve, and end caps (one of them containing an air inlet). Though, bending contractor pMA has an extra plastic layer (plastic rod) interceding only one side of the actuator as shown in Figure 4.16. Reinforcement of the muscle occurs throughout one side and with the presence of the plastic rod within that side the length remains unchanged. While the other side- lacking the plastic rod –contracts, resulting in a difference in length between both sides leading to the desired bending action. The bending extensor pMA is fixed from one side of the actuator using a high-tension thread around 500N and the thread restrains the actuator from expansion as illustrated in Figure 4.17. Meanwhile the opposite side remains free to extend when applying pressurised air. The difference in length of both sides results in bending the extensor pMA to the thread side. Table 4.7 shows the specification of the bending contractor and bending extensor pMA.

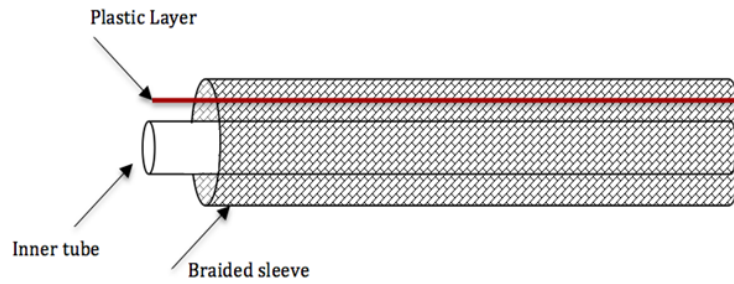


Figure 4.16. Illustrative construction of bending contractor pMA

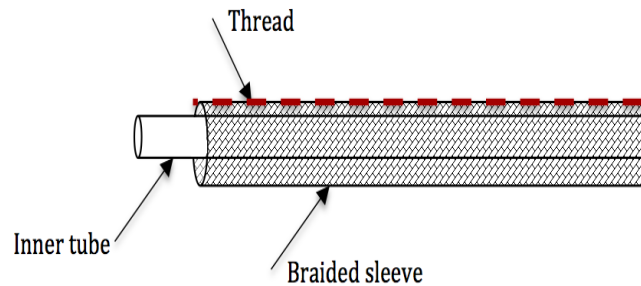


Figure 4.17. Illustrative construction of bending extensor pMA

Table 4.7. Specification of bending pMAs

Muscle Type	Initial Length (m)	Rubber Thickness (m)	Braided sleeve Thickness (m)	Inner tube Diameter (m)	Braided sleeve Diameter (m)
Bending Extensor	0.34	1.1×10^{-3}	0.5×10^{-3}	20×10^{-3}	20×10^{-3}
Bending Contractor	0.3	1.1×10^{-3}	0.5×10^{-3}	20×10^{-3}	20×10^{-3}

4.5.2 Experimental Inspection of Bending Contractor and Extensor pMA

Both bending contractor and extensor pMA are operated by inflow of pressurised air regulator as mentioned in the contraction pMA section. When the bending pMA is supplied with pressurised air the diameter of the pMA increases/decreases depends on the type of the actuator resulting in compression/expansion. However, using reinforcement techniques on either side of the muscle will result in bending action. The purpose of the experiment is to determine the bending angle for both bending pMAs and the force produced at different pressure levels. In addition, to examine the relationship of pressure versus bending angle and pressure versus force. To measure the force of bending pMA same technique as traditional contraction and extension pMA was employed. The bending pMA was fixed to a rig in an

isometric configuration as shown in Figure 4.18, and different pressures were applied varies from 0-5 bar; 0.5 bar per step. The experiment was repeated at specific bending angles, 90°, 45°, and 90° for bending extensor (Al-Fahaam, Davis , & Nefti-Meziani, 2018), bending contractor (Al-Ibadi, Davis, & Nefti-meziani, Design, Kinematics and Controlling a Novel Soft Robot Arm with Parallel Motion, 2018) , and double bending extensor respectively.



Figure 4.18. Bending pMA experimental setup to measure the bending angle and the force, fixed to a rig

Figure 4.19 demonstrates the relationship of the bending angle at different pressures differs from 0-5 bar, 0.5 bar per step. The maximum angle for the unloaded single extensor pMA was about 420° at 5 bar. It shows a proportional relationship, as the bending extensor pMAs increases with increasing the level of pressurised air. However, the bending extensor pMAs diverges at high pressures when both end clashes resulting in unpredicted behaviour as shown in Figure 4.20. Therefore, the pressure level was limited to 4 bar to avoid clash between muscle ends.

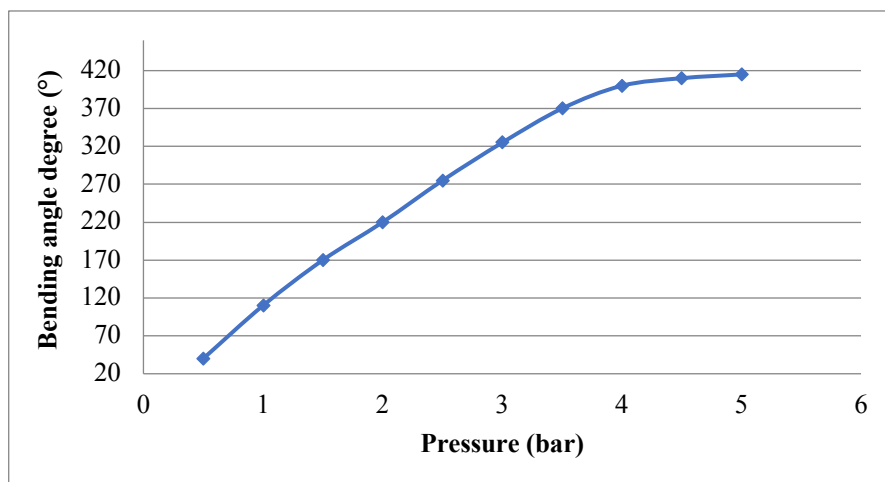


Figure 4.19. The Relationship between the bending angle and pressure of bending extensor pMA.

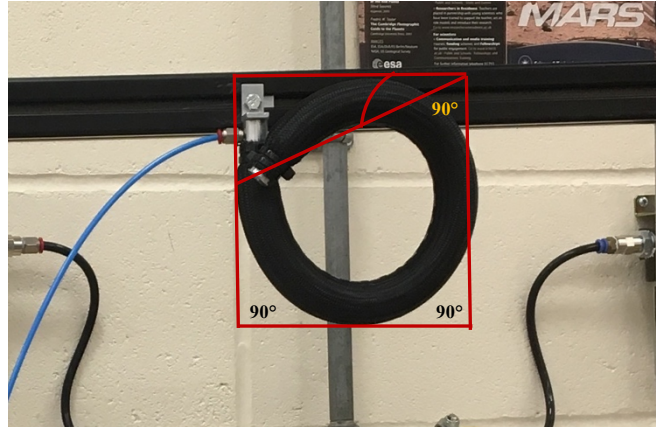


Figure 4.20. Bending angle of extensor pMA more than 360° showing unpredicted behaviour

Figure 4.21 shows the relationship of the bending contractor pMA against applied pressure that varies from 0 to 5 bar. It can be noted that the bending angle increases with the increase of the pressurised air. The bending angle of contractor pMA is less than the extensor pMA at a given pressure. This is due to the difference in construction and length. *e.g.* the contractor and extensor pMA bending angle 180° as shown in Figure 4.22.

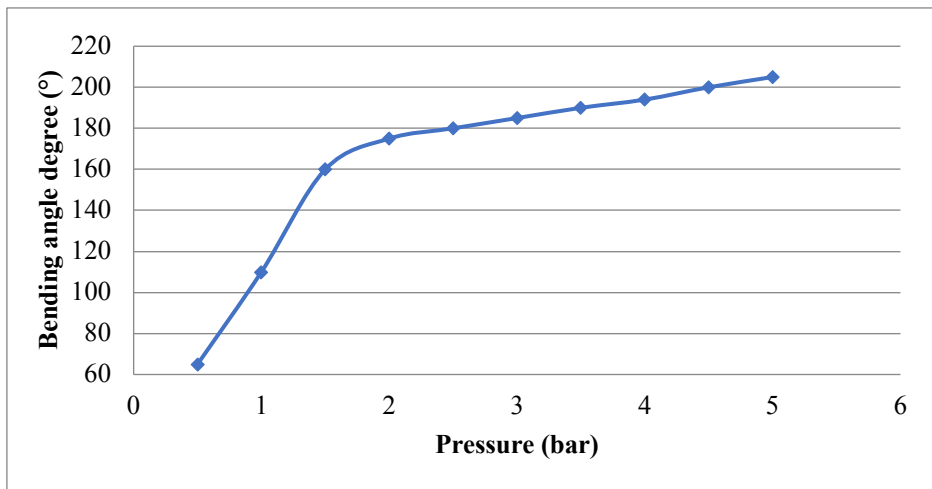


Figure 4.21. The Relationship between the bending Angle and the Pressure of the bending Contractor pMA

The relationship of the generated force against the applied pressure was tested experimentally for different bending pMAs. Figure 4.23 shows a linear relationship between the force and the pressure; the bending contractor generates 18% larger force than the bending extensor. However, the generated force in the double extensor is 93% of the single bending extensor pMA. The reason that the double extensor pMA generated force is not double the single extensor pMA is because of the dissipated energy between the two muscles. The maximum payload for the single bending extensor pMA is about 1.7 kg, and the payload for the double

bending pMA was about 3.2 kg. However, the bending contractor pMA payload is about 2 kg.

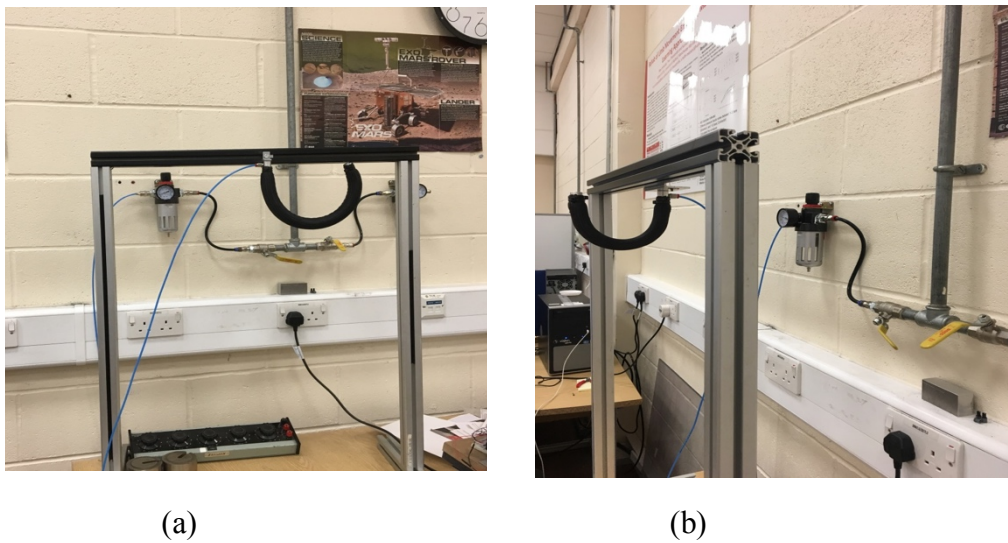


Figure 4.22 Bending Angle 180° of Contractor pMA and Extensor pMA, (a) extensor bending angle at 2.5 bar, (b) contractor bending angle at 1.5 bar

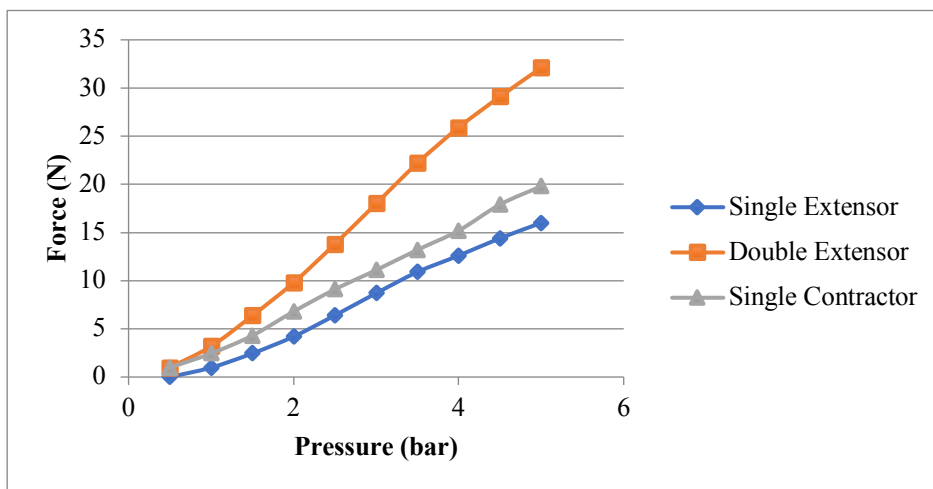


Figure 4.23. Relationship of the generated force at different pressure levels in an isometric configuration; the blue curve for the single extensor pMA and the grey curve for contractor pMA at, and the orange curve for double extensor pMA

4.5.3 Geometrical Model of Bending Contractor and Extensor pMA

To analyse the bending contractor and extensor pMA behaviour it is assumed that; the cross-sectional area of the muscles remains in a circular shape during the bending of the muscle, the plastic rod/ high tension thread used to reinforce the pMA from one side to cause bending is inextensible, there is no elastic force in the inner tube, and there is no friction force between the inner tube and the braided sleeve and between the braided sleeve and the reinforcement material.

The length of the bending pMA is calculated based on the geometry of the bending pMA, as shown in Figure 4.24. Where L_o is the length of bending pMA on the reinforced side, L_n is the length of bending pMA on the opposite side, L_b is the length of the neutral axis of the bending pMA; in this case the average length is calculated based on the assumption that the cross sectional area shape of the bending pMA is circular, r_o is the inner radius of the bending pMA, r_n is the outer radius of the bending pMA, φ is the bending angles of the pMA, and D_b is the diameter of the bending pMA. The average length of the bending pMA is calculated as:

$$L_b = \frac{L_o + L_n}{2} = \frac{b \cos \theta_{max} + b \cos \theta}{2} \quad (4.17)$$

The diameter of the bending pMA is given by:

$$D_b = r_n - r_o \quad (4.18)$$

r_o and r_n are calculated based on the value of θ , where in r_o it is calculated based on the maximum value of θ , which is constant due to the reinforcement. While the r_n is calculated based on θ value at different pressures that decreases during the bending. So, based on the geometry of traditional pMA in Equation 3.5 the initial length and the length at certain pressure level of the bending angle is given by:

$$L_o = b \cos \theta_{max} = r_o \varphi \quad (4.19)$$

$$L_n = b \cos \theta = r_n \varphi$$

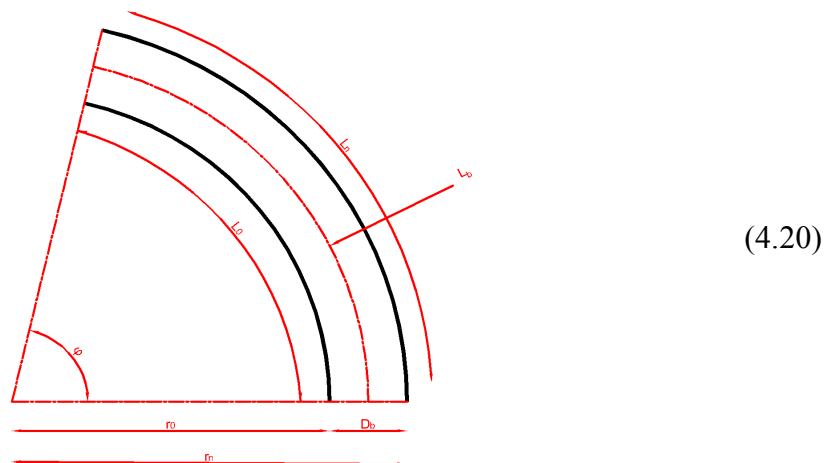


Figure 4.24. Bending pMA geometry

The diameter of the bending pMA is related to the change of θ in the braided sleeve, considering that the cross-sectional of the bending pMA is circular in shape. Then D_b is calculated as:

$$D_b = r_1 + r_2 \quad (4.21)$$

$$r_1 = D_1/2 = b \sin \theta / 2\pi n ; r_2 = D_2/2 = b \sin \theta_{max} / 2\pi n \quad (4.22)$$

According to the traditional pMA geometry and substituting in equation (2) D_b is calculated as:

$$D_b = \frac{b \sin \theta + b \sin \theta_{max}}{2\pi n} \quad (4.23)$$

The bending angle φ of the bending pMA can be derived as a function of θ as:

$$\varphi = \frac{b \cos \theta - b \cos \theta_{max}}{D_b} \quad (4.24)$$

In order to understand the behaviour of the force generated by the bending pMA, the same theory as the traditional pMA is utilised; the energy conservation theory, as was conducted by (Chou & Hannaford, 1996), The input work W_{in} is done in the bending pMAs when the pressurised air inflow distributes across the tube inner surface area resulting in radial forces. This will equally result in a mechanical motion initiated by volume change and consequently bending instead of contraction/ expansion with corresponding force along the major axis of the pMA due to the reinforcement at one side of the pMA; where P is the relative pressure, dV_b is the change in volume, and dL_b is the change length of the bending pMA.

$$W_{out} = W_{in} \quad (4.25)$$

$$-F dl = PdV_b \quad (4.26)$$

$$V = \frac{D^2 \pi L}{4} \quad (4.27)$$

Thus, the volume of the bending pMA is given as:

$$V_b = \frac{D_b^2 \pi L_b}{4} \quad (4.28)$$

Substituting the equations (4.14) and (4.20) in equation (4.25), V_b is given by:

$$V_b = \frac{b^3 (\cos \theta + \cos \theta_{max}) (\sin^2 \theta + 2 \sin \theta \sin \theta_{max} + \sin^2 \theta_{max})}{32\pi n^2} \quad (4.29)$$

Differentiating the length and volume of the bending muscle with respect to θ

$$\frac{dL_b}{d\theta} = \frac{-b \sin \theta}{2} \quad (4.30)$$

$$\begin{aligned} \frac{dV_b}{d\theta} = \frac{b^3}{32\pi n^2} [& (\cos \theta + \cos \theta_{max})(2 \cos \theta \sin \theta + 2 \sin \theta_{max} \cos \theta) \\ & - \sin \theta (\sin^2 \theta + 2 \sin \theta \sin \theta_{max} + \sin^2 \theta_{max})] \end{aligned} \quad (4.31)$$

The generated force in the bending extensor pMA is given as:

$$\begin{aligned} F_{ext} = P \frac{dV_b}{dL_b} = \frac{Pb^2}{8\pi n^2} \left[\frac{(\cos \theta + \cos \theta_{max})(\cos \theta \sin \theta + \sin \theta_{max} \cos \theta)}{\sin \theta} \right. \\ \left. - \frac{(\sin \theta + \sin \theta_{max})^2}{2} \right] \end{aligned} \quad (4.32)$$

The same equations are used to calculate the force and length of the bending contractor pMA, however, the direction of the generated force is opposite to the generated force in the bending extensor pMA. Therefore, the generated force in the bending contractor pMA is described as:

$$\begin{aligned} F_{cont} = P \frac{dV_b}{dL_b} = - \frac{Pb^2}{8\pi n^2} \left[\frac{(\cos \theta + \cos \theta_{max})(\cos \theta \sin \theta + \sin \theta_{max} \cos \theta)}{\sin \theta} \right. \\ \left. - \frac{(\sin \theta + \sin \theta_{max})^2}{2} \right] \end{aligned} \quad (4.33)$$

In the next section an experimental model was designed and tested in order to validate the mathematical model.

4.5.4 Experimental Model vs. Mathematical Model

Figure 4.25 represents a plot of the generated force of different bending pMAs versus the applied pressure using the experimental model and the mathematical model. Qualitatively, both models behave similarly in terms of their shapes. However, the results obtained from mathematical model overpredicts the experimental model with a MFE = 1.43, 2.3, and 1.76 for the single bending contractor, single bending extensor, and double bending extensor respectively.

The relationship between both models, i.e., geometrical and experimental, a regression model was developed the resulting equation are:

$$y = 1.0921x + 1.8702 \text{ (single bending contractor pMA), } R^2 : 0.99821$$

$$y = 1.1274x + 3.1194 \text{ (single bending extensor pMA), } R^2 : 0.99422$$

$$y = 1.1705x + 4.6217 \text{ (double bending extensor pMA), } R^2 : 0.99631$$

where x and y represent the bending angle of the bending contractor ($^\circ$) obtained from the geometrical model results and observed data, respectively. The model has a relatively large efR^2 of 0.9908 and the value of the gradient is approximately 1.

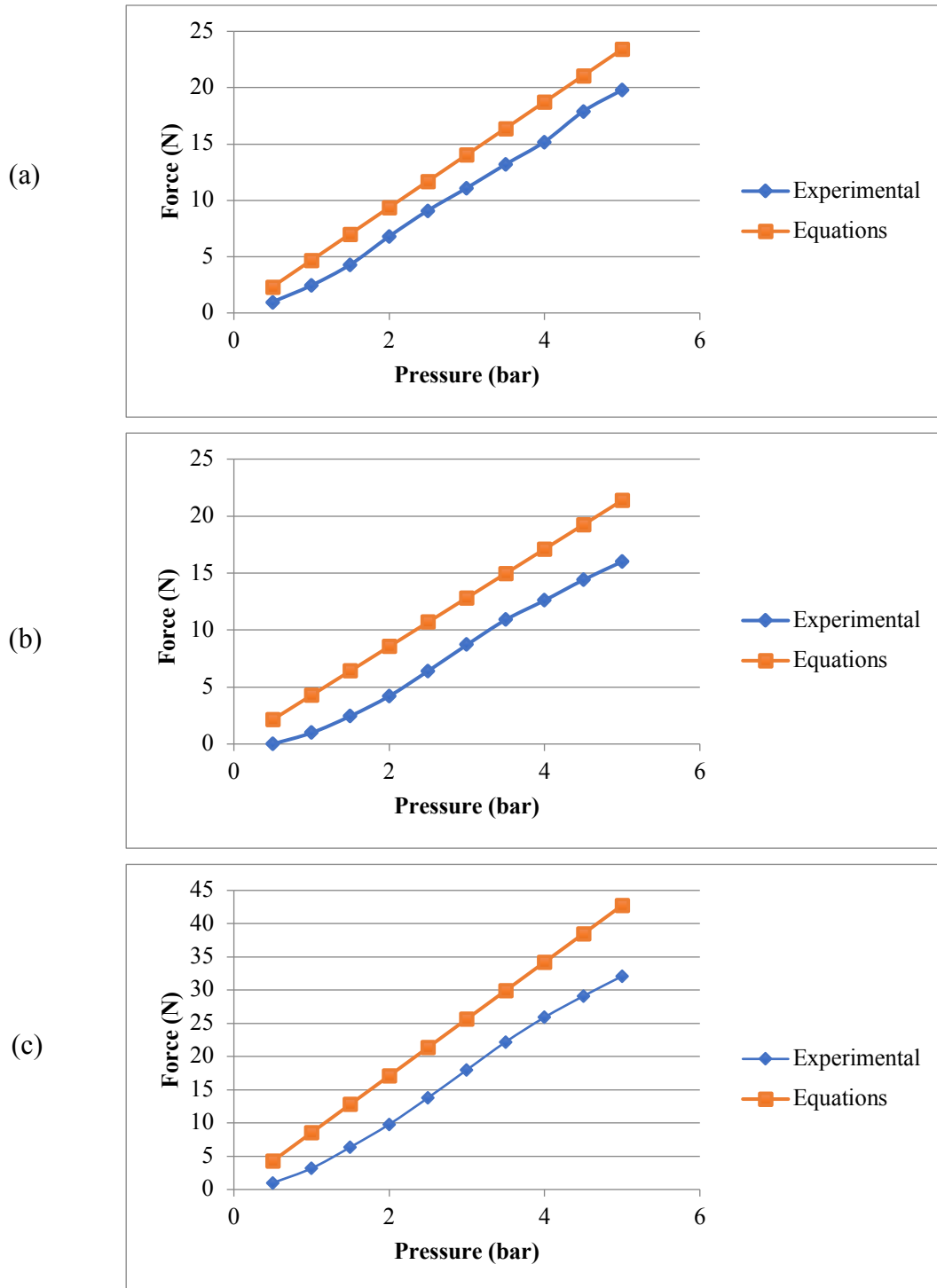


Figure 4.25. A comparison between the mathematical model and the experimental model to demonstrate the relationship of the generated force at different pressure levels in an isometric configuration; (a) for the extensor pMA at 90° , (b) contractor pMA at 45° , and (c) for the double bending extensor pMA at 90° .

There is a noticeable error between the observed and the calculated force generated in the bending pMA . The average error for the bending pMA was 22.5%, 11.8%, and 10.7% for the double bending extensor, single bending contractor, and single bending extensor respectively. The error is expected due to the dissipated energy in the bending pMA before the inner tube contact the braided sleeve, and friction between the braided sleeve and the inner tube, and the friction between the plastic rod/thread and braided sleeve. Especially in the case of double bending extensor pMA, additional energy dissipation occurs in the lateral direction, and the friction between the two muscles.

Figure 4.26 represents a plot of the bending angle of the bending contractor pMA versus the applied pressure using the experimental model and the geometrical model. Qualitatively, both models behave similarly in terms of their shapes. However, the results obtained from mathematical model overpredicts the experimental model with a MFE = 1.10.

The relationship between both models, i.e., geometrical and experimental, a regression model was developed, and the resulting equation is:

$$y = 1.0325x + 10.329$$

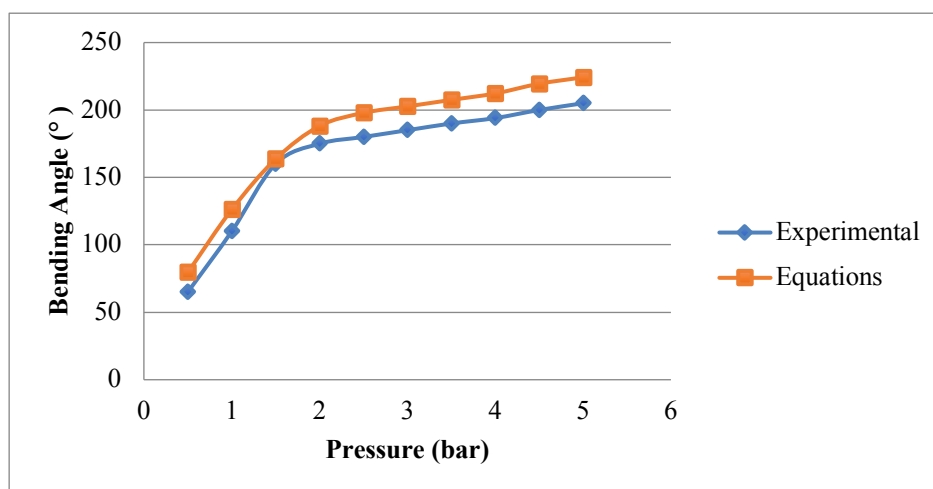


Figure 4.26. The observed and predicted bending angle for the bending contractor pMA; where the blue curve shows the experimental results and the orange one shows the calculated results

Where x and y represent the bending angle of the bending contractor (°) obtained from the geometrical model results and observed data, respectively. The model has a relatively large R^2 of 0.9908 and the value of the gradient is approximately 1.

In the case of bending extensor pMA, the results obtained from mathematical model and the experimental model has a MFE = 1.46, there is a noticeable error between the observed and the calculated bending angle in the bending extensor pMA. Due to the bending extensor

construction, the friction between the inner tube and the sleeve, the dicipated pressure before the inner tube contacts the sleeve, and the tube properties, as shown in Figure 4.27.

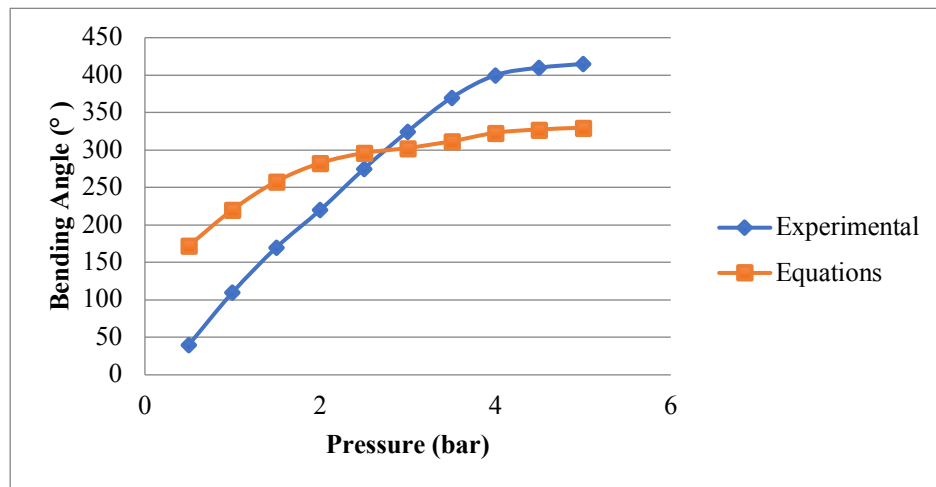


Figure 4.27. The observed and predicted bending angle for the bending extensor pMA; where the blue curve shows the experimental results and the orange one shows the calculated results

4.6 A Novel Elbow pMA Exoskeleton Arm (EpMAE)

The proposed prototype with 1DOF is devised to rehab the elbow joint, the prototype consists of two bending extensor pMAs and one bending contractor pMA.

4.6.1 EpMAE Construction

The construction of the proposed prototype depends on the arthrometric data, see appendix (A), as the average mass for the forearm for both genders is 1.5 kg. The (EpMAE) is distinguished by being soft not only because of the actuators but also the other parts of the exoskeleton arm are bendable and soft. In addition, it does not have any discrete joints; to avoid aligning the exoskeleton arm to the user's arm that might lead to injuries if it does not attach correctly resulting in more adjustments to fit any person. The (EpMAE) assist the user to perform 1 DOF at the elbow joint; extension and flexion when the EpMAE is pressurised. The pressurised air will result in generating force in the pMAs which will cause bending of the muscle.

The bending pMAs are sewn onto the adjustable elbow support as shown in Figure 4.28, three bending pMAs are used to increase the generated force to flex and extend the arm when the pMAs are pressurised; two bending extensors, on the distal side of the arm, and one bending contractor pMAs, on the opposite side. EpMAE has a total weight of 0.35 kg and the same construction as in the traditional pMAs and the bending pMAs are implemented.

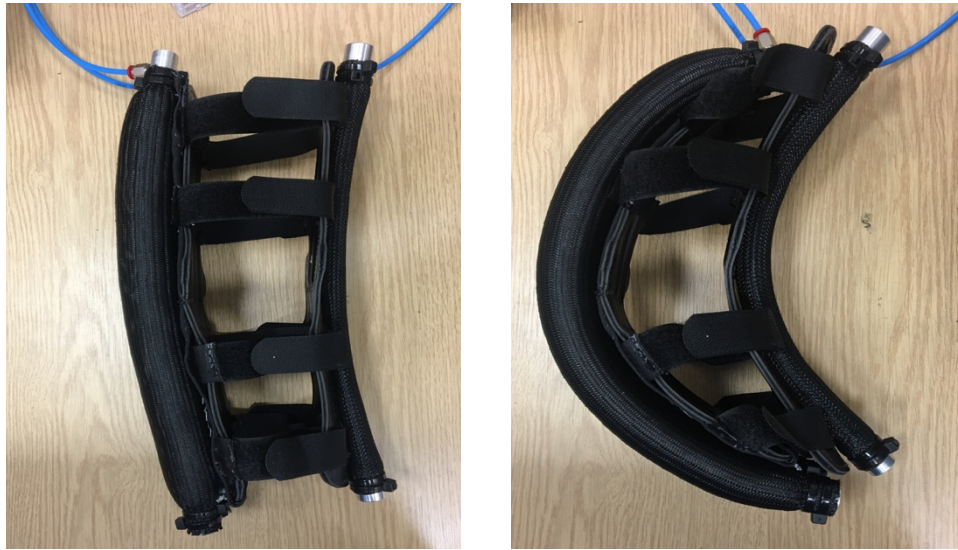


Figure 4.28. The proposed soft arm (EpMAE), the one on the left when it's unpressurised, and the one on the right when the soft arm is pressured

4.6.2 Experimental Inspection for EpMAE

Few experiments are conducted in order to validate the effectiveness of the EpMAE in case of the prototype is unloaded and loaded with 1.5 kg. Also, to find the relationship between the bending angle of the prototype and the pressure applied. And then an isometric configuration is set to find the relationship of the generated force at different pressure levels as shown in Figure 4.29.



Figure 4.29. The prototype setup to find the force of the at different pressure level; e.g. the load is 4 kg at 4 bar

Figure 4.30 represents a plot of the bending angle of the proposed prototype versus the applied pressure using the experimental model and the geometrical model. Qualitatively, both models behave similarly in terms of their shapes in both case as in the case (a) the prototype

is unloaded, but in the case (b) it is loaded with 1.5 kg. The results obtained from mathematical model overpredicts the experimental model with MFE = 1.05, and 1.06 for when it is unloaded and when it is loaded respectively.

The relationship between both models, i.e., geometrical and experimental, a regression model is developed, and the resulting equation is:

$$y = 1.0819x - 5.8623 \text{ (unloaded)}$$

$$y = 1.0473x + 0.6856 \text{ (loaded 1.5 kg)}$$

where x and y represent the bending angle of the prototype ($^{\circ}$) obtained from the geometrical model results and observed data, respectively. The model has a relatively large R^2 of 0.9992 and 0.9984 and the value of the gradient is approximately 1.

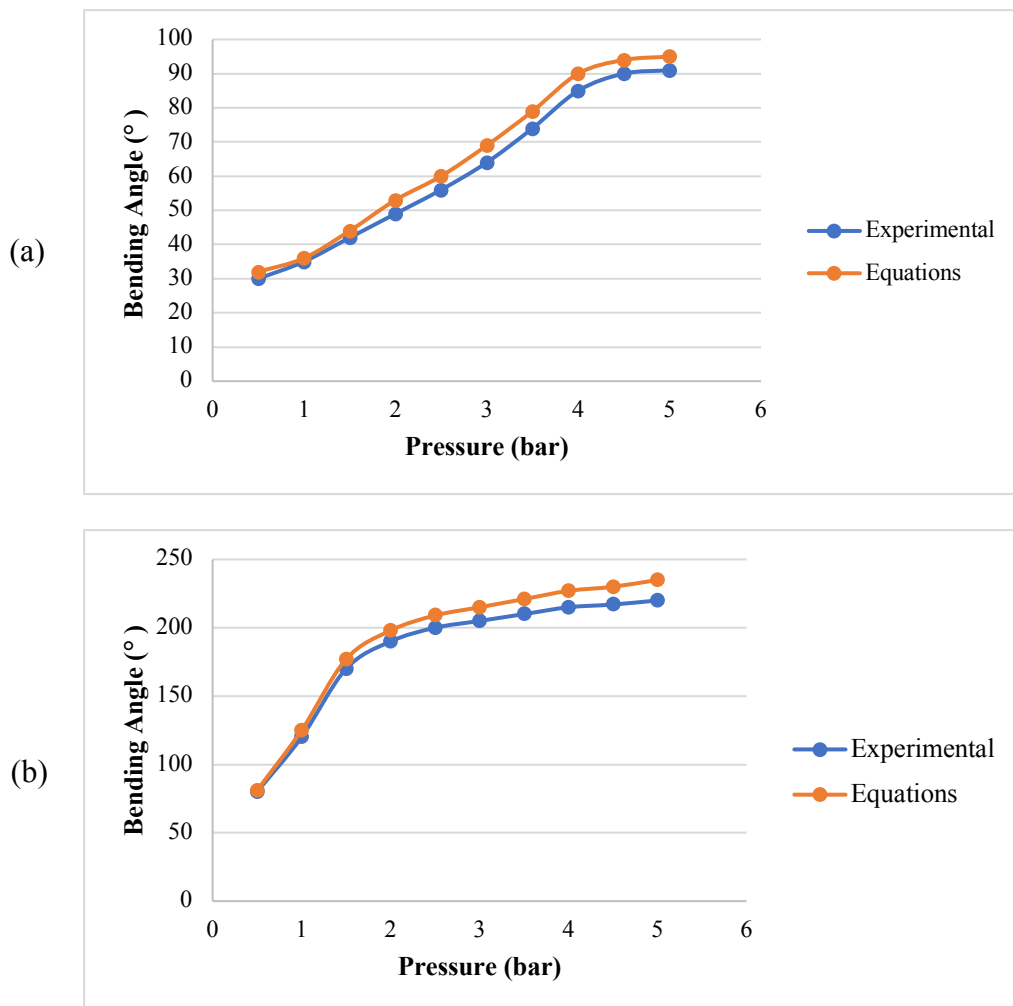


Figure 4.30 The observed and predicted bending angles for the bending prototype at different pressure levels; (a) shows the relationship between the angle and the pressure when it the prototype is unloaded, (b) when the prototype is loaded with 1.5 kg, the blue curve shows the experimental results and the orange curve demonstrates the calculated results.

The generated force of the prototype was measured experimentally using the same procedure mentioned previously. Figure 4.31 shows the direction of the generated force for the proposed prototype, which consists of two bending extensor pMA and one bending contractor pMA. The direction of the force in the bending contractor is opposite to the force generated in the bending extensor as was mention previously. The resultant force was calculated using the force Equations (4.32) and (4.33). The total force generated by the prototype is calculated as:

$$F_{pro} = 2F_{ext} + F_{cont} \quad (4.34)$$

where F_{pro} is the resultant force of the prototype, F_{ext} is the bending extensor pMA force, and F_{cont} is the force generated by the bending contractor pMA.

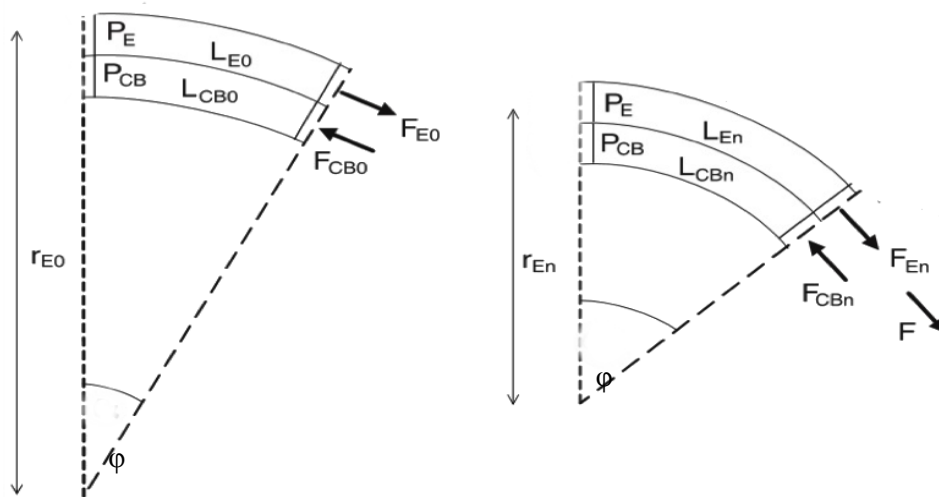


Figure 4.31. The proposed output force direction;

F_{E0} is the extensor force at the initial point, F_{CB0} is the bending contractor force at point 0, L_{E0} is the initial length of the extensor, L_{CB0} is the initial length of the bending contractor, r_{E0} is the initial radius, F_{En} is the extensor force at n pressure level, F_{CBn} is the bending contractor force at n pressure level, L_{En} is the length of the extensor at n pressure level, L_{CBn} is the length of the bending contractor at n pressure level, and r_{En} is the radius at n pressure level

Figure 4.32 represents a plot of the generated force of the proposed prototype versus the applied pressure using the experimental model and the mathematical model. Qualitatively, both models behave similarly in terms of their shapes. However, the results obtained from mathematical model overpredicts the experimental model with MFE = 1.29.

The relationship between both models, i.e., geometrical and experimental, a regression model is developed the resulting equation is:

$$y = 1.0389x + 5.5389$$

There is an obvious error between the observed and the calculated force generated in the proposed prototype. The model has a relatively large R^2 of 0.99982. The average error is 31%. The error is expected due to the dissipated energy in the prototype before the inner tube contact the braided sleeve, and friction between the braided sleeve and the inner tube, and the friction between the plastic rod/thread and braided sleeve.

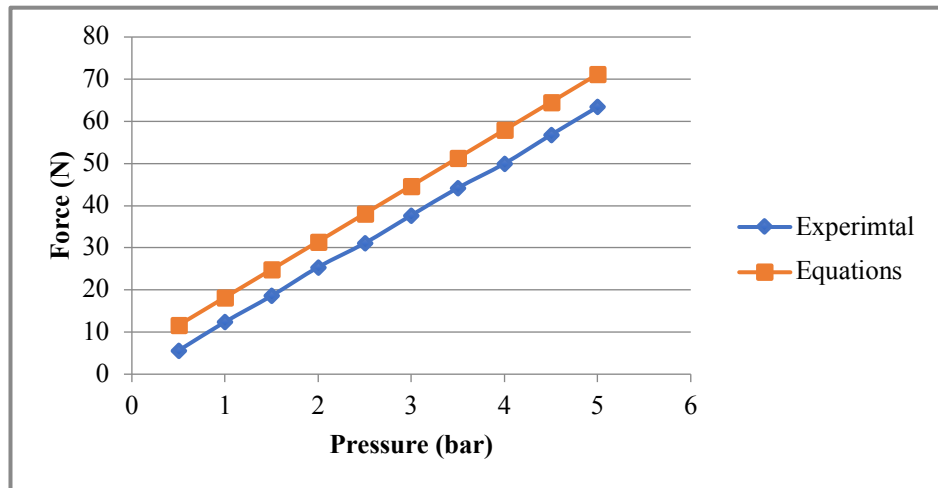


Figure 4.32. A Comparison between the mathematical model and experimental model for the prototype force vs. pressure level; the blue curve shows the experimental results, the orange curve shows the equation results

4.6.3 Enhancement to the Mathematical Model

Based on the previous section, it can be clearly seen that there is a gap between the predicted and observed results in the generated force. There are many factors that can affect the theoretical results that have been neglected to ease the calculations. The correction factor is used because some of geometrical factors are neglected in the calculation, such as energy loss, friction between the braided sleeve and the bladder, and between the threads in the braided sleeve, the tension is distributed evenly among the pMA but not in the experimental case, the stress fluctuates, and the threads in the braided sleeve adjust itself in pursuit of attaining lower stress.

A correction factor of 4.521 (constant) is considered to be added to the predicted resultant force of the geometrical model. So, the new force model is as:

$$F_{pro} = 2F_{ext} + F_{cont} + 4.521 \quad (4.35)$$

4.6.4 Experimental Verification of Enhanced Model

Figure 4.33 shows the performance of the new model of the new model compares to the experimental model and the predicted model. It can be clearly shown that the gap between

the new model and the experimental model is less than the previous modelled results. It is clear that the average error percentage is reduced to 9.09% after adding the correction factor. The error between the experimental results and the previous predicted model was 31.11%.

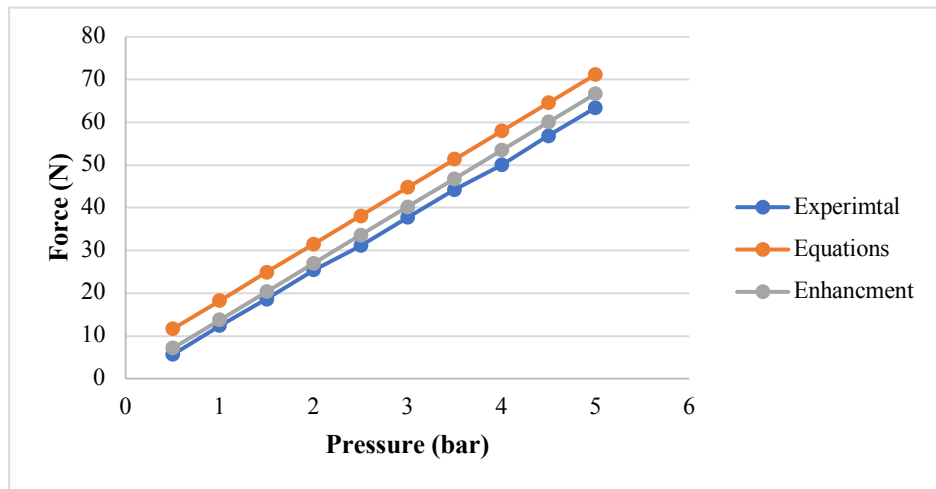


Figure 4.33 A Comparison among the new model, the mathematical model and experimental model for the prototype force vs. pressure level; the blue curve shows the experimental results, the orange curve shows the equation results, and the grey curve shows the enhanced results.

Qualitatively, the models behave similarly in terms of their shapes in all cases. The results obtained from enhanced model overpredicts the experimental model with a MFE = 1.09.

The relationship between both models, i.e., enhanced and experimental, a regression model is developed, and the resulting equation is:

$$y = 0.9624x - 0.9732$$

where x and y represent the resultant force of the prototype obtained from the enhanced model results and observed data, respectively. The model has a relatively large R^2 of 0.998 the value of the gradient is approximately 1.

4.7 Summary

In this chapter a novel elbow pMA exoskeleton arm was introduced, this arm consists of various pMAs, the construction and behaviour of each pMA was described in detail. An experimental model for each pMA was designed to understand the behaviour of the pMA in reality and then it was compared to the geometrical model that depends on different parameters to demonstrate the force generated as a function of input pressure in each pMA. These pMAs were combined together to best fit the forearm and to generate more force to move the forearm (extension and flexion).

However, there is an error between the predicted results and the observed results because of the assumption that has been set at the beginning, that the muscle is a perfect cylinder, the cross-section of the pMA is circular, there is no friction among the components, the energy loss in the inner tube before it contacts the braided sleeve, and the air leakage. Therefore, an enhanced model was introduced, using a correction factor to reduce the percentage of the average error.

5 MODELLING PNEUMATIC MUSCLE ACTUATORS

A number of mathematical models were conducted to examine the linear behaviour of pMAs, however, few were conducted to study the non-linear behaviour of pMAs as mentioned previously in chapter 2: Literature Review. This showed lack of genuine geometric characteristics, real parameters of the inner tube (bladder), and the properties of the material used in: inner tube, braided sleeve, and end caps. This chapter will discuss a novel non-linear Finite Element (FEA) numerical model of the proposed pMAs. The model is validated after series of experiments, using the real parameters of the pMAs. The experimental model and design was previously discussed in detail in chapter 3: Mechanical Design. A comparison is held between the experimental results of the model and the numerical model using FEA.

5.1 Numerical Model Consideration

Empirical data and/or mathematical modelling without loading are used to justify the viability of design. Such methods may become unreliable, especially when unpredictable and random deformation occurs once a soft actuator is in contact with unknown and varying objects. A more systematic and detailed design process is needed for analysis of optimum conditions in actuating the pMAs. The non-linear behaviour of the pMA is a direct result of the non-linearity of the inner tube material (Butyl rubber). Therefore, a realistic numerical model was designed in order to aid in understanding the real-world behaviour.

A systematic finite element analysis (FEA) is carried out to evaluate the elongation/contraction, force, and bending profile of the actuators. The actuator was then validated by actuating at different pressures and adaptive control. Analysis of pMAs model was made using finite element analysis (FEA) and observations are compared with the experimental results.

A 3D CAD model is built to match the experimental model. This model has 3 components, the inner tube (bladder), braided sleeve and end caps. The model was produced in Fusion 360 software package Student Version provided by Autodesk. The model is built based on the material properties and real dimensions that were used experimentally. The Butyl rubber is used for the inner tube, PET is used for the braided sleeve, and stainless steel is used for the end caps as shown in Table 5.2. The construction of the numerical model is based on the definition of material type used, the node set construction, element set construction, and boundary conditions. A number of assumptions are taken into consideration in order to design the numerical model, these include: (a) there is no friction between the strands, and

(b) the braided sleeve is always in contact with the inner tube (Tondu & Lopez, 2000).. The following geometrical parameters are used in the numerical model as shown in Table 5.1.

Table 5.1 Geometrical parameters description

Parameter	Description
θ	The helix angle ($^{\circ}$)
L_0	Initial Length (mm)
D_0	Initial Diameter (mm)
t	Thickness of the inner tube (mm)
P	Pressure (pa)
F	Force, for isometric test simulation (N)
ΔL	Displacement for isotonic test simulation (mm)

5.1.1 Material Type Definition

The material modelling in Ansys Workbench provides the hyperplastic modelling. The butyl rubber is adopted as a material of a 1.1 mm thick inner tube (bladder) due to its hyper elasticity. The behaviour of hyperplastic response of butyl rubber is modelled based on the Mooney Rivlin parameters C_1 and C_2 (Manuello Bertetto & Ruggiu, 2014). The two constants and the values of density of each component are as given in Table 5.2.

Table 5.2 Materials properties

Component	Material assignment	Properties
Bladder	Butyl Rubber	$C_1= 0.0698\text{Mpa}$ $C_2= 0.0628\text{Mpa}$ D factor= 0 Density= 1040kg/m^3 , Mooney Rivlin model
Braided Sleeve	PET threads	Density: 1300 kg/m^3 Elastic Modulus: 2500MPa Poisson's ratio: 0.4
Inextensible layer	Nylon thread/Paper layer	Density: 730 kg/m^3 Elastic Modulus: 6500MPa Poisson's ratio: 0.2
Caps	Structural steel	Density: $7,800\text{ kg/m}^3$ Elastic Modulus: 200MPa Poisson's ratio: 0.26

Butyl rubber-like materials show nonlinear behaviour. These are isotropic and generally incompressible materials which undergo large elastic deformations. They are also called green elastic materials, a special case of Cauchy materials that is defined by its strain energy

function (Mansouri & Darijani, 2014). The whole approach of FEA is to produce the necessary deformation and derive the energy functions that follow a set of constraints in the form of differential equations, governed by the physical phenomenon.

The strain energy function of hyperplastic materials is a function of stretch ratio α , which is also the sum of a unit and the engineering strain during deformation.

$$\alpha = 1 + \epsilon_{eng \text{ strain}} \quad (5.1)$$

The Mooney Rivlin class of model expresses the energy in terms of strain invariants I_1 , I_2 , and I_3 , and stretch ratios, given as:

$$\begin{aligned} I_1 &= \alpha_1^2 + \alpha_2^2 + \alpha_3^2 \\ I_2 &= \alpha_1^2 \alpha_2^2 + \alpha_2^2 \alpha_3^2 + \alpha_3^2 \alpha_1^2 \\ I_3 &= \alpha_1^2 \alpha_2^2 \alpha_3^2 \end{aligned} \quad (5.2)$$

Under the assumption of incompressible materials, and uniform transverse and biaxial extension, where, J is the elastic volume ratio:

$$I_3 = 1 = J, \alpha_1 = \alpha_2 \quad (5.3)$$

$$I_1 = 2\alpha^2 + \frac{1}{\alpha^4} \quad (5.4)$$

Mooney-Rivlin constants from the experimental data were used in material modelling for FEM analysis. The data fit better in the third-order reduced polynomial Yeoh model equation than Ogden, with the constant values as given in equation (Shahzad, Kamran, Zeeshan Siddiqui, & Farhan, 2015). The models also have to be selected according to the applied strain range. Mooney Rivlin model can handle about 30-200% of strain whereas Ogden up to 700% strains (Guo & Sluys, 2006). But the fitting of curve is priority criteria, so Mooney Rivlin was adopted, the equation is given as:

$$M(I_1, I_2) = C_1(I_1 - 3) + C_2(I_2 - 3)^1 + \frac{1}{d_1}(J - 1)^2 \quad (5.5)$$

where I_1 is the deviatoric first principal invariant, J is the Jacobian and the required input parameters are defined as:

$$\begin{aligned} C_1 &= 0.0689 \text{Mpa}, C_2 = 0.0628 \text{Mpa} \\ d_1 &= \frac{2}{K} = 0.299 \text{E} - 5 \end{aligned} \quad (5.6)$$

In FEA, the incompressibility parameter d is assumed to be 0 . The Engineering stress can be calculated by Cauchy stress tensor σ_{ij} equation and can be equated to the pressure applied to get the principal engineering strain values.

$$\sigma_{11} = -p + 2\alpha^2 \frac{\partial U}{\partial I_1} = \sigma_{22}, \sigma_{33} = -p + \frac{2}{\alpha^4} \frac{\partial U}{\partial I_1} \quad (5.7)$$

$$S = \frac{\sigma}{\alpha} \quad (5.8)$$

Although analytically one can approximate the result, but more precise solution could be attained by FEA. The model is a hollow cylinder made of butyl rubber. This has been attached to a fixed support at the top of the muscle.

5.1.2 Hyperplastic FEA Matrix Formulation Methodology

The structural finite element methodology is based upon creation of the stiffness matrix for each element developed after successful discretisation. The number of DOFs in a continuum problem is infinite, whereas for a finite element method the elements are finite and are governed by equation:

$$L(\phi) + f = 0 \quad (5.9)$$

For solving the variables, there must be equal number of equations representing the boundary conditions of the form:

$$B(\phi) + g = 0 \quad (5.10)$$

An approximate solution of these differential governing equations is a force stiffness equation that is calculated at each node in relation to the neighbouring nodes using finite difference method or other evolved methodologies.

$$[K]\{x\} = [F] \quad (5.11)$$

Where K is the stiffness and x the displacement is. The given force is based on the boundary condition equations, where the number of rows depends on the number of elements.

The stresses on the body in post-processing solution (and even to produce the stiffness matrix from stress-displacement matrix) are determined by derivative of strain energy density function W given by:

$$S_{ij} = \frac{\delta W}{\delta E_{ij}} = 2 \frac{\partial W}{\partial C_{ij}} \quad (5.12)$$

Where i and j are rows and columns of the matrix and E is strain energy function, whereas C being the strain constants as defined before. Strain energy density functions are defined in terms of finite deformation quantities: invariants of the Cauchy- green deformation tensor or principal stretch ratios as defined and calculated for hyperplastic material properties. The deformation or displacements in x , y , and z direction in local coordinates of each nodes are u , v , and w . These displacements can be used to determine the mapping functions f , g , and h .

$$\begin{aligned} f &= x + u(x, y, z) \\ g &= y + v(x, y, z) \\ h &= z + w(x, y, z) \end{aligned} \quad (5.13)$$

As per the finite deformation theory (Mingrui & Zhan, 2000), the deformation gradient is defined as differential nodal changes in coordinates of deformed or undeformed regions of the configuration.

$$\begin{aligned} dx^* &= \frac{\partial f}{\partial x} dx + \frac{\partial f}{\partial y} dy + \frac{\partial f}{\partial z} dz \\ \{dx^*\} &= [F]\{dx\} \end{aligned} \quad (5.14)$$

Thus,

$$[F] = \begin{bmatrix} \frac{\partial f}{\partial x} & \frac{\partial f}{\partial y} & \frac{\partial f}{\partial z} \\ \frac{\partial g}{\partial x} & \frac{\partial g}{\partial y} & \frac{\partial g}{\partial z} \\ \frac{\partial h}{\partial x} & \frac{\partial h}{\partial y} & \frac{\partial h}{\partial z} \end{bmatrix} \quad (5.15)$$

Using this equation and the mapping functions, the final deformation matrix is as:

$$[F] = \begin{bmatrix} 1 + \frac{\partial u}{\partial x} & \frac{\partial v}{\partial y} & \frac{\partial w}{\partial z} \\ \frac{\partial u}{\partial x} & 1 + \frac{\partial v}{\partial y} & \frac{\partial w}{\partial z} \\ \frac{\partial u}{\partial x} & \frac{\partial v}{\partial y} & 1 + \frac{\partial w}{\partial z} \end{bmatrix} \quad (5.16)$$

This deformation gradient vector can be broken down to 2 matrices.

$$[F] = [R][U] = [V][R] \quad (5.17)$$

The matrix R is called the orthogonal rotation matrix and U and V are symmetric matrices called right and left stretch tensors according to their position in the matrix multiplication.

The principle stretch ratios are found or calculated by extracting the eigen values of U and V matrices. Mostly this is not followed as it would require the value of rotation matrix R . Hence the value of the stretch ratio squared is found by obtaining eigen values of the Cauchy-green deformation tensor. C is the tensor given by:

$$C = [F]^T [F] \quad (5.18)$$

The square of change in length of each line element, is given by:

$$dS^2 = \{dx^*\}^T \{dx^*\} = \{dx\}^T [C] \{dx\} \quad (5.19)$$

Substituting the right stretch tensor () in Cauchy-green tensor ():

$$\begin{aligned} \text{As, } [R]^T [R] &= [I] \\ [C] &= [U]^T [U] = [U]^2 \end{aligned} \quad (5.20)$$

For finding the eigen values, *i.e.* the squared principal stretch ratios can be found by the equation:

$$\det \begin{bmatrix} (C_{11} - \alpha^2) & C_{12} & C_{13} \\ C_{21} & (C_{22} - \alpha^2) & C_{23} \\ C_{31} & C_{32} & (C_{33} - \alpha^2) \end{bmatrix} = 0 \quad (5.21)$$

This results in the characteristic equations of principal stretch ratios giving the values of I_1 , I_2 and I_3 as shown in the equation 5.2. Thus, the energy density function is calculated using the above stretch ratios, the stress-displacement, and force-stiffness matrices.

5.1.3 Nonlinearity of the Model

A Static nonlinear analysis is an investigation where a nonlinear relation holds between applied forces and displacements. These non-linear effects can originate from non-linearity of the material; *i.e.* elasto-plastic material, non-linearity of the geometrical model, *i.e.* large deformations, and contact between the braided sleeve and the inner tube, and the braided sleeve and reinforcement material in the case of bending. These effects consequence is a stiffness matrix that is not persistent during the load application. Such is in contrast to the linear static structural analysis, where the stiffness-matrix remains constant. Therefore, a different solving strategy is required for the non-linear analysis rather than the conventional

one. Appropriate model and solution parameters need to be specified considerably to obtain a successful converged solution.

The nonlinear behaviour of the proposed model is initiated from:

- Material nonlinearity
- Geometric nonlinearity
- Constraint/Contact nonlinearity

Material Nonlinearity

This involves the non-linear behaviour of a material based on a present deformation, previous deformation (history), rate of deformation, pressure, temperature and so on. Hyper elasticity is one of the examples of large strain material non-linearity. The behaviour poses a nonlinear problem, where the inner tube (bladder) in this model is of a hyperplastic material, hence the convergence of its elements; force and displacement pose non-linear issues.

Geometric Nonlinearity

In analysis involving this geometric non-linearity, changes in geometry as the structure deforms are considered in formulating the intrinsic and equilibrium equations. Many engineering applications require the use of large deformation analysis based on geometric non-linearity. Thus, geometry also plays a significant role in obtaining a successful solution.

Constraint/Contact Nonlinearity

Contact non-linearity in a system can occur if the kinematic constraints are represented in the model. Kinematic DOF of a model can be constrained by imposing restrictions on its movement. These can also be identified as the boundary conditions (BCs). The changes in BCs due to the deformations occurring in the runtime of calculations such as changing geometry, sudden contact of surfaces, or self-contact due to changing geometry.

The stiffness matrix that used in Lagrange contact was created in the following way: If a penetration of a slave node into the master surface is detected, another additional constraint is added to force, the node lies on the master surface exactly (Tur, Albelda, Manuel , & Ji, 2015). This problem of penetration poses a certain range of problems due to the other nonlinearity problems.

5.1.4 Contacts in FEA

In ANSYS or any FEA package, contact status is continuously changing nonlinearity status. That is because the stiffness matrix of the system depends on the contact status; when parts are touching or separated. Physically contacting bodies do not inter-penetrate. Therefore, the background programme must establish a relationship between the two surfaces in order to prevent them from crossing through each other during the analysis.

For nonlinear solid body contact of faces, Pure Penalty (integration point detection) or Augmented Lagrange (nodal detection) formulations can be used: both of these are penalty-based contact formulations:

$$F_{normal} = K_{normal} x_{penetration} \quad (5.22)$$

For a finite contact force F_n there is a concept of contact stiffness K . The higher the contact stiffness, the lower the penetration x , as shown in Figure 5.1.

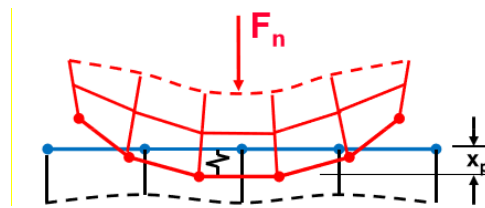


Figure 5.1. Contact compatibility

The main difference between Pure Penalty and Augmented Lagrange methods is that the latter augments the contact force (pressure) as:

$$F_{normal} = K_{normal} x_{penetration} + \lambda \quad (5.23)$$

Because of the factor λ , the augmented Lagrange method is less sensitive to the magnitude of the contact stiffness K_{normal} .

In Augmented Lagrange conditions, due to the large elemental contact between the sleeve and the bladder, the solution failed to converge in the slightest distortion or difference in penetration in different locations (elemental locations) on the same body between the contact surfaces; this is due to difference in the value of λ at these locations. The force convergence is based on reaction force calculations, balancing that become an issue when a contact problem like this occurs in the same body.

Other type of advanced formulations includes Lagrange multiplier formulation and also for the specific case of “Bonded” and “No Separation” type of contact between two faces, a multi-point constraint (MPC) formulation is available. This approach is not penalty-based or Lagrange multiplier-based. This formulation is used when the surfaces of contact regions are direct, and bonded, this formulation can be also used in large deformations.

As a solution for excessive contacts in same body, the pure penalty approach is generally used rather than the latter. The Pure penalty approach is used to attain the solutions for this model, where the detection method is chosen to be on Gauss element node points with penetration tolerance of 0.2 mm. This value is chosen in successive iterations of the model to achieve a reasonable convergence time in time-step iterations.

5.1.5 Contact Modelling of Actuator

Contact property between the inner tube and braided sleeve is defined as tangential to target in FEA simulation, with the approximated static friction coefficient. Contact force is estimated by summing all the normal forces applied to elements along the contact surface on the object. The weight of object that the soft arm is capable of handling then was estimated by finding the product of normal force and frictional coefficient. In the case of bonded contacts, there is no displacement between the layers of materials as in braids. The contact formulation in the proposed model is chosen to be Pure Penalty, where the penetration tolerance value is provided. This value is considered as a variable and it is modified according to convergence demand. However, in case of frictionless, the formulations are programme controlled.

When modelling pMAs the contact between the braided sleeve surfaces and the inner tube surface is considered as bonded for the fact that the pretension in the braided sleeve cannot be modelled. The same Pure Penalty formulation is applied. Whereas in the case of bending, the gap effect is predominant. *i.e.* the gap affects the bending angle of the actuator as well as the force. Thus, a frictional contact is provided with a static friction coefficient 0.2 (μ) as specified in the properties in Table 4.3 and shown in Figure 5.2.

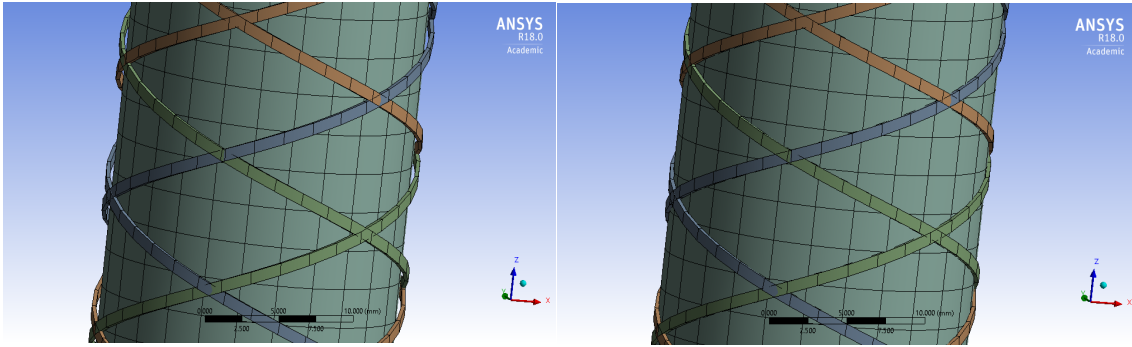


Figure 5.2 Contact Modelling of the pMAs, the left figure shows a gap between the inner tube and the braided sleeve, the right figure shows a bonded model

Table 5.3 Contact Properties

Braid	Braid	Bonded /Rough
Braid	Bladder	Frictional/Bonded
Braid	Thread/plastic rod	Frictionless /Rough
Bladder	Thread/plastic rod	Bonded /Rough
Caps	Braid	Bonded /Rough
Bladder	Braid	Bonded/Rough

5.1.6 Braided Sleeve and Element Type Controls

Solution convergence depends on the mesh uniformity and profile. The convergence should be obtained in minimum number of elements for minimal time of solution. Sleeve threads were modelled as surfaces and then the programme-controlled mode of meshing is using the SHELL181 Finite Strain Shell elements that are largely used for bending degree of freedom. Using the MPC technique, ANSYS generates internally some coupling equations to establish the correct kinematics at the coupling point. The coupling point between SOLID 185 of cuppings and the SHELL element were defined as MPC bonded contact points similarly. Shell elements based on the REISSNER MINDLIN theory were considered taken into account the shear stress distribution over the thickness. As a consequence of that these elements typically show softer deformation behaviour.

For the bladder geometry, SOLID186 Homogeneous Structural Solid Element is used with Hex Dominant method. The end caps are defined as SOLID 187 Tetrahedral elements. Modelling the braided sleeve is adaptive and uniform with body edge and face sizing to produce mesh with minimum elements. As shown in table 5.4, as here the shell elements of sleeve are more than the number of nodes.

Table 5.4. Nodes and Element sets of pMA

PMA	Threads no.	Nodes	Element
Contractor	7	32114	120453
	5	15013	33469
Extensor	7	47392	142056
	5	24215	23968

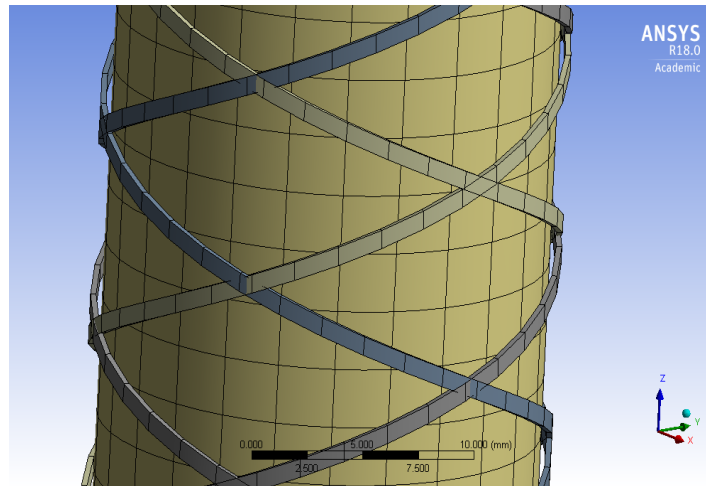


Figure 5.3. Braided sleeve modelling

It is observed that the skewness is not criteria for getting the convergence. As long as the surface of the body is uniformly meshed with tetrahedrons preferably or hexahedral elements, the solution is supposed to provide a smooth and continuous deflection. Although, while modifying the mesh it is necessary to be meticulous on fact that more distribution of number of elements over the element matrices would lead to difficulties in transferring loads to elements. Also, as the large deflection is switched on, the distortion of the elements due to loads would lead to increased skewness in each step. A solution in light of this problem would be increasing the number of elements keeping the mid-side nodes. This will improve the accuracy. But the randomness in volume mesh sizes would again pose a problem in skewness. So, a balance of element sizes and skewness along with uniform face sizing will generate the mesh for finding solution for all pressure loads. When the mesh is over refined, the areas of peak strain become more distorted than with a coarser mesh, becoming more prone to failure. Thus, this process involves iterations of meshing and refining. Skewness should be maximum. In Static structural analysis, an option of nonlinear adaptive remeshing is available to ensure against the failure. This increases the remeshing in the areas of more skewness and distortion. But as this analysis is limited to already converged and solved

models and difficult to incorporate in an unsteady model, hence this feature has not been considered. Multizone meshing with Hexa mapped mesh and tetra free mesh along with face sizing of 0.8333mm and other faces with necessary sizes and body sizing are provided to obtain the mesh for the body as shown in Figure 5.4. More the uniform mesh, better convergence characteristics of hyperplastic materials.

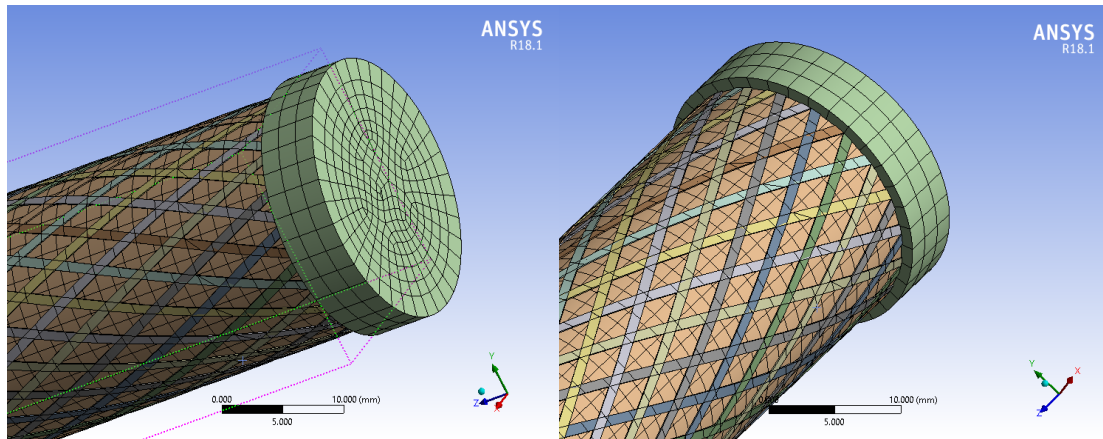


Figure 5.4. Hexa-mapped mesh and tetra free mesh

5.1.7 Boundary Conditions

For simulating the fluid structural interaction, it is important to consider the right conditions of the experiment onto the model. The inside of the bladder is imposed with a pressure value to replicate the actuating scenario. The magnitude of pressure is ramped to the required value in certain interval of time. The change in the interval of actuation has little or no effect in case of Static Structural Analysis. However, changing the time interval and the time steps assists in convergence of the actuation. Other than pressure loads, the fixed support and the standard earth gravity load play an important role. The fixed support is specified for the open end of the actuator on the end cap where the inlet is connected. The actuation is observed over the motion of the other end of the actuator; the same end of the braid is also provided a fixed support as constructed experimentally. The corresponding edges of the braid of the model is approximated the fixed support boundary condition. The gravitational load on the bodies is provided in the cases of bending actuation but not in case of extensors and contractors. As the bodies are assumed to be in horizontal position, the effect of gravitational load is minimal and can be neglected as shown in Figure 5.5, Where (a) is pressure at certain level, (b and c) are fixed supports, and (d) is displacement.

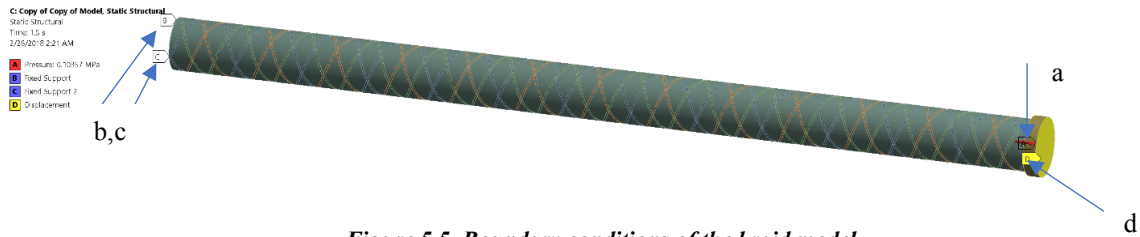


Figure 5.5. Boundary conditions of the braid model

5.1.8 Convergence Criteria

The following Figure 5.6 shows the force convergence at each time steps with corresponding iterations. The force criterion is specified to be a percentage of the exact energy balance, because of the nonlinearity of the model. Thus, iterations are conducted for each time step. Energy put into the model through loads roughly should be equal to the energy output of the model through reaction loads. So, the convergence criteria define how close to this exact balance is acceptable. An unbalance of about 40% is allowed in the simulations done on all models. The convergence criteria are 60% of force convergence. $F = 0.6 F_{\text{actual}}$, thus, the force is converged.

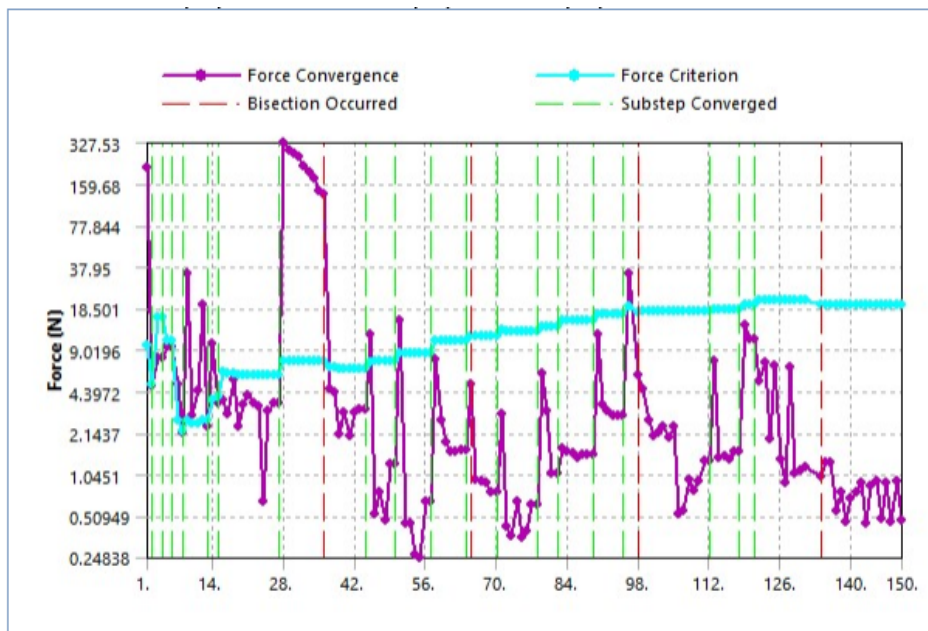


Figure 5.6. Force convergence with respect to number of iterations and number of sub steps

5.1.9 Mathematical Formulation

The gap between the braided sleeve and the rubber inner tube is necessary for the actuator to work like an extensor, contractor, bending contractor, or bending extensor. The major difference between the contractor and the extensor is the pretension on the sleeve. When the length of inner tube and braided sleeve are equal, the helix angle of the braided sleeve is less

than 54.7° , it behaves as a contractor. While in the extensor the length of the braided sleeve is greater than the inner tube length to form an angle greater than 54.7° .

This relationship has been proved analytically as well as through the data. One of the reason behind this behaviour is that the braided sleeve is always in contact with the inner tube. At even an instant of bladder expansion, the sleeve restricts further by constraining and transferring the strain energy in expansion to that in changing the helix geometry of threads in sleeve, eventually producing tension in itself and enduring all the stresses that is imposed on it in this restriction. This produces a twisting action along with compression of the bladder.

While in bending pMAs, when the inner tube touches the braided sleeve, the braided sleeve it starts to restrict the expansion or contraction. The initial bending can be expressed by a cantilever beam subjected to uniformly distributed load on one side, causing bending on the other. In bending extensor; the pMA bends towards the side of the inner tube that is in contact with a restricting material with less Poisson's ratio and Young's Modulus like plastic or a nylon thread. However, in bending contractor, the pMA bends on the opposite direction of the restricting material layer (plastic rod). The bi-material expansion elevates the bending effect, the bending equation for bending displacement can be simply given as:

$$\frac{\partial^2 y}{\partial x^2} = \frac{Wx^2}{2EI} \quad (5.24)$$

The equation of radius of curvature is given as:

$$R = \left(\frac{\partial^2 y}{\partial x^2} \right)^{-1} \quad (5.25)$$

The bend is not of a constant radius of curvature and hence varies with expansion and bend angle. The differential equation for this is given as:

$$L = R\theta \quad (5.26)$$

$$\frac{dL}{L} = \frac{dR}{R} + \frac{d\theta}{\theta} \quad (5.27)$$

The relation in energy conservation is given as:

$$F = P \left(\frac{dV/d\theta}{dL/d\theta} \right) \quad (5.28)$$

Hence it is shown that the tension force on the braids is directly proportional to the change in volume and inversely to the change in the length of the assembly. The relation between the braided sleeve length and the length of the inner tube with respect to the helix angle equation (5.29), representing the diameter too in terms of braid length equation (5.30). Also, the relation between the length of the actuator and the helix angle is given as below. Where b is the length of the threads in the braided sleeve.

$$L = b \cos \theta \quad (5.29)$$

$$V = \frac{\pi D^2 L}{4} = \frac{b^3}{4\pi n^2} \sin^2 \theta \cos \theta \quad (5.30)$$

In the case of contractor pMA, substituting after differentiating the variables, the force is given as:

$$F = \frac{P b^2}{4\pi n^2} \sin \theta (3 \cos^2 \theta - 1) \quad (5.31)$$

This equation states some specific conditions of the model. The strings of the sleeve will have 0 tension only when they break off. Hence when $F = 0$, the angle attained is 54.74. If the angle is increased above this value, then the tension increases causing extension. Whereas if the angle is decreased, the tension is negative, resulting in contraction action.

Assuming the whole of the work in changing the volume of the bladder is provided by the pressure forces on the faces, the relation in energy conservation is given as:

$$F = P' \left(\frac{dV/d\theta}{dL/d\theta} \right) \quad (5.32)$$

5.2 Novel Model for contraction Muscle

The experiments on the contractor are based on a specific model dimensions and the same has been followed in the 3D geometry considerations. The experimental model has a length of about 30 cm and the diameter of 2 cm. When all the components of the model are assembled, the cross section at the middle of the length had the diameter of about 1.6 cm. This is mostly due to the pretension produced in the sleeve when the sleeve length is not larger than that of the tube. The change in the cross section is unpredictable and hence cannot be accurately 3D modelled. It is assumed that the tube bladder is of uniform concentric circular cross section. While the sleeve is modelled to be consisting of a certain number of threads. This is only to simplify the model. The whole braided configuration is complex with

numerous amount of contact surfaces with self-contacts. The contact property complexity is neglected and so the contact modelling is simplified by considering specific thread number. Specific contacts are modified to be frictionless, frictional and rough as well, which is further explained in detail.

5.2.1 Braided Sleeve Model

Modelling of the sleeve geometry is complex with intersections, to simplify the model, each of the thread is assumed to be of perfect helical shape. The helix, in case of contractors, has 2 revolutions and a pitch of 150 mm making the total length of 300 mm and diameter larger than that of the tube in the case when gap is provided. When the gap between the sleeve and tube is not considered, the helix is of 2 cm diameter. By this configuration, the helix angle comes to around 22° , which is in the range of angles to provide the contraction action; the only major difference between the contractor and extensor model is the helix angle.

The threads of the braided sleeve are specifically made of surface bodies with negligible thickness. ANSYS considers surface bodies to be specifically assigned the SHELL 181 type elements. This simplifies the 3D CAD model even further. Also, the threads are defined as PET (polyethylene terephthalate).

Another important part of the pMA model is the endcaps that are connected directly to the end of the tube.; which are made of structural steel material. The dimensions of these are similar to the steel caps used in the experiment. Although the weight of the caps is dependent on the volume, which in turn is dependent on the length, it was observed that the weight effects on the actuations between a range of values are negligible. Hence an arbitrary length of 20 mm was assigned to the end cap. While the diameter is larger than that of the sleeve diameter. It is assumed that the tube is hollow and closed by the steel cap. The direct connection is assumed to be a bonded contact in ANSYS Non-linear Structural analysis. The interface between the two bodies is not singular but defined by the meshing elements as two walls. The sleeve is meshed in hexahedral BRICK elements whereas the capping's made of Tetrahedral 3D solid elements.

The other end of the actuator is not connected to any material as it is assigned the fixed support Boundary condition. As in case of experimental study, only one end of the model shows actuation motion while other is fixed. Hence the sleeve thread ends, and the tube end are given fixed boundary condition while the other end cap provides desired motion.

5.2.2 Thread Study

Representing the sleeve in terms of number of threads pose some problems. This means the number of threads adds up as a variable, so the amount of deformation in the actuation depends on the thread geometry as mentioned before as well as the number of these. Considering couple of threads as a set, the stress and deformation depends on these sets. Hence at first the comparison thread study is made, and observations were made to provide conclusive explanations.

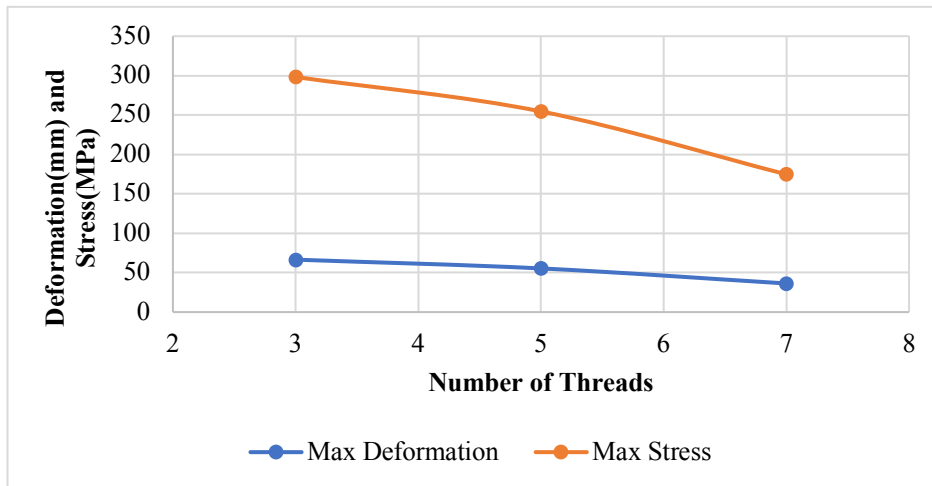


Figure 5.7. A comparison of threads number of the contraction pMA at 1 bar against the deformation and the stress; the blue curve shows the max. deformation, and the red curve shows the max. stress.

Figure 5.7 and 5.8 provides the approximation in effects of number of threads in meshing, deformation and stress. In the case of contractors, the study was done for 1 bar of pressure on the inside surfaces of bladder. These results are compared with that of the experimental. When the pressure is constant, the increase in number of threads led to more accurate and realistic results in terms of deformation, while the maximum stress on the sleeve decreased. The stresses induced over the sleeve is distributed in the threads, and as that number is increased, lesser the possibility of the sleeve failing in operation. The maximum stress did not cross the ultimate tensile limit, though at higher pressures the shear stress produced in cross sections would be enough to break the threads.

Creep effects have been neglected in these computer models. In higher temperature environment (about 50-100°), the properties of PET changes and these effects dominates leading to pre-tensed failure of sleeve.

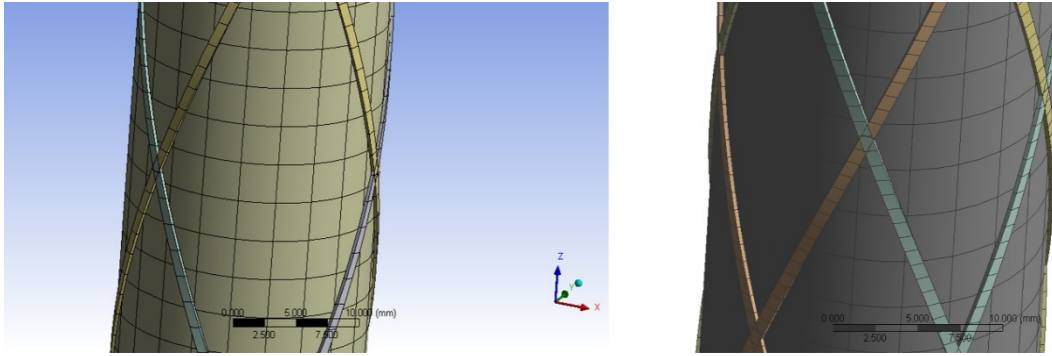


Figure 5.8. Contraction pMA at 1 bar with different number of threads.

5.2.3 Contraction pMA: Displacement vs. Pressure

Pressure based study followed the thread-study to observe the relationship between deformations stresses and forces. The computer model is subjected to the boundary conditions as mentioned in the previous section, in addition to which is the varied pressure on face. The pressure is discontinuous, meaning that for each observation, the pressure is ramped from 0 to the required in the sufficient pseudo time-steps of 1E-4 seconds over 1second of calculations. Figure 5.9 shows the curves for the experimental data and computer model calculation data in the case of contraction pMA.

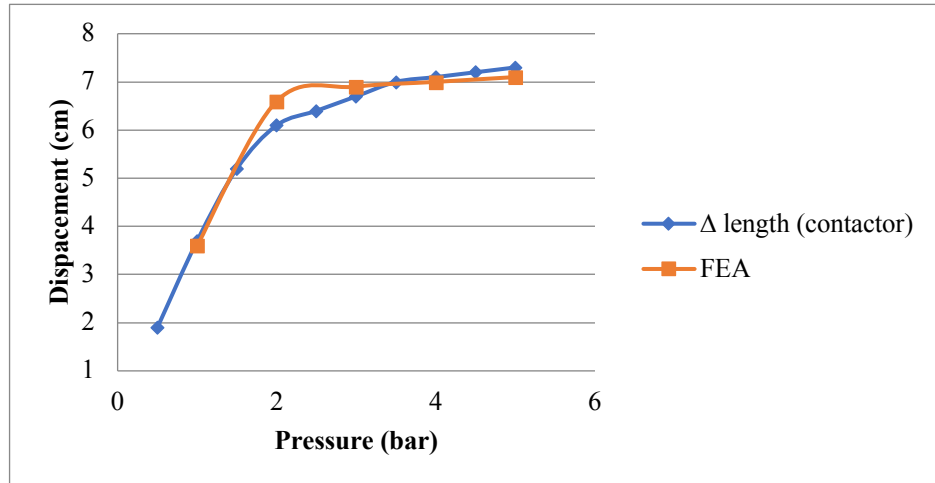


Figure 5.9 A comparison between FEA and experimental results to show the displacement at different pressure levels; the red curve shows the FEA results; the blue curve shows the experimental results.

The plot provides observations in good agreement of the experimental and finite element simulation data. The curve although follows a predictable trend in all designs of contraction pMA. But for this design specifically, it follows a curve predicted by Equation. For almost all size of pMA, the behaviour of deformation with respect to the pressure is always quadratic in nature.

$$y = 0.3174825 + 3.620932 * x - 0.4620047 * x^2$$

$$y = -0.1202797 + 5.012044 * x - 1.191608 * x^2 + 0.0972805 * x^3$$

Cubic equations tend to show more agreement in the curve fitting as shown in Figure 5.10.

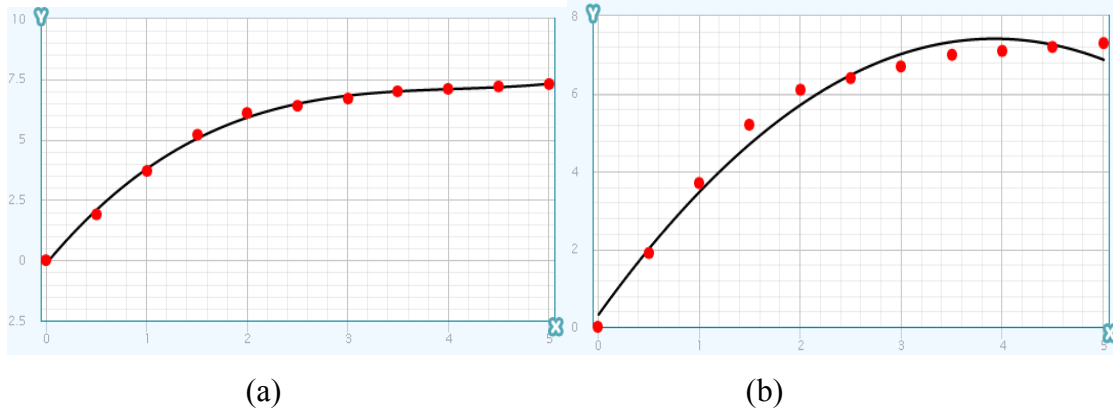


Figure 5.10 Curve fitting showing better approximation by quadratic representation over cubic, (a) quadratic, (b) cubic

This shows that the contraction pMA displacement is quadratic in nature and will dampen down to a maximum value where any increase in pressure will enhance the stresses to the point of bursting. The maximum displacement at 0 load is the maximum load carrying capability of the muscle which can be defined as load-capability ratio given as:

$$\text{Load - Capability ratio} = \frac{\text{Maximum displacement}}{\text{Pressure at zero slope in displacement Pressure plot}} \quad (5.33)$$

The LC ratio by the experiment is 2 whereas by FEM is 2.8. More the LC ratio signifies more strength and usefulness of the muscle. Hence less wastage of pressure energy. Whereas less the LC ratio, more energy losses in application.

Figure 5.10 shows the FEA deformations of contraction pMA at 3 and 5 bars. These observations are based on the model of 5 threads that is assumed enough to accurately represent the experimental model. The threads of PET provide enough constriction to compress and express useful work during one cycle of work, the maximum stress and deformation as expected is found to be at free end cap.

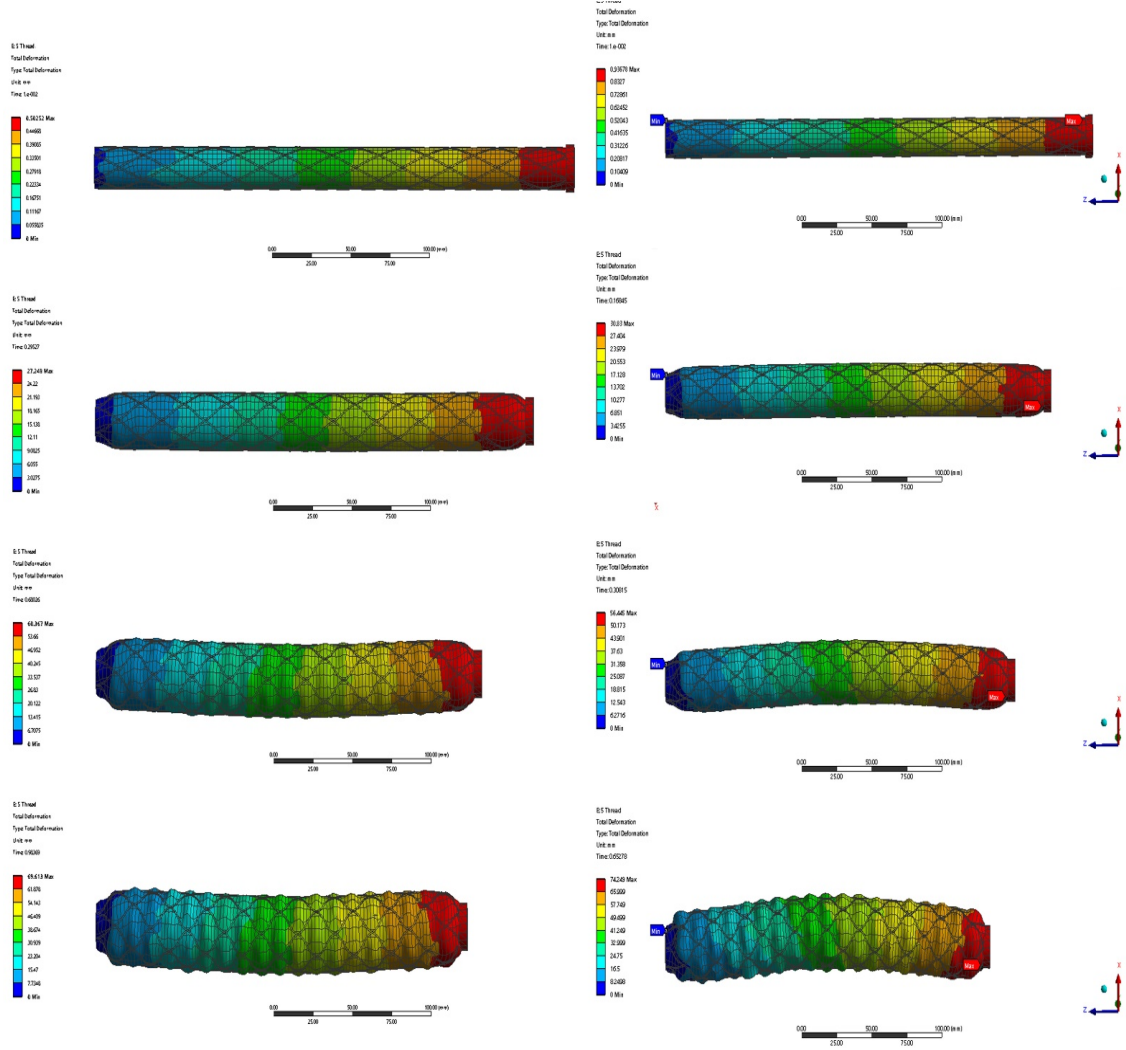


Figure 5.11. FEA deformations of contraction pMA at 3 and 5 bars

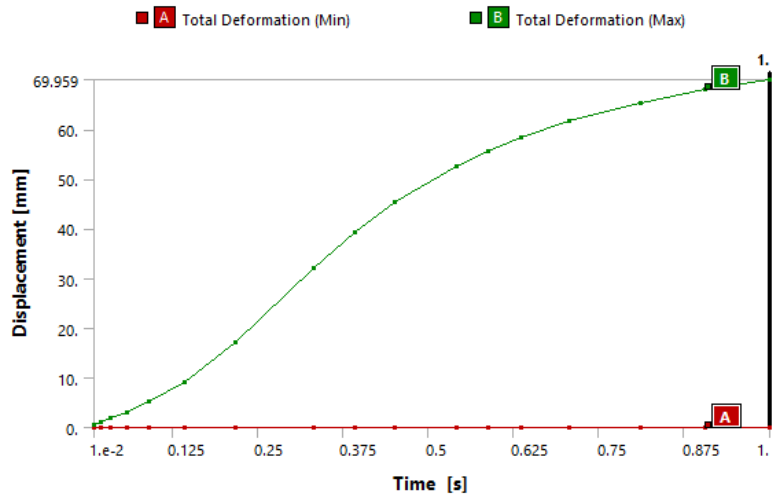


Figure 5.12. The deformation with respect to the time

When the pressure profile is ramped to a certain end pressure in static structural for a certain model end expected pressure, the deformation with respect to the time is observed to be as shown in Figure 5.11. The initial deformation is slow in time, and when the restriction time passes excessive relaxation in material leads to steep deformation in time. After a Threshold pressure at the end of relaxation time the slope decreases showing slow deformation. This is a case at all iteration of simulations with end pressures 1,2,3,4 and 5 bar. The curve is true for all and has also been found to be similar to the experimental curves.

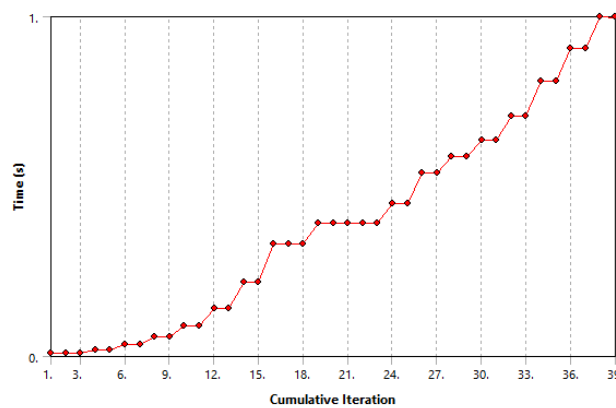


Figure 5.13. Iterations to enhance contact convergence

Most of the rubber modelled nonlinear material components face convergence issues that are resolved by introducing more number of substeps. But in this methodology the variable in iterations were time steps. Time stepping is allowed to be of variable spacing and to counter contact nonlinearity, bisection of time step is also allowed. This bisection allows time step variability at contact regions where penetration is more. Figure 5.12 describes the iterations followed in the same time step to enhance contact convergence.

5.2.4 Contraction pMA: Force vs. Pressure

Most of the elastomeric materials have rapidly changing strains in particular directions when bombarded with external forces because of high poisson's ratio. This changing strain is to counter the residual stresses; restriction of the strain with high strength low strain materials allows these materials to withstand these external forces without much deformation. Hyperplastic materials act the same; the force that can be used to counter the deformation is calculated by the stresses acting on the given surface while facing the deformation. In this case the deformation is the displacement of end caps. This is a novel type of contractor actuator where the sleeve bladder material combination can be used as muscle to do work in handling forces in displacements. The data calculated from the FEM solution at each node is

compared with the experimental data. A separate boundary condition of force is used for the same purpose in providing the same displacement using the equation:

$$F = P * (\pi * r^2) \tag{5.34}$$

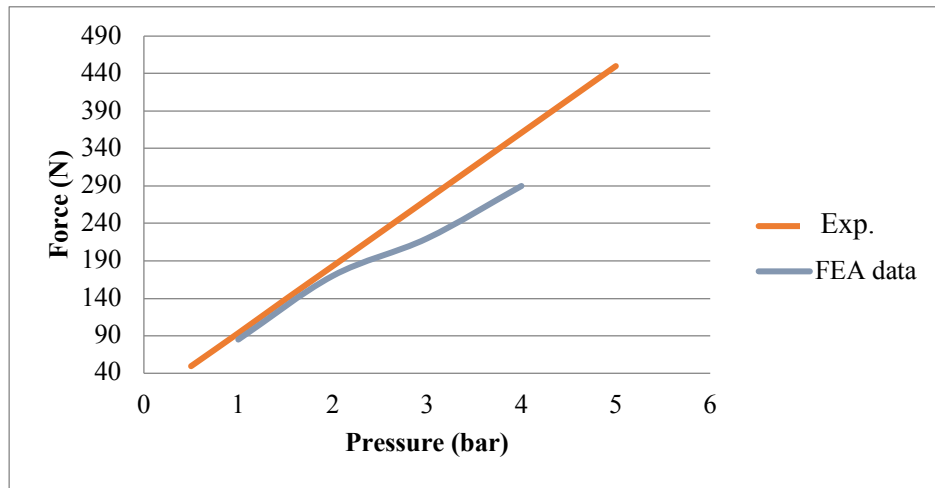


Figure 5.14. A comparison between the experimental results and the FEA results

5.2.5 Stress Observations

Most of the elastomeric materials have the tendency to provide deformations of higher than 300% of its own dimensions. Hence it is safe to say that chance of bursting is less. Although, hysteresis losses are a factor that has been not considered in this study. One of the side effect of over-pressurising a muscle for higher load bearing capacity will results in weakness of the material itself due to heat produced in friction between layers of materials leading to minor molecular random rearrangements and hence energy losses. The hysteresis of the muscles can be studied further, the peak stresses that a contractor experiences over the course of time defines the life of the actuator too. Figure 5.14 shows a stress and strain plots are indicators of maximum and minimum areas indicators of future failures.

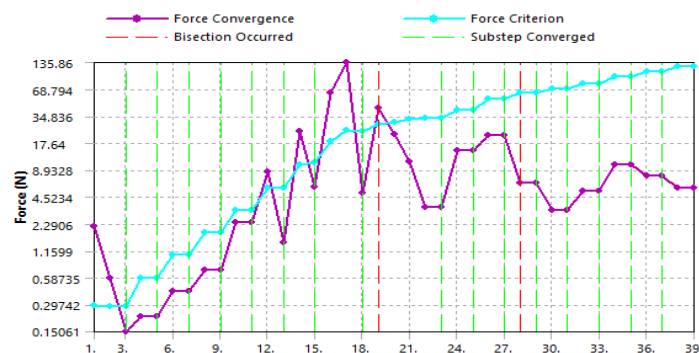


Figure 5.15. Stress and strain plots, that shows the force convergence, force criterion, and substep converged

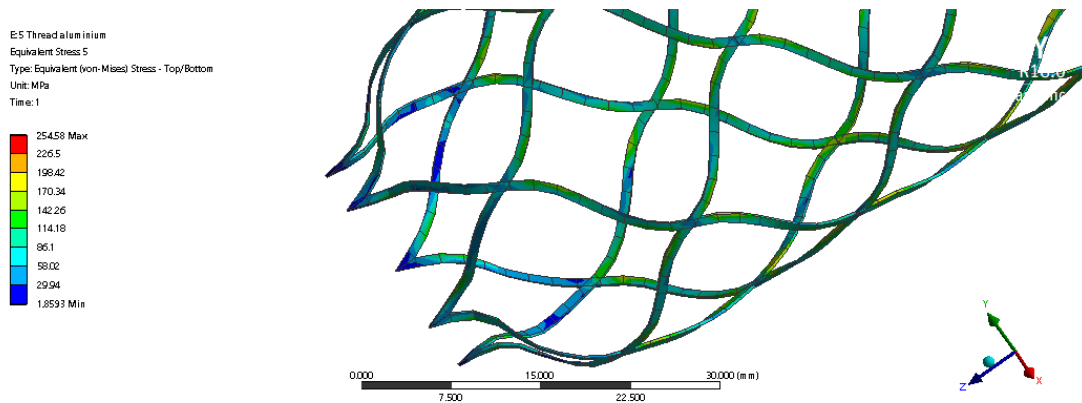
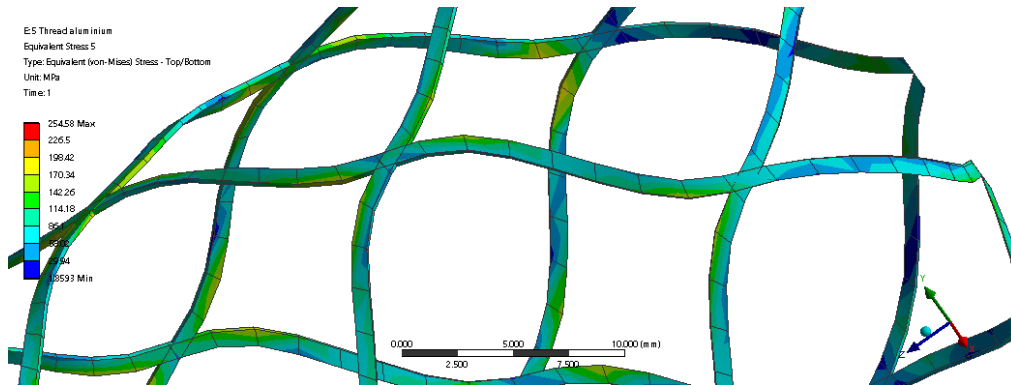
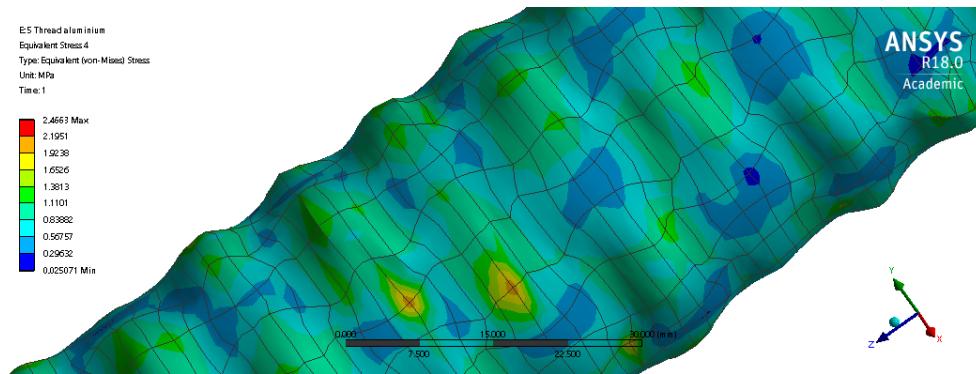
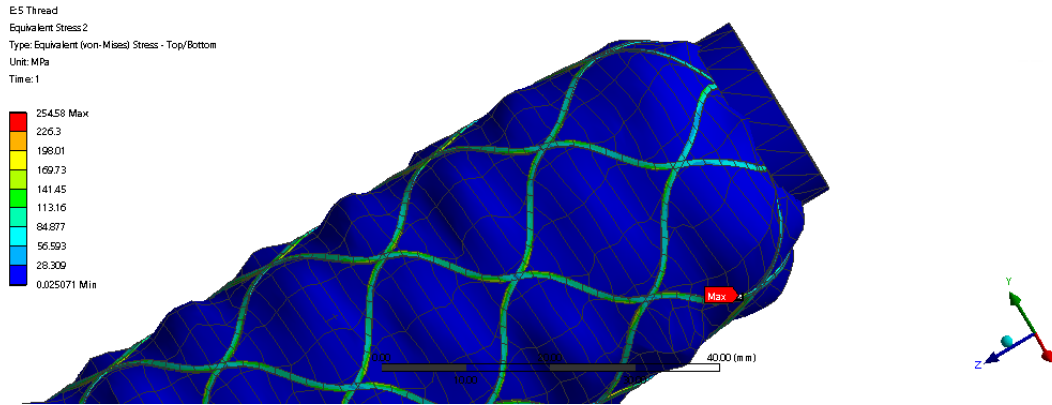


Figure 5.16. A close observation on the stresses provides insights on the probable failure regions

Figure 5.15 shows A close observation on the stresses provides insights on the probable failure regions. The maximum stress is found in the thread *i.e.* 0.254 Gpa of stress. This high value indicates the overstretched nature of the material and exposes it to chances of tear on warping. The stress on the tube is only 2.56 Mpa that is much less compared to that of threads. Hence it is shown that the chances of thread failure are more in contraction pMA. The gradient also shows the changes in stress over the notch regions over the regions away from crossings.

5.3 Novel Model for Extension pMA

The experiments on the extension pMA are based on a specific model dimension and same has been followed in the 3D geometry considerations. A Novel extension pMA has been also been simulated to provide the extension values by numerical calculations. This uses FEA equations that have been mentioned in contractor section. The geometry of the extensor model is the same and has a length of about 34 cm and the diameter of 2 cm. The cross-section is bulged in after the assembly in the experimental model. This is mostly due to the slack produced in the sleeve when the sleeve length is much larger than the tube in contrary to contractors. The change in the cross-section is unpredictable and hence again cannot be accurately 3D modelled. So, the cross-section is assumed to be constant, although two cases are compared where there is a gap between the thread and tube and the other when there is none. Along with this another variable *i.e.* the number of threads has also been considered. This is only to simplify the model; the whole braided sleeve configuration is complex with numerous amount of contact surfaces with self-contacts. The contact property complexity is neglected and so the contact modelling is simplified by considering specific thread number. Specific contacts are modified to be frictionless, frictional and rough as well which is explained in previous sections.

As shown in Figure 5.16; gapping between the sleeve and the tubing is used and solved that posed many contact convergence problems. It is due to the nature of the contact, where the tube was given the 'Contact' property and the sleeve thread the 'Target' property.

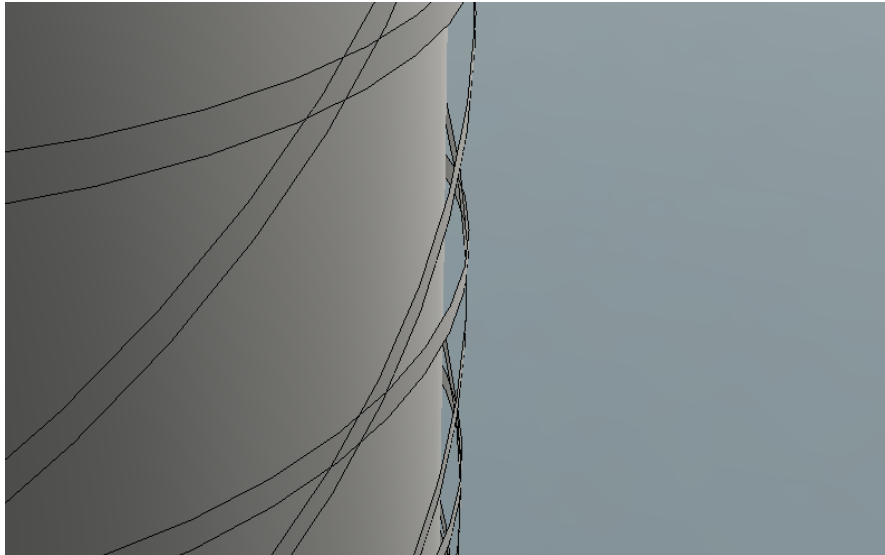


Figure 5.17. Gapping between the braided sleeve and the bladder

This helps in determining the minimum penetration in pure penalty method that updates the stiffness aggressively at each successive nonconverted iteration. The nature of in total 42 contact regions for 7 thread model to immense nonlinearity in stiffness matrix. This failed to provide solution in further iterations. This led to unconverted solution at the required time steps that can be illustrated in the Figure 5.18 with the 0.5 converged relaxation time. The deformations at each node is calculated to the last converged time step. Hence the steep line after 0.5s. This simulation is done in 5 bar for 1s in the model with gap inclusive.

Due to this unstable nature of the model, the gaps are neglected in the next iterations and initial contacts were produced with sleeve and tube nodes coincident.

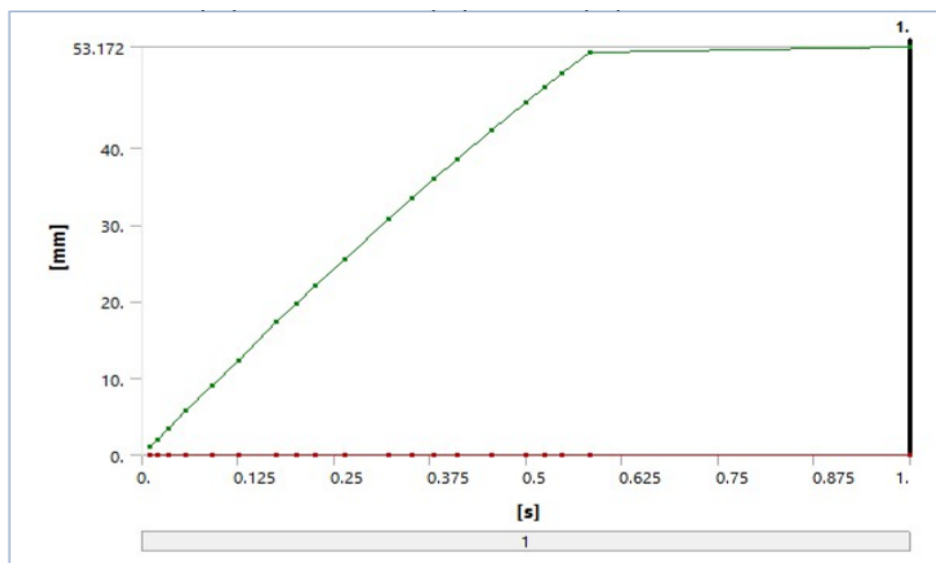


Figure 5.18. The deformations at each timestep

5.3.1 Thread study

Similar to the issues in contractor study, representing the sleeve in terms of number of threads pose some problems. This means the number of threads adds up as a variable. So, the amount of deformation *i.e.* the actuation depends on the thread geometry as mentioned before as well as the number of these. Considering couple of threads as a set, the stress and deformation depends on these sets. Hence at first the comparison thread study is made, and observations are made to provide conclusive explanations.

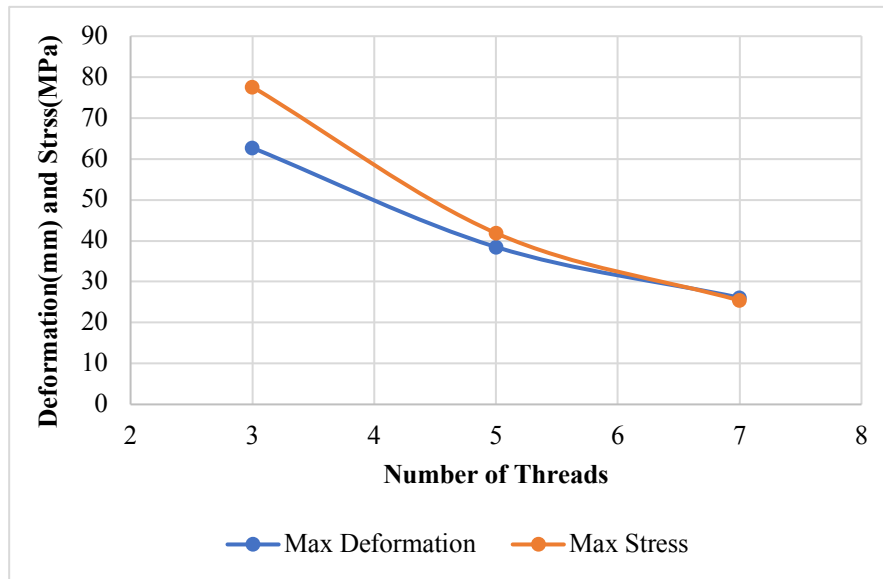


Figure 5.19. A comparison of threads number of the extension pMA at 1 bar against the deformation and the stress; the blue curve shows the max. deformation, and the red curve shows the max. stress.

On the 1 bar study of extensors, the relation is somewhat inverse of that of contractors. The less the number of threads would lead to less restriction in extension and hence more displacement of the actuator tip.

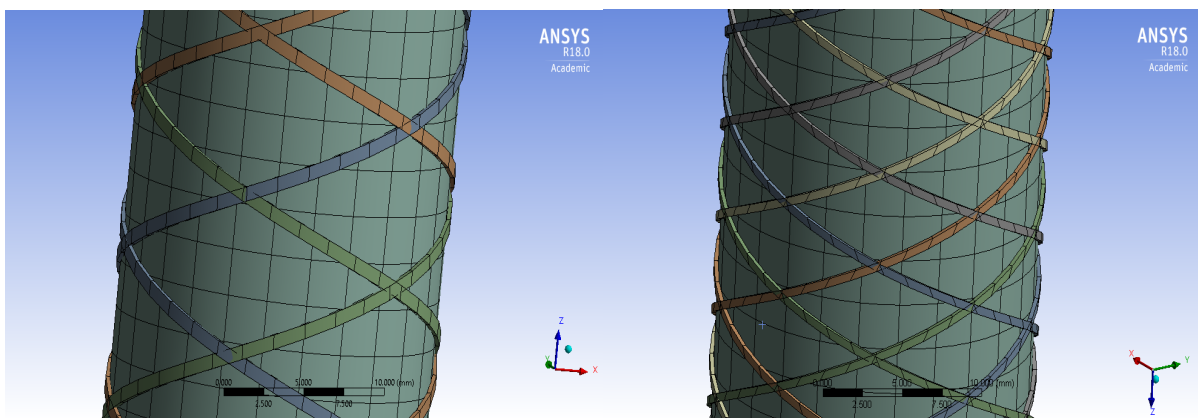


Figure 5.20. Extension pMA at 1 bar with different number of threads.

Though the deformation, the stresses on sleeve in this case is much lower than that of contractors that indicate larger longitudinal strain enhancement possibilities. In experimental study, the extensor sleeve of 80cm is made into 34cm that caused relaxations on the sleeve in actuation concentrating all stress due to pressure, on the bladder itself. This pre-relaxed nature of extensors could not be represented in computer model leading to a degree of divergence from experimental result and hence lesser deformations. Although, the behaviour can be accurately predicted in simulations.

Figure 5.19 shows the difference in the extension produced in models with different number of threads. The number of nodes and elements increased as the threads increased, so does the matrix distributed space in drive and also the calculation time. The mesh study for this part is not done as it is irrelevant to the type of elements used. The SHELL 181 elements were given a minimum size of 0.1mm and decreasing that exponentially increases run time and space. Also, the refinement in mesh would be redundant as more shell elements will be ineffective to the solution.

Hence a simple hexahedral mesh is chosen for the hyperplastic tube and shell elements for the threads. The analysis settings are same as that used in contractors, but rough contact is used between the sleeve and bladder. Frictionless contacts gives diverged solution as the slippage between the sleeve and tube would be nonlinear, and thus uneven deformations thought the sleeve. Rough contact restricts the tube elements to have even deformations between each thread.

The thread study is done, and it is observed that the increasing threads drastically effects the elongation. Figure 5.21 shows the deformation at different pressures namely, 1,2 3, and 5 bar, the deformation is closely related to that of experimental and has a slight offset.

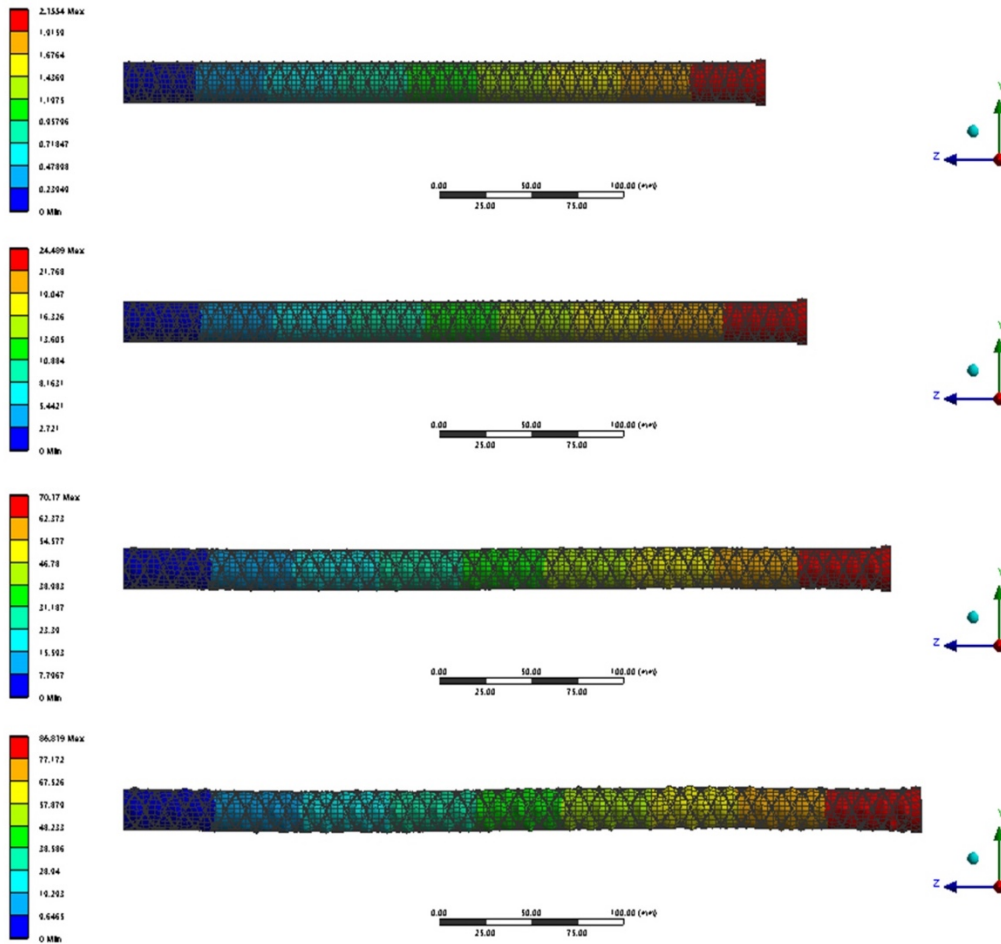


Figure 5.21. The deformation at different pressures for extension pMA

5.3.2 Extensor displacement- data

Boundary conditions as mentioned above that are used to model the extensor, the pressure is discontinuous, meaning that for each observation, the pressure is ramped from 0 to the required in the sufficient pseudo time-steps of $1E-4$ sec over 1second of calculations. The shows the curves in experimental data and computer model calculation data in the case of contractors.

Figure 5.22 shows deviation in the extensor change in length with respect to the experimental result is because of the neglecting of the gap which is deviation from the real experimental model. Hence pretension and slack of sleeve are major contributors in the motion produced. The curve although follows a predictable trend in all designs of extensor actuator. For almost all size of actuators, the behaviour of deformation with respect to the pressure is always quadratic in nature.

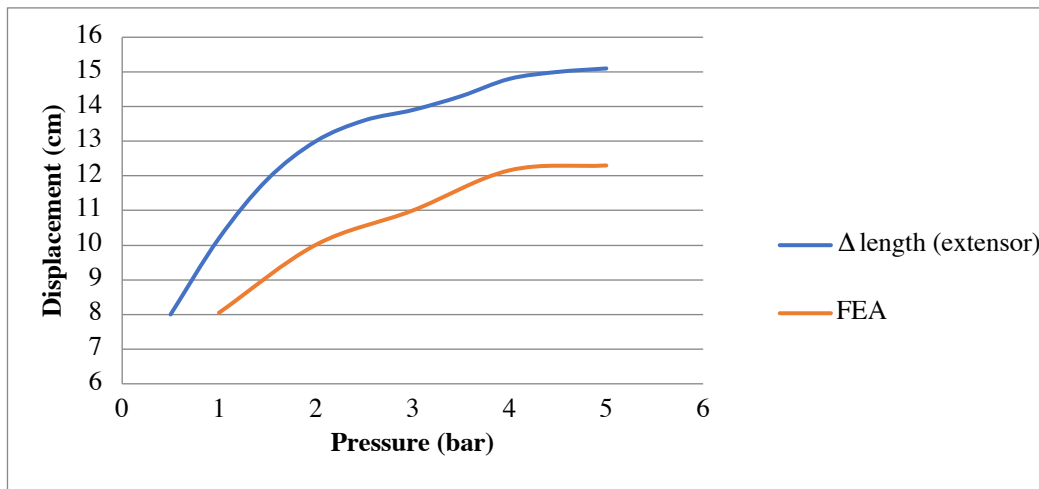


Figure 5.22. A comparison between the experimental results and the FEA results in the extensor change in length.

5.4 Summary

It was necessary to adopt a reference experimental model to validate the numerical model. A prototype has been designed and built according to the classical scheme of McKibben. A model validation is carried out by a comparison of experimental and numerical results in quasi-static and isometric test. The same values of the basic parameters of the experimental McKibben are implemented into the FEM, for counting the exact number of nodes and elements. The results of the contractor pMA in both cases numerically and experimentally behave the same, with a small deviation. However, the deviation in the extensor change in length with respect to the experimental result is bigger. This difference is because of the friction between the bladder and the braided sleeve, threads in the braided sleeve. contact between the components. There is a good agreement between the numerical and the experimental results; the number of the threads plays a significant role deformation. When the number of threads increases the deformation increase as it depends on the thread set. The construction of pMA numerical model, implemented by FE using ANSYS software and other softwares' such as Fusion 360 and 3D CAD, was based on different parameters such as the internal diameter of the tube, thickness of the bladder, axial and diagonal braid structure, the helix angle, of the mesh, the length of the pMA, and the end caps.

The bladder made of butyl rubber, is modelled by the two coefficients Moony-Rivilin formulation ($C_{10}= 0.0694$, $C_{01}=0.0628$) and the material of the braided sleeve is PET, and a strand made of 5 and 7 threads. The obtained results in this model suggest that this model can be used to predict the behaviour of the pMA.

6 CONTROL OF THE SOFT ARM

The proposed prototype is made of 3 bending pMAs as mentioned in chapter 3: Mechanical design of the soft arm. An elbow soft arm range of motion varies from about 0° to 180° , under its best conditions. A control system is needed in order to perform the required tasks; *i.e.* extension and flexion (for filling and for discharging). In the form of pressure pulse, the compressed air flow into the muscles through the solenoid inlet valve and that way the resulting pressure (P) in the muscles is manipulated variable with different values from about 0 to 5 bar. The throttle valve is used to adjust the actuator dynamics and the outlet solenoid valve is used to discharge muscles. To control the bending angle of the proposed pMAs (angle of rotation arm (θ)) the pressure is controlled via a solenoid valve through a balance of both tensile forces depending on load (m) and the air pressure in each muscles of the actuator arm. The pneumatic system of the wearable soft arm is a classical pneumatic system for output bending angle.

6.1 Pneumatic System Design

Pneumatic system is designed to control the air flow required to operate the proposed pMAs. The following components in Figure 6.1; a schematic overview of the complete pneumatic system is shown. Figure 6.2 shows the Pneumatic diagram of the experimental setup of the actuator, the following components were utilised in the pneumatic system:

- Tubes
- Connectors
- Pneumatic Muscle Actuators (pMAs)
- Solenoid Valve
- The driver's circuit
- Pressure regulator
- Pressure Sensor

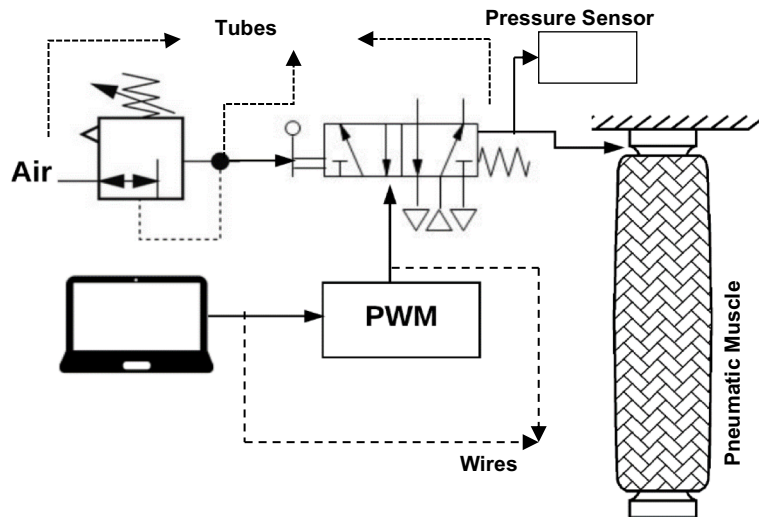


Figure 6.1 A Schematic Representation of the Pneumatic System Setup

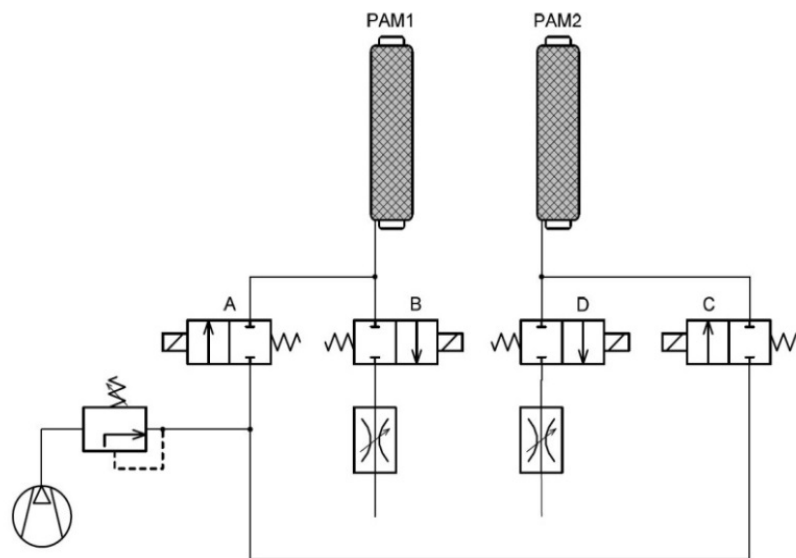


Figure 6.2. Pneumatic diagram of the experimental actuator

The programmable solenoid valve is used to control the air flow to perform the two rehabilitation tasks flexion (inflation), and extension (deflation); as it is a simple on/off valve type. The MATRIX 3/3 750 series solenoid valve, normally closed valve that can vent or fill actively, with four ports is controlled by the PWM signal from the control unit - Arduino UNO (Mechatronics). In addition, the pMAs maintains in its position without consuming energy due to the valve nature. The valve shown in Figure 6.3 below has many advantages, see appendix (C):

- Compact dimension
- Short response time

- Insensitivity to both frequency work and vibrations
- Low absorbed power
- Precision, repetitiveness, flexibility and long operation life.

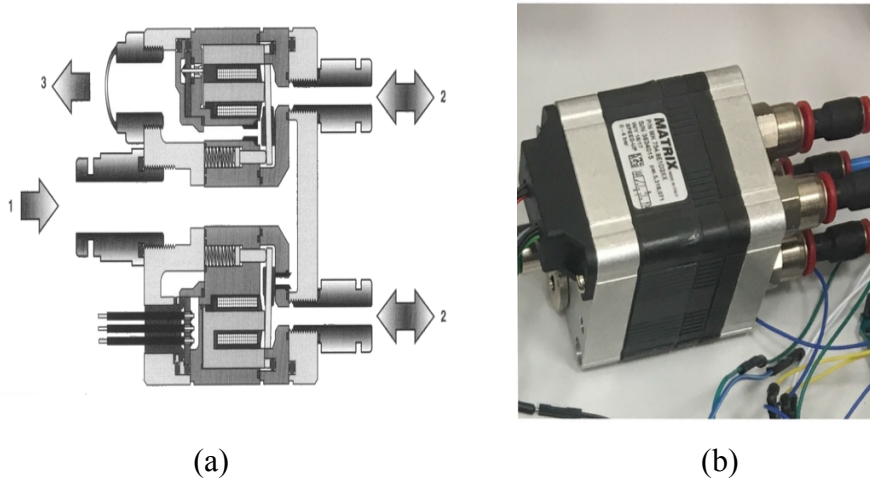


Figure 6.3 A MATRIX3/3 750 Series Solenoid Valve, (a) is a schematic MATRIX valve showing the 4 ports, (b) the solenoid valve.

A closed-loop direct control method, proportional, integral, and derivative controller (PID) is used to control the pressure in order to obtain the desired bending angle of the pMAs. This is achieved by using a pressure transducer sensor in the pneumatic circuit, and pulse width modulation (PWM), and a driver's circuit. The driver's circuit (board) provides an interface between the solenoid valve and the control unit. The solenoid valve requires 24 v to operate, yet, it was found that the Arduino PWM is only 5 v. Figure 6.4 shows the driver's circuit used to amplify the PWM signal.

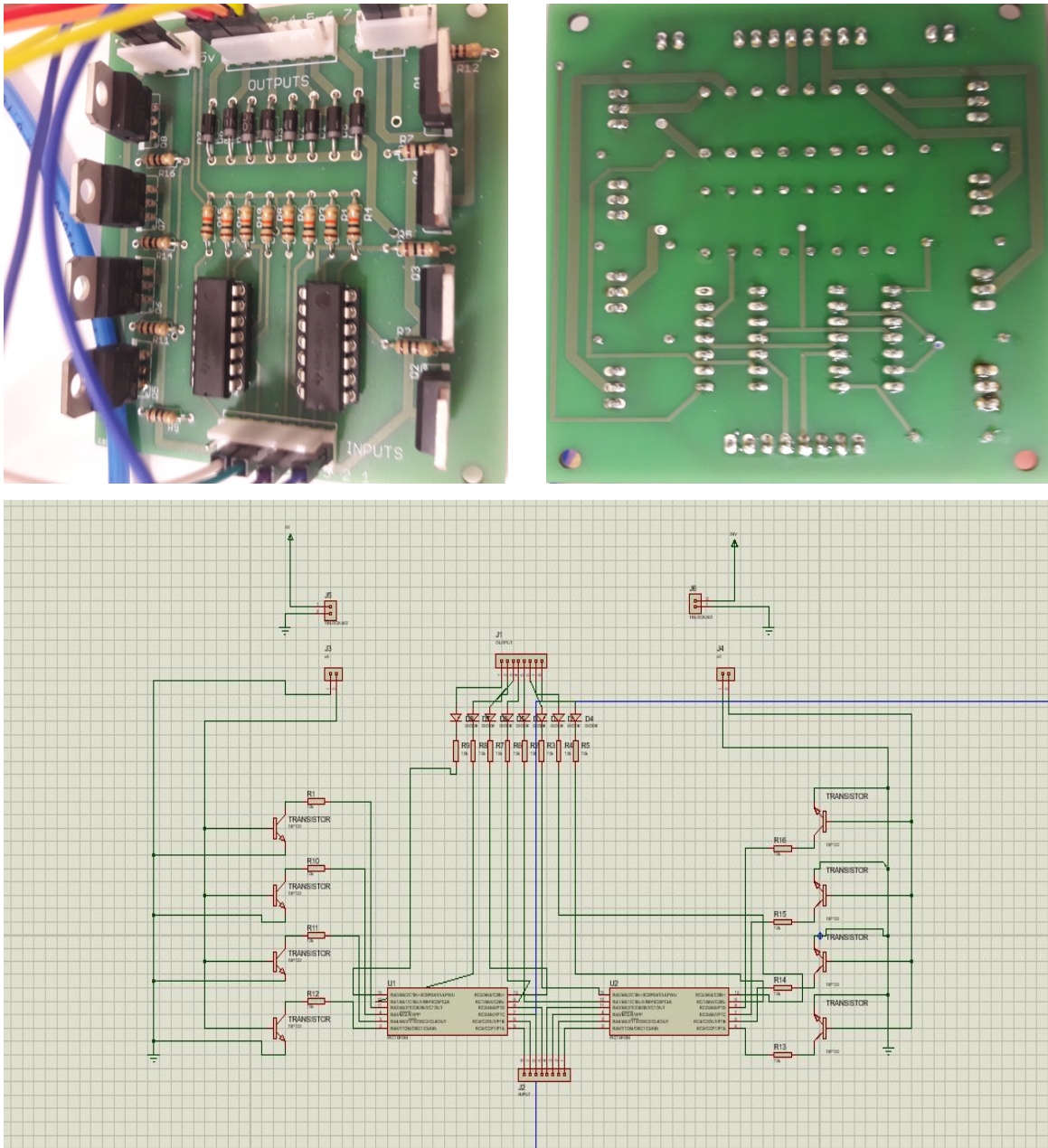


Figure 6.4 the driver's circuit, the first two figure shows the connection in the driver's circuit and last figure shows the schematic connection of the driver's circuit

Within the actuator pressure transducer sensor have been incorporated to monitor the internal state of the muscle and provide feedback to the control system. The complete unit can safely withstand pressures up to 1.2 MPa, although 500 kPa (5 bar) is the operating pressure for the proposed system as shown in figure 6.2. The pressure sensor is connected directly to the pMAs and the control unit, as it works on the same range of voltage as Arduino of 5v. The output of the pressure sensor is in volt ranges between 0.5 to 4.5 VDC.



Figure 6.5 The pressure sensor

6.2 Simulink Simulation

A typical Simulink block consists of inputs, states, and outputs, where the outputs are a function of the sample time, the inputs, and the block states. During simulation, the model execution follows a series of steps. The first step is the initialization of the model, where Simulink incorporates library blocks into the model; propagates signal widths, data types, and sample times; evaluates block parameters; determines block execution order; and allocates memory. Simulink then enters a simulation loop. Each pass through the loop is referred to as a simulation step. During each simulation step, Simulink executes each of the model blocks in the order determined during initialization. For each block, Simulink invokes functions that compute the values of the block states, the derivatives, and the outputs for the current sample time. The simulation is then incremented to the next step. This process continues until the simulation is stopped.

It is easier to change the model than to change the code, the controller can be analysed in terms of the Simulink model.

6.3 Control System Design

An pneumatic muscle actuator (pMAs) is non-linear static characteristic, non-linear system with dead zone as well as time delay with saturation due to non-linear characteristics of solenoid valves and artificial muscles. A linear controller such as P,PI, and PID with fixed gains (K_P) is not able to provide a satisfactory performance in the whole range of actuator. The dynamic simulation hybrid Model Reference Adaptive Control algorithm (MRAC) with a reference model of such actuator was designed in Matlab/Simulink environment in two cases. The first case based on Simulink blocks and the second case based on neural network simulation. These two cases simulated and the simulation results were compared with real measured data on the experimental actuator such as dynamic characteristics of pressure in the

muscles, force of the muscles and position of the actuator arm. The nonlinear dynamic model (MRAC) of a one-DOF actuator was used for the subsystem of pneumatic muscle actuator in this simulation model which based on advanced geometric muscle model. The linear PID controller with fixed gain does not satisfy the required performance for the whole prototype during pMAs arm movement, this bad performance appears under conditions of varying inertia moment. To overcome this problem and enhance the prototype performance, a hybrid Model Reference Adaptive Control algorithm (MRAC) scheme of the pMAs as shown in figure 6.6 was proposed to can adapt the changing parameters (capable of handling the PMA’s nonlinear properties) and could be able to compensate the changes of the inertia moment due to the variation in external load of the PMA. The PMA stiffness will be selfaligning and the stiffness control loop can be avoided.

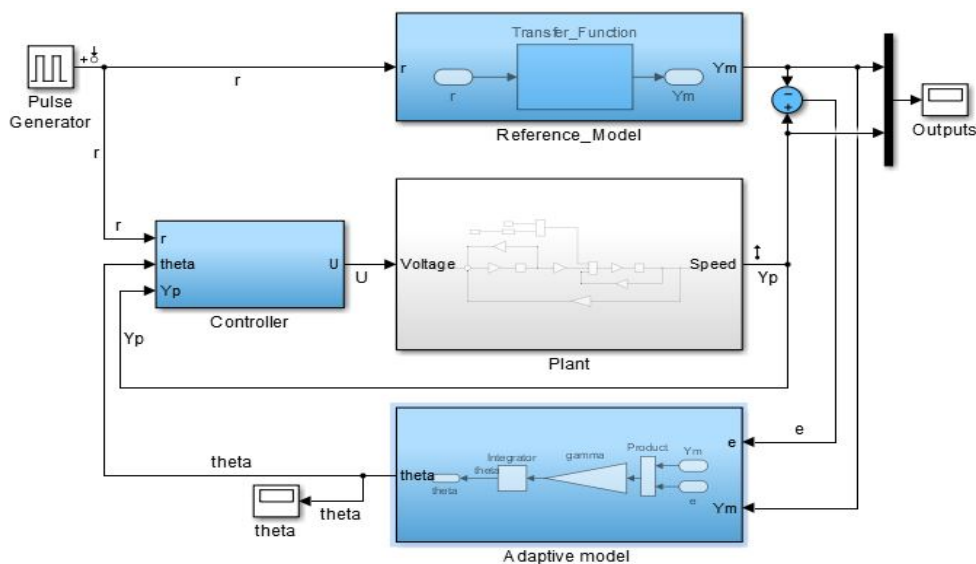


Figure 6.6. MRAC scheme of the pMAs

The implementation of the control system using MRAC is divided into two phases; a closed-loop controller, and adaptive control algorithm, to control the proposed prototype. The closed-loop control algorithm was achieved by using a solenoid valve that is controlled by Arduino-UNO, and PWM driver’s circuit as shown in Figure 6.7.

The first phase is implemented to control the bending angle of the exoskeleton soft arm relying on the pressure supplied to the pMAs. The closed-loop PID control is used later as a reference for the adaptive control where its parameter can be updated to change the response

of the system. MRAC is designed and modeled in Simulink/MATLAB® to control and tune the bending angle of the proposed prototype, controlling filling and venting of the prototype. Two models are designed one is based on neural network (NN) and the other one without NN.

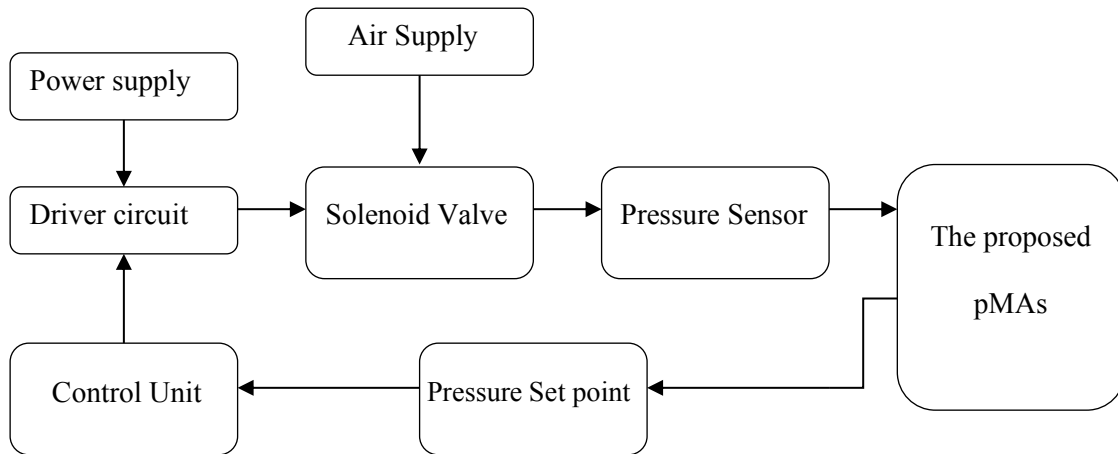


Figure 6.7 Control System

6.4 Model Reference Adaptive Control (MRAC)

Controlling the pressure inside the pMAs remains a challenge. Thus, a solenoid valve is utilised to ease the control process and preserve constant pressure inside the pMAs. The MRAC is used, where the input of the MRAC control is the output from the closed-loop PID controller, and the prototype angle is the feedback. MRAC is a general adaptive control that has been utilised in many systems to ensure repeatability of the process. It uses a dynamic reference model for the desired behavior of the plant. The system compares the input of reference model to the plant model; thus, it changes and updates the input applied to the plant to match the model behavior. MRAC has been widely devised in rehabilitation robotics but in hard robotics, this approach is implemented to the proposed prototype to improve the repeatability, accuracy, and precision.

The MRAC consists of three main elements:

- Reference model.
- Plant model
- Adaptive model

An adaptive control strategy has been developed combining PID with MRAC, where the PID controller is used as a reference model that generates the trajectory command for the adaptive control. MRAC has been simulated in two scenarios; firstly: without tuning, and secondly: with NN tuning. The solenoid valve was controlled via PID controller to control the pressure inside the pMAs (the proposed prototype). The control deviation of the arm position (e) is an input to the linear PID position controller. The total control effort on the PMA (in the form of manipulated variable u) is a result of interaction between linear PID position controller output and adaptation gain of MRAC. The task of the MRAC is to force the system to follow the trajectory determined by the reference model response. When multiplied with the control signal of the linear PID position controller, it produces corrective efforts to minimize the deviations from the reference model trajectory and change the bending angle according to pressure changing. The output of the model is the bending angle that is used as inputs. The controller parameters are adapted during iterations within the NN utilising the plant inputs and outputs.

6.4.1 Reference Model

The reference model is a controller model that describes the behavior of the closed-loop PID controller; it demonstrates how the prototype interacts for given inputs. The reference model is utilised as a transfer function, where the signal is generated from the closed-loop system as shown in Figure 6.8.

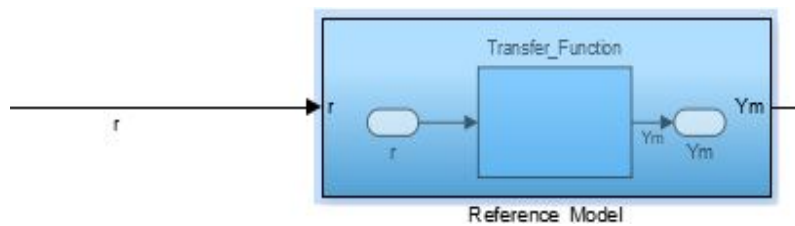


Figure 6.8 Reference model in Simulink

Where the desired rise time is 0.5 sec, setting time is 0.8 sec and steady state error is 0. Y_m is the desired reference trajectory, and r is a small disturbance. For this a second order linear transfer function can be developed (Dorf 2010) in complex s domain as shown in Figure 6.9:

$$\text{transfer function} = G_p(s) = \frac{5}{s^2 + 5s + 5} \quad (6.1)$$

$$G_c(s) = K_p + K_i \frac{1}{s} + K_d \frac{1}{K_f + (\frac{1}{s})} \quad (6.2)$$

Where $G_c(s)$, $G_p(s)$ are the controller and plant transfer function, K_p , K_i , K_d and K_f are the proportional, integral, derivative gains.

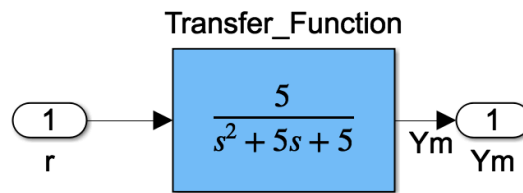


Figure 6.9 Transfer Function

The closed-loop PID controller consists of proportional controller that updates the outputs that is proportional to the current error value. Thus, the time rise and steady state error decrease. The integral controller is used to sum the direct error over time, multiplied it by an integral gain, then add it to the output of the controller, which also result in decreasing the steady state error and the time rise. The derivative controller multiplies the error change rate by derivatives gain in order to reduce the controller output change rate. The controller is designed to track the bending angle of the proposed prototype; to use it's out as inputs for the adaptive controller.

6.4.2 Plant Model

In this part, plant is solenoid valve, which controls the bending angle, normally closed valve that can vent or fill. K_f –Damping is considered to be varying. Initial value is assumed 0.4. In addition, PID controller is tuned to achieve desired response (control the pressure in order to obtain the desired bending angle of the pMAs) with this initial value of K_f . Now as valve goes through ageing and impact of other environmental conditions, K_f changes, this will change model behaviour. Plant output is Y_p . Hence controller has to adapt/change its parameter values to achieve desired response as:

$$e = Y_p - Y_m = 0 \tag{6.3}$$

Where e is error, Y_p is the plant output, and Y_m is the model output.

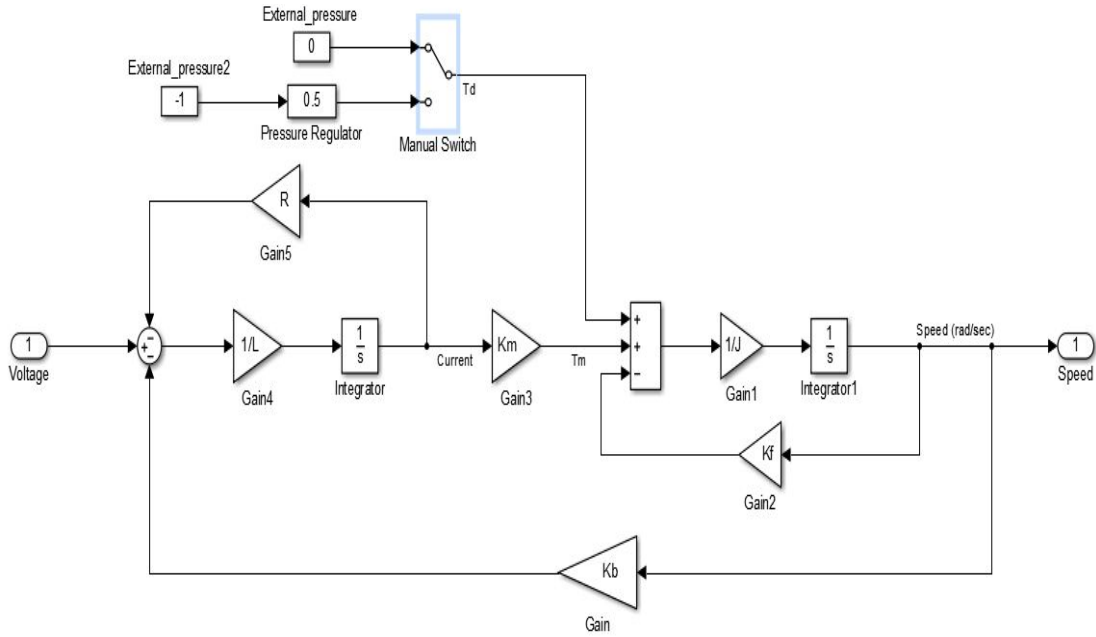


Figure 6.10 Plant model configuration

The plant model equations in time domain t can be expressed by matrix relationships:

$$\dot{x}^o(t) = A(t) x(t) + B(t)u(t) \quad (6.4)$$

$$y(t) = C(t) x(t) + D(t)u(t) \quad (6.5)$$

where x is state, u is input, y is output and A , B , C and D are related parameters with appropriate dimensions (Dorf 2010),

With $D(t)=0$, then

$$y(t) = C(t) x(t) \quad (6.6)$$

$$\dot{x}_k^o = A_k x_k + B_k U_k \quad (6.7)$$

$$y_k^o = C_k x_k + D_k U_k \quad (6.8)$$

$U(s)$ and $Y(s)$ are Laplace transform of $u(t)$ and $y(t)$ respectively and equations of plant closed loop can be expressed as a polynomial in s as:

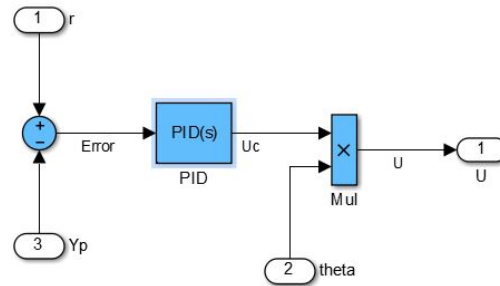
$$P_K(s) = \sum_{i=0}^n a_i s^{n-i} \quad (6.9)$$

6.4.3 Model Reference Adaptive controller

There are two sub components of this controller:

6.4.3.1 PID Controller

This part of controller is fixed, and gains have been tuned for keeping initial plant condition in mind and to achieve overall stability. Output of PID controller is U_c as shown in Figure 6.11.



6.4.3.2 Figure 6.11. PID control Adaptive Control

This goal of this part of controller is to change its output ($theta$) based on error (e) between plant output (Y_p) and reference model output (Y_m). How fast it can adapt (or change its output) depends on parameter called learning rate, gamma. Higher the value of gamma, faster it can adapt to any changes in plant. Controller output (U) is calculated by: $U = U_c * theta$.

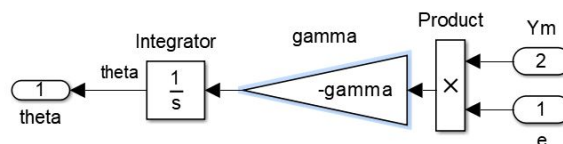


Figure 6.12 Adaptive control

The pulse is generated from the pneumatic system where the signal it is considered as an external source as follows:

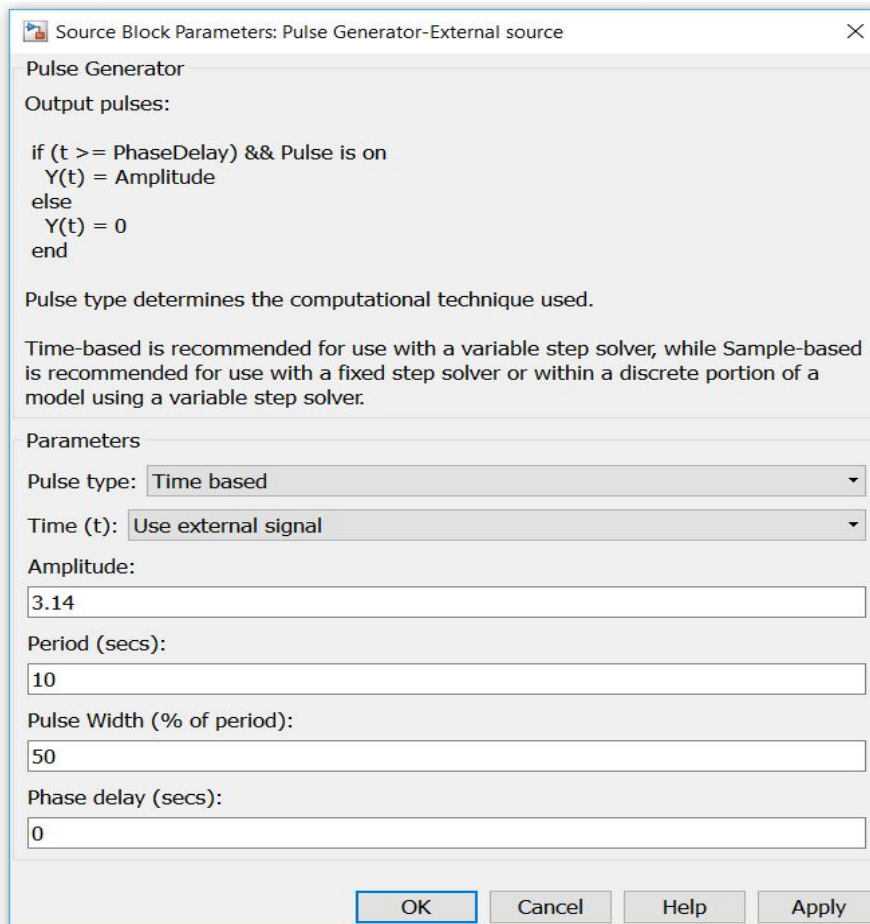


Figure 6.13 Generator pulse diagram properties

The resulting position θ (*Bending angle*) of the actuator arm changes due to the nonlinearity (MRAC) and it depends on the Pressures / forces difference of the both artificial muscles. As shown in Figure 5.12 there is a small difference between Y_m and Y_p . This small error is due to well-tuned PID controller for known plant values (K_f and others). Nonlinearity MRAC for pMAs simulation model based on simple geometric muscle model is given by the static Characteristic of the actuator, which is measured on experimental actuator. Input variable is pressure difference in the muscles ($P_1 - P_2$) and the output variable is the angle θ of actuator arm rotation. Pressure sensors with accuracy 0.5 % and measuring range of 50-500 kPa are used for pressure measuring in the muscles. At the beginning both muscles were fully pressurized and actuator arm is in zero initial position ($\theta = 30^\circ$) at pressure 50 kPa. Measured results are shown in Figure 6.14.

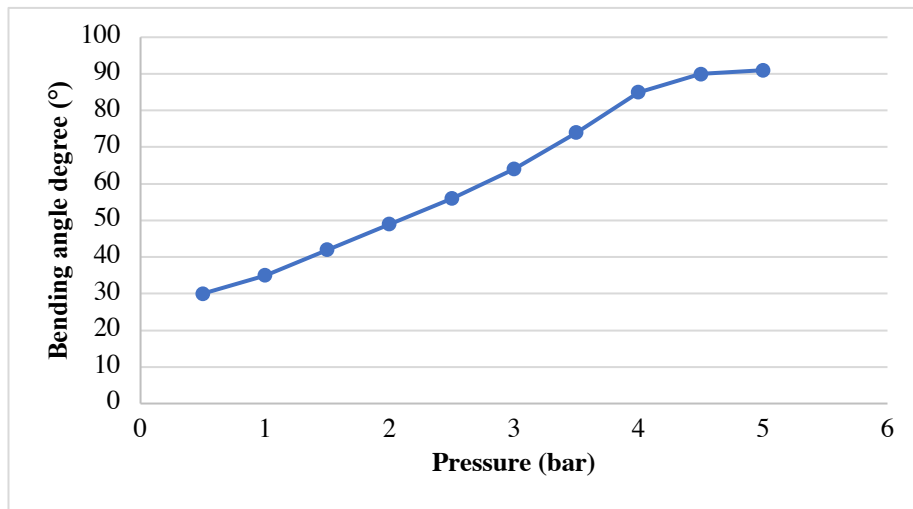


Figure 6.14. Measured bending angle of the soft Arm

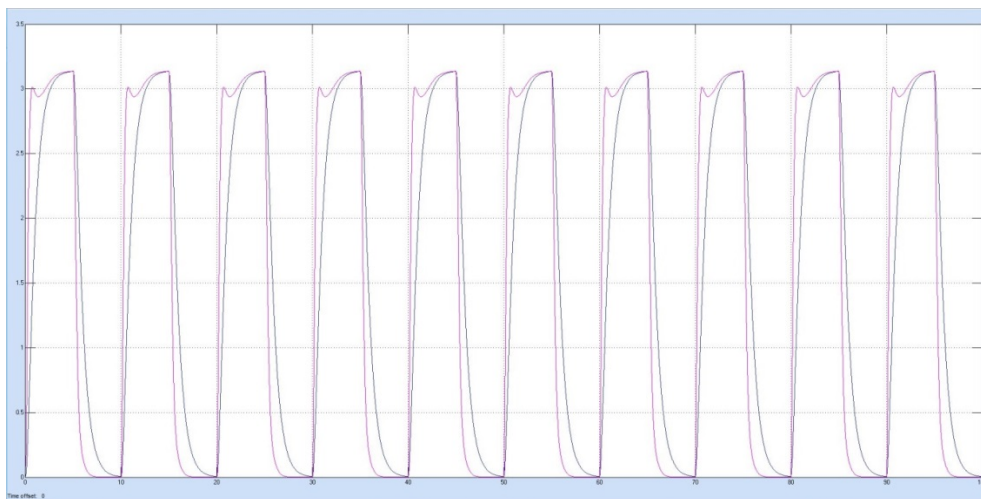


Figure 6.15. A comparison between Y_m vs Y_p values

6.4.4 Control Structure

The structure of the control system without NN tuning is shown in Figure 6.16, each block represents a set of control calculations performed at each iteration with data flow between blocks. Where the input of the system is generated from the pulse generator as mentioned before. The plant block run calculations to determine the suitable pressure value to the proportional pressure to produce the correct pressure in order to obtain the desired bending angle of the prototype. The reference model block is a closed-loop PIC control that is based on the bending angle of the proposed prototype, the PID controller is used to adjust the pressure values of the prototype according to the pressure error.

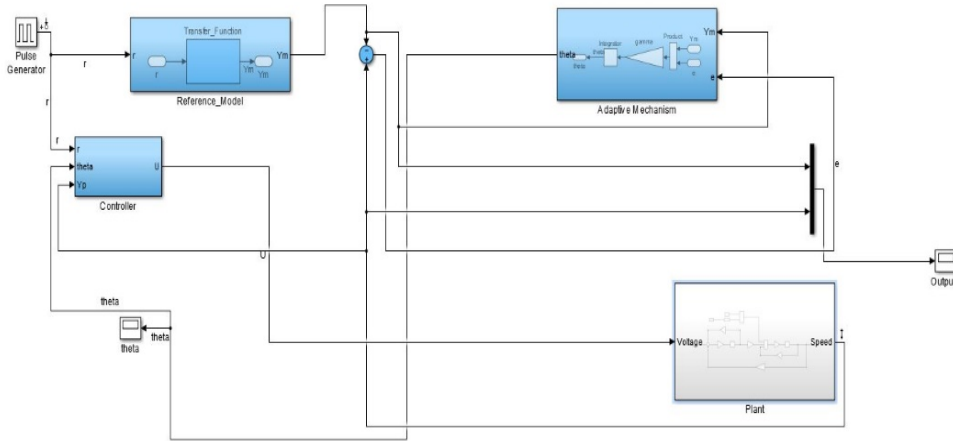


Figure 6.16. General Block Diagram for Reference model adaptive control

6.5 Adaptive Control Based on Neural Network

6.5.1 NN Main Configuration

The neural model reference control architecture uses two neural networks: a controller network and a plant model network, as shown in the following Figure 6.17. The plant model is identified first, and then the controller is trained so that the plant output follows the reference model output.

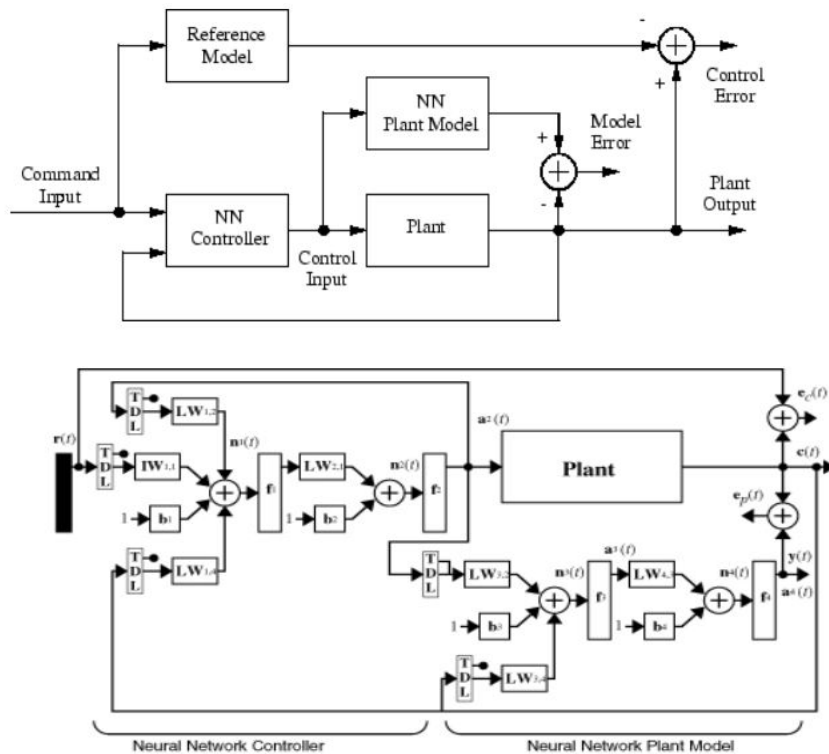


Figure 6.17 NN Reference model adaptive control

The proposed closed loop configuration of a neural network control system is shown in Figure 6.18.

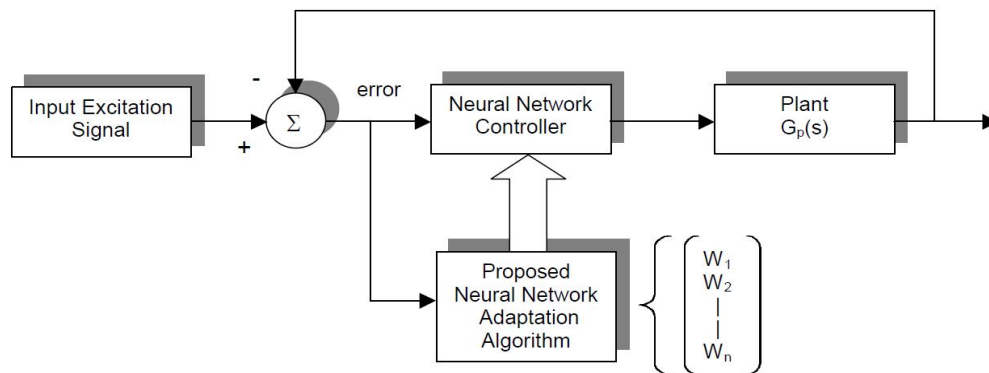


Figure 6.18. Proposed configuration

To demonstrate the previous adaptive neural network theory and approve the concept, software simulation has been performed. The MATLAB/Simulink model is shown in Figure 6.19. The MRAC consists of two subnetworks; one subnetwork is the model of the plant, to control the pMA and the other one is the controller. pMAs outputs is used to represent the plant model that was trained by using neural network. The attached code in appendix () is utilised to implement the observed data. Neural Network for pMAS model is designed by Simulink/MATLAB®, the NN consists of 10 neurons in one hidden layer, 2 delayed plant inputs, and 2 delayed plant outputs; it is trained by trained for 300 epochs. As shown in Figure 5.20 at Input Signal with Amplitude is 3.14, and frequency: 0.01 Hz and learning rate $\gamma=10$ as shown in Figure 6.22.

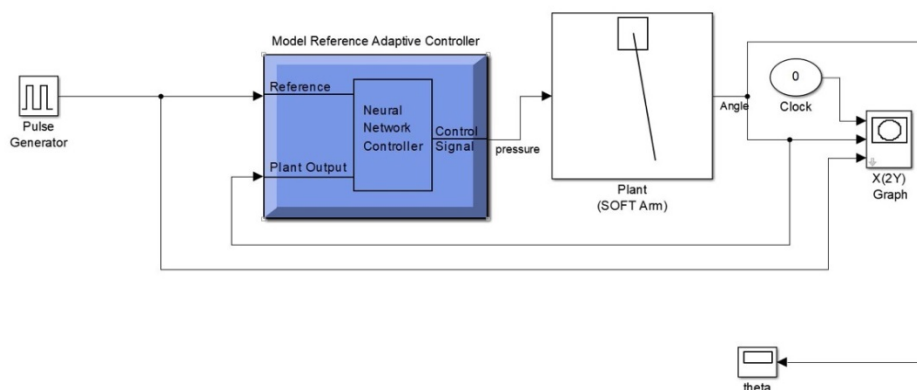


Figure 6.19. Simulink model of the adaptive NN controller

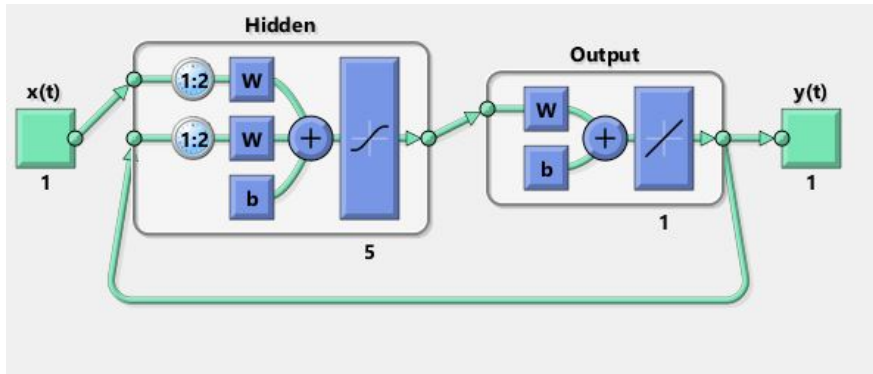


Figure 6.20. Plant model resulting Network

Figure 6.20 shows the plant model training, the whole MRAC system consists of NN model that begins with a feedforward network, and feedback connections.

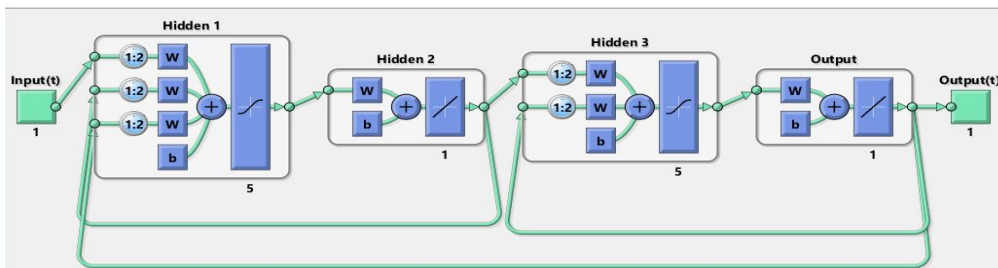


Figure 6.21. MRAC NN View

Figure 6.21 shows the MRAC NN view, where layer 1 and layer 2 represent the controller. While layer 3 and layer 4 (output) represent the plant model subnetwork

```

Pulse Generator
Output pulses:

if (t >= PhaseDelay) && Pulse is on
    Y(t) = Amplitude
else
    Y(t) = 0
end

Pulse type determines the computational technique used.

Time-based is recommended for use with a variable step solver; while
Sample-based is recommended for use with a fixed step solver or with
a discrete portion of a model using a variable step solver.

Parameters
Pulse type: Time based
Time (t): Use simulation time
Amplitude:
3.14
Period (secs):
10
Pulse Width (% of period):
50
Phase delay (secs):

```

Figure 6.22. Input Signal

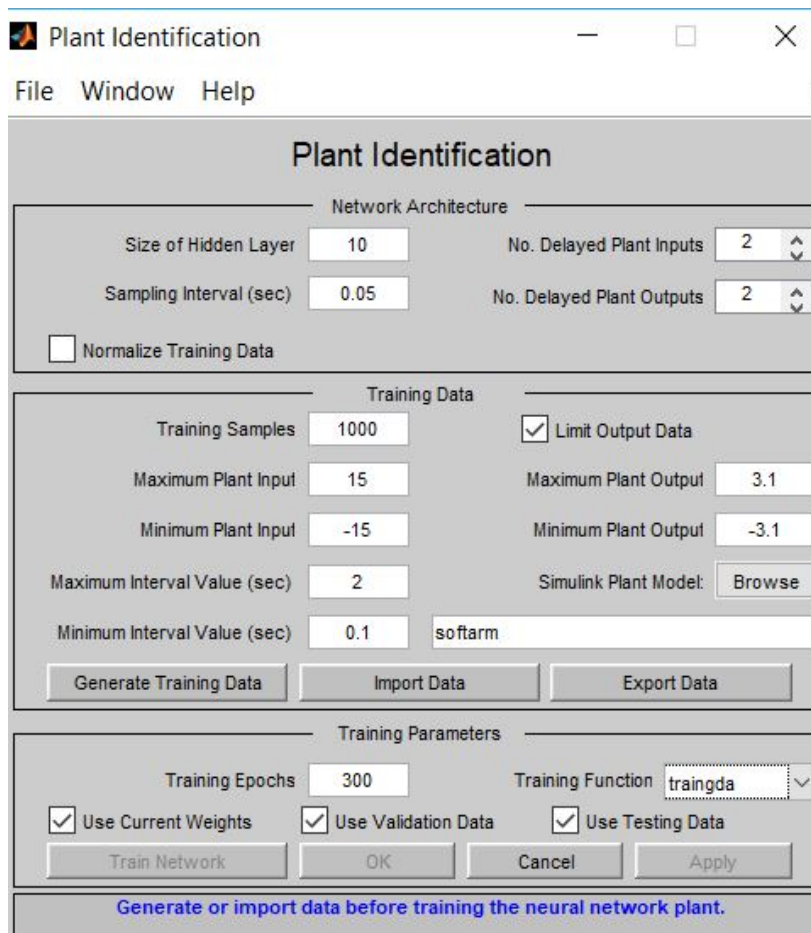


Figure 6.23 Plant Neural Network identification

The error for the training, testing, and validating is about 10^{-4} as shown in figure 6.24. The neural networks feedback; the neural network model has an almost identical output as the plant output for the same input, thus the performance is high for the time interval form 0- 50 seconds and from 0- 100 seconds.

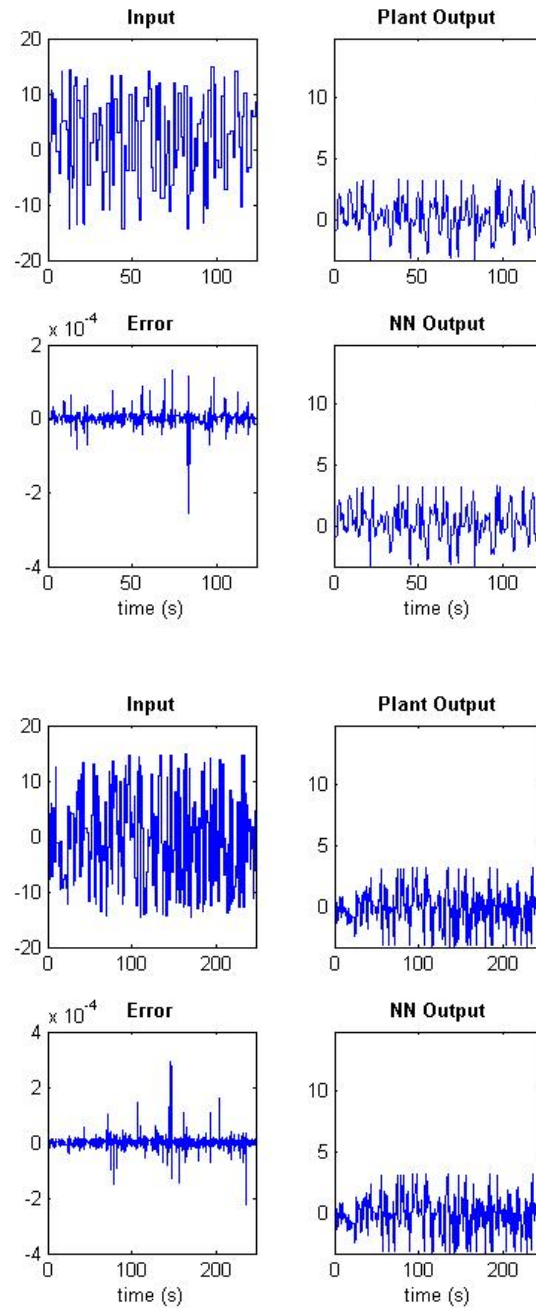


Figure 6.24 Validation results for model reference adaptive control

To further show the advantage of using NN as shown in Figure 6.25, the mean square error is 3.2094×10^{-4} at the 0 iteration. Therefore, using NN can improve the accuracy of the bending angle for the proposed prototype. In addition, it can accelerate the convergence ratio and decrease the fitting error.

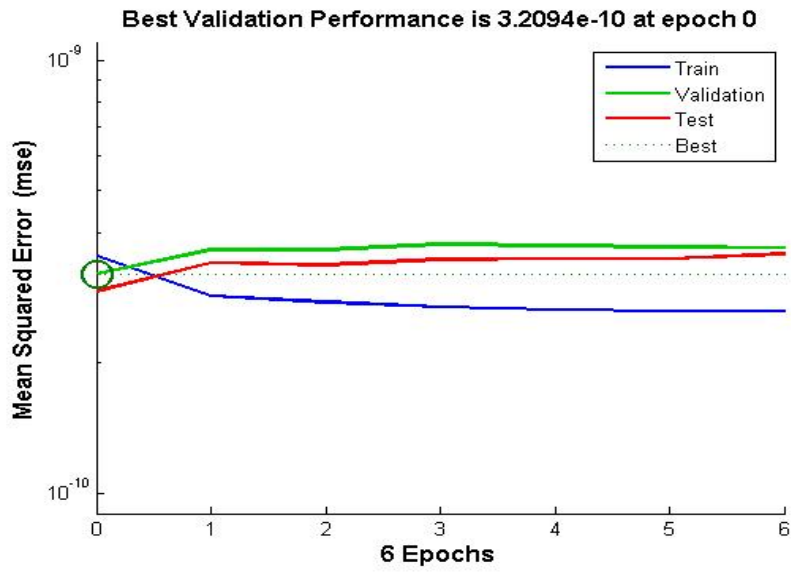


Figure 6.25 Mean Square Error curve for the NN for 6 epochs

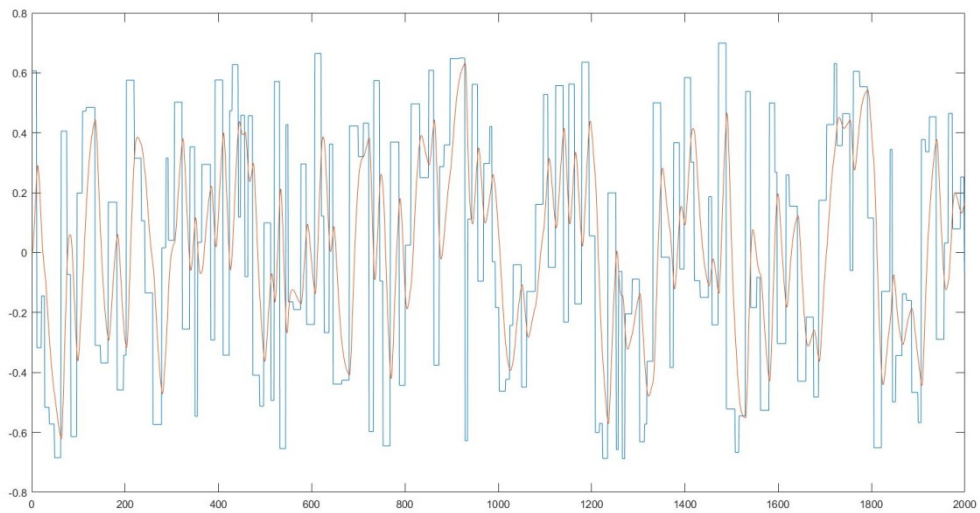


Figure 6.26. Training Data

Sample training data is required in order to configure the network. Figure 6.26, plots the training data, and the network configuration. Where 6.27 represents the reference arm angle at each time step.

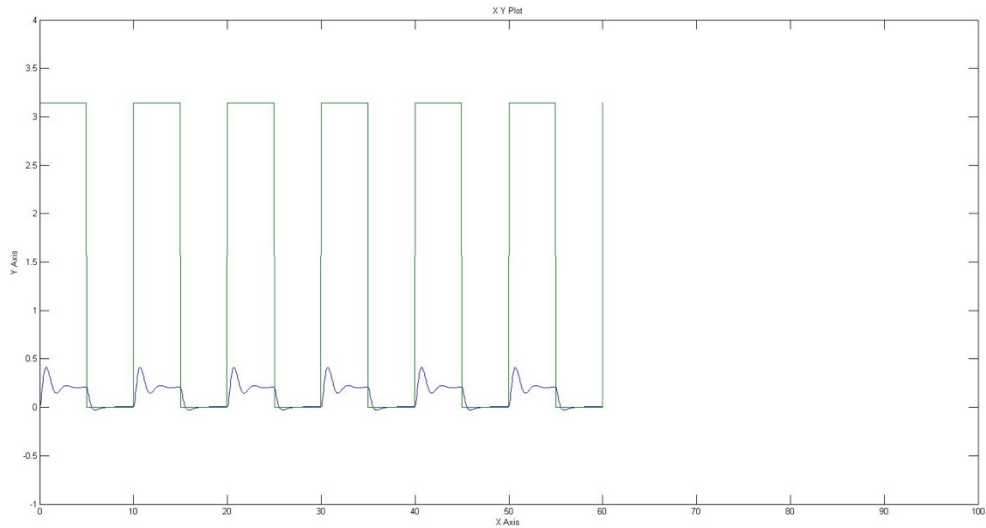


Figure 6.27. Y axis represent reference arm angle, and X axis represent time (s)

6.6 Comparison

Figure 5.28, shows a comparison between the input and the plant model output, where the reference input should follow the plant model output with correct critical damped response, although the input sequence is not the same as the input sequence in the training data. The steady state response is not perfect for each step. However, this can be improved by adding more hidden neurons and a larger training set.

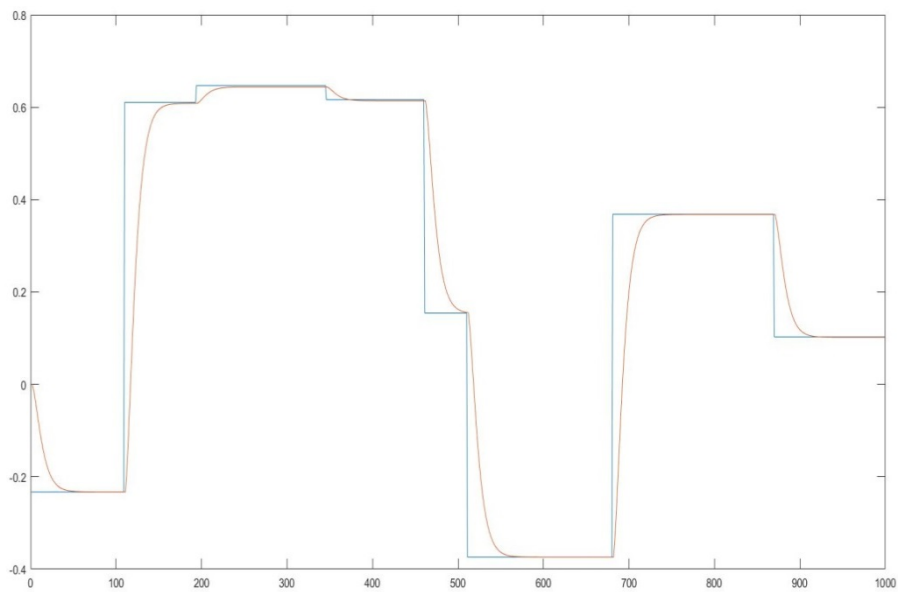


Figure 6.28. Reference input vs plant model output

The performance of adaptive PID control based on NN is better than the conventional PID, Figure 6.29 shows the bending angle using NN. Figure 6.30 shows the bending angle values without NN.

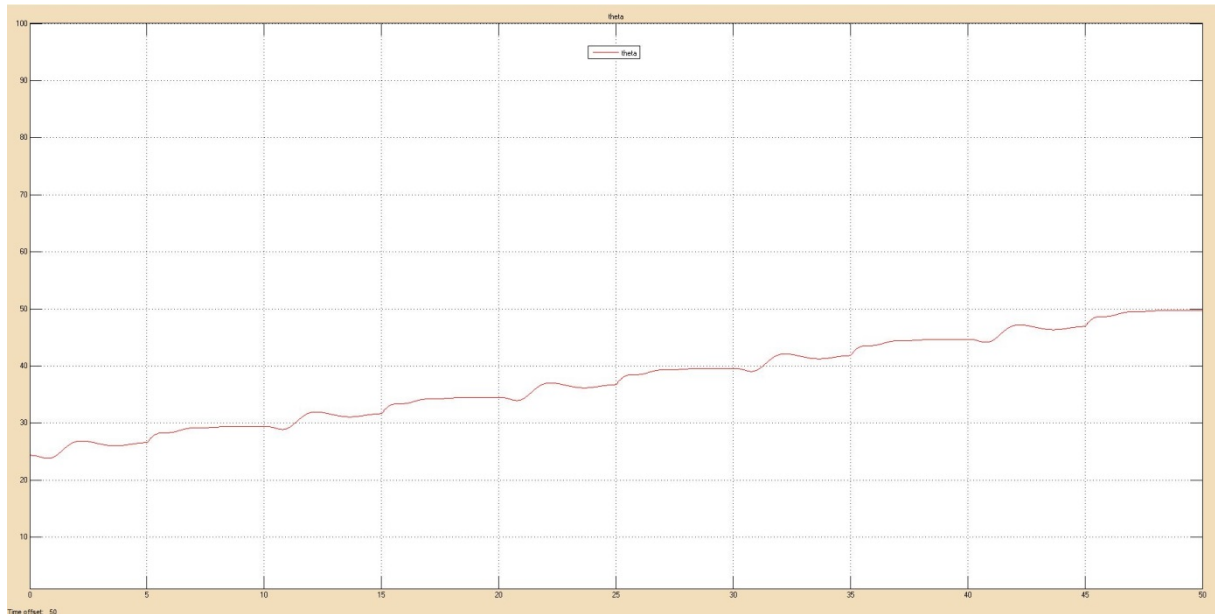


Figure 6.29. Bending angle theta output from NN

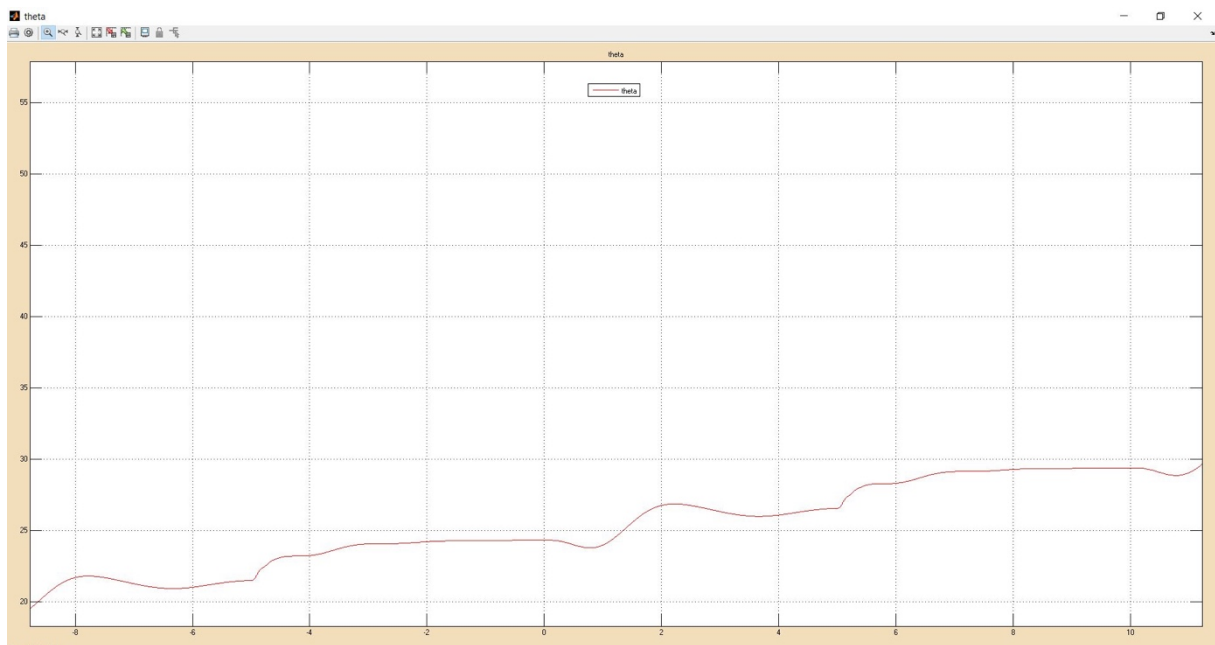


Figure 6.30. Bending angle theta output without NN

6.7 Summary

The aim of this chapter is to test and design non-linear model of 1 DOF pMA (extension and flexion) as a reference model in adaptation mechanism using NN. The simulation results proved that using NN with MRAC has better results than MRAC without NN, PID controller is used as a reference for MRAC. Different simulation is conducted to validate the experimental results. It has been shown that both controllers exhibit a stable behaviour, however MRAC with NN was able to capture wider dynamic range of the system and therefore perform better. The proposed control model catches the aim of the research.

7 CONCLUSION AD FUTURE WORK

Throughout the literature reviews (i.e., journals and conference papers) on existing research studies of the rehabilitation robotic systems, the evaluation and comparison of the developed upper-limb rehabilitation orthosis using pneumatic muscle type of actuators are thoroughly reviewed. These reviews include various design, modelling and control algorithms and strategies, intended to analyse the pMA behaviour and relationship among length, force, bending angle and pressure. Even though a considerable amount of work has now been employed, it could be said that the field is still rapidly evolving. Based on the review findings, it is understood that the issues of which are the most effective control algorithms are still wide open.

To conclude, I recall from earlier the research question of this thesis. Specifically:

“Is the Novel soft arm design and control are suited to application in elbow rehabilitation?”

This research introduces a novel exoskeleton upper limb soft arm, a novel numerical model, and a developed control strategy. In numerous experiments, spanning different setups of pMA we have shown that our soft arm is effective due to many reasons such as lightweight, low cost, high performance, and safety..

We now summarise the contributions made in this thesis and propose future work.

7.1 Summary of Contributions

In short, the significant contributions of this thesis can be summarised as follows:

Design a Novel Soft Arm for Elbow Rehabilitation Using Pneumatic Muscle Actuators (pMA)

In Chapter 4, we satisfied research objective RO1 by developing lightweight, safe, low cost, low impedance, high power to weight ratio, and adjustable soft arm that can satisfy the dynamic and adaptive characteristics of the rehabilitation process. A number of experiments were conducted on various pMA to illustrate and analyse the behaviour of pMA and the relationship among pressure, length, force, and bending profile. These all contributed to the conclusion that, given the good applicable design to rehab the elbow joint with many advantages.

Devise a Novel Model for Various Pneumatic Muscle Actuators.

Predominantly in Chapter 5 the mathematical design is discussed in detail, but also in Chapter 4 the numerical model was presented in detail using ANSYS and other softwares such as Fusion 360 and 3D CAD. The material and pMA fabrication was modelled. A model validation is carried out by a comparison of experimental and numerical results in quasi-static and isometric tests. The same values of the basic parameters of the experimental McKibben are implemented into the FEM, for counting the exact number of nodes and elements. The results of the contractor pMA in both cases numerically and experimentally behave the same, with a small deviation. However, the deviation in the extensor change in length with respect to the experimental result is bigger. This difference is because of the friction between the bladder and the braided sleeve, threads in the braided sleeve, and contact between the components. There is a good agreement between the numerical and the experimental results; the number of the threads plays a significant role in the deformation. When the number of threads increases the deformation increase as it depends on the thread set. The bladder is made of butyl rubber, and is modelled by the two coefficients from the Moony-Rivlin formulation ($C_{10}= 0.0694$, $C_{01}=0.0628$) and the material of the braided sleeve is PET, and a strand made of 5 and 7 threads. The obtained results for this model suggests that this model can be used to predict the behaviour of the pMA. This, therefore, satisfied our research objectives RO2, RO3, and RO4.

Develop an Adaptive Controller Using Simulink/ Matlab

In Chapter 5 an adaptive control approach (MRAC) tuned by NN was developed to validate the results. An extensive set of simulation were performed in Matlab/Simulink to control the amount of pressure required to bend the soft arm. PID controller was used as an input (reference model) for the MRAC. Two cases were conducted the first scenario without NN and the second one was with NN, the performance of the controller was better when NN was used. This is not only because 1000 samples were taken for training but also because NN was able to capture wider dynamic range of the system into considerations. This result in getting higher performance than the other one. Hence, RO5 was achieved.

7.2 Limitations

Despite the contributions listed in the previous section, this thesis also has its limitations. Some of the important limitations can be listed as follows:

Platform Specifications

All the experiments shown in this thesis were performed by a person, so human errors are expected. In Chapter 4, and 5. Overcoming these issues may need some changes in the algorithm that may be subject to future work.

Nonlinearity of pMA

One of the challenges of the pMA is its difficulty to describe the behaviour in a physical model. In the models there is still an error present, which makes the force response not optimal. This is due to the hysteresis effect of the friction between the bladder and the braided sleeve and between the threads in the braided sleeve. Thus, the mathematical model is not accurate due to the assumptions that were taken into considerations in this thesis. In addition, structural parameters and the operating conditions. By lacking an accurate model it's difficult to predict the non-linear behaviour of the muscle.

Modelling the pMA

It was one of the biggest challenges because of the material definition, nonlinearity, and contact in pMA. Because meshing becomes more difficult when each thread is considered as helices with SHELL 181 elements.

7.3 Future Work

The ultimate aim of this research is to provide a soft robotic device to assist many individuals suffering from stroke or similar disabling illness and living with reduced mobility of the arms, hands and other joint. Especially it is anticipated that this device can be used at home independently without therapist. Unfortunately this was not possible within a PhD research project and further research work needs to be done.

Firstly further investigation is required to address a few open problems that we think would be beneficial to explore in the future. For example it is advisable to apply further stress and strain analysis for McKibben muscles. This yields a larger working area as the tube touches the braid at a lower pressure and therefore might cause a few issues in long term.

While performing above analysis, it is also recommendable to extend FEA to analysis the extension and contraction while bending. This will help to understand the behaviour and the range of motion of the McKibben muscle better. Above analysis can be then extend to the whole EpMAE prototype and to evaluate analytically the arm performance as one piece.

Lack of real-time measurements for angles was the main reason behind absence of real-time control for whole EpMAE prototype. Therefore real-time angle measurements by any motion capture system such as VICON or Kinect will be helpful in providing feedback signal that can utilise designed controllers in previous section and inverse kinematic of the EpMAE.

In our design also we have not considered motions such as pronation and supination, which are also required for elbow rehabilitation. In order to achieve this more pneumatic muscle actuators should be used in different direction to force the elbow joint to rotate. Moreover, another test should be conducted to understand the behaviour of the pMA when the angle is 54.7° whether it twists or not.

There are other requirements related to rehabilitation regimes, which have widely been studied by many researchers. From a system engineering point of view, developing an optimal pattern of rehabilitation regimes including, applied torque in repetitive motion according to rehabilitation specific and human resistance, will make the EpMAE more user friendly, comfortable and effective in its performance. In doing so, we can develop machine learning algorithms and apply them to both healthy subjects and patients in different stage. This will result in obtaining an optimal rehabilitation regime that accelerates the rehabilitation process.

Building and testing this elbow rehabilitation device has shown us that we can expand the system functionalities to other joints: therefore there is a potential to extend the design, for example to build rehabilitation EpMAE devices for shoulder and wrist with different DOFs. This is especially straightforward for the wrist because it has the same movements as in the elbow but with less range of motion.

APPENDICES

Appendix (A)

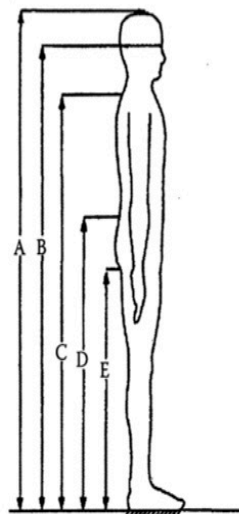
Anthropometric Data

Table 1: Normalized Mass and Length of Body Segments (Standard Human)

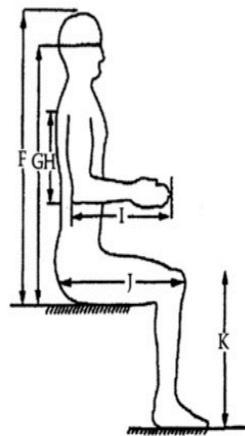
Segment	Segment Mass / Total Body Mass	Center of Mass / Segment Length		Density (kg/l)
		Proximal	Distal	
Hand	0.006	0.506	0.494	1.16
Forearm	0.016	0.430	0.570	1.13
Upper Arm	0.028	0.436	0.564	1.07
Forearm and Hand	0.022	0.682	0.318	1.14
Total Arm	0.050	0.530	0.470	1.11
Foot	0.0145	0.500	0.500	1.10
Lower Leg (calf)	0.0465	0.433	0.567	1.09
Foot and Lower Leg	0.061	0.606	0.394	1.09
Upper Leg (thigh)	0.100	0.433	0.567	1.05
Total Leg	0.161	0.447	0.553	1.06
Head and Neck	0.081	1.000	—	1.11
Trunk	0.497	0.500	0.500	1.03

Table 2: Standing and Sitting Dimensions in meters

Name	Dimension	Male			Female		
		5th%	50th%	95th%	5th%	50th%	95th%
Stature	A	1.649	1.759	1.869	1.518	1.618	1.724
Eye height (standing)	B	1.545	1.644	1.748	1.427	1.520	1.630
Mid shoulder height	C	1.346	1.444	1.564	1.210	1.314	1.441
Waist height	D	0.993	1.102	1.168	0.907	0.985	1.107
Buttocks height	E	0.761	0.839	0.919	0.691	0.742	0.832
Sitting height	F	0.859	0.927	0.975	0.797	0.853	0.911
Eye height (sitting)	G	0.743	0.800	0.855	0.692	0.743	0.791
Upper arm length	H	0.333	0.361	0.389	0.306	0.332	0.358
Lower arm + hand length	I	0.451	0.483	0.517	0.396	0.428	0.458
Upper leg length	J	0.558	0.605	0.660	0.531	0.578	0.628
Lower leg length	K	0.506	0.553	0.599	0.461	0.502	0.546



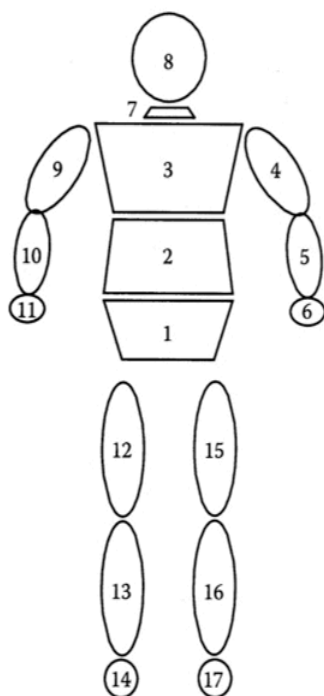
- A. Stature
- B. Eye height (standing)
- C. Mid shoulder height
- D. Waist height
- E. Buttocks height



- F. Sitting height
- G. Eye height (sitting)
- H. Upper arm length
- I. Lower arm/hand length
- J. Upper leg length
- K. Lower leg length

Table 3: Body Segment Masses in kilograms

Name	Body Segment	Male			Female		
		5th%	50th%	95th%	5th%	50th%	95th%
Lower torso (pelvis)	1	8.24	10.00	11.99	8.27	10.00	12.11
Middle torso (lumbar)	2	9.01	10.95	13.13	5.45	6.59	7.98
Upper torso (chest)	3	15.30	18.58	22.28	7.69	9.30	11.25
Upper arm	4, 9	1.84	2.23	2.67	1.41	1.71	2.07
Lower arm	5, 10	1.14	1.39	1.66	0.84	1.02	1.24
Hand	6, 11	0.43	0.52	0.63	0.34	0.42	0.50
Neck	7	1.48	1.80	2.16	1.20	1.45	1.76
Head	8	4.07	4.95	5.93	3.31	4.01	4.85
Upper leg	12, 15	6.96	8.45	10.13	6.22	7.53	9.11
Lower leg	13, 16	2.84	3.45	4.14	2.24	2.71	3.28
Foot	14, 17	0.85	1.03	1.23	0.71	0.86	1.04
Total		66.22	80.42	96.41	49.44	59.85	72.43



Appendix (B)

1. General code for contractor and extensor calculations

```
clc;
clear;
d=20*10(-3);
sr=363.33;
x=[0.0126,14882,-2;2*10(-5),-0.5375,11777];
y=[1;(d/sr);((d2)/(sr2))];
s=x*y;
Leo=.34;
k=0;
for
p=[0.5*105,1*105,1.5*105,2*105,2.5*105,3*105,3.5*105,4*105,4.5*105,5*105]
k=k+1;
Lec(k)=Leo-((s(1)*Leo)/(1+exp((-s(2)*(d/sr)*p)))6.214);
end

global thmax be ne bc thmin nc
dn=.02; % nominal muscle diameter.
thn=45; % nominal braid angle.
Len=.8;% nominal length for Extensor
Leo=.34;
be=Len/cosd(thn);
ne=Len*tand(thn)/(pi*dn);
do=be/(ne*pi) ; %actual bending muscle diameter.
thmax=acosd(Leo/be);
dmax=be*sind(thmax)/(ne*pi);
k=0;
p=0.5:0.5:5;
r=[.9 10];
% w=fsolve(@myfun4,r)
z= fsolve(@myfun,r);

for Lec=[.42,.445,.464,.474,.482,.485,.488,.493,.496,.498];% the length
of bending extensor muscle
k=k+1;
thc(k)=acosd( (1/be).* Lec); %angel of braided thread for
extensor
dce(k)=be*(sind(thc(k))+sind(thmax))/(2*pi*ne);
alfae(k)=180*be*(cosd(thc(k))-cosd(thmax))/(dce(k)*pi);
fex(k)=(((104)*p(k).*be.2)/(8*pi*ne2)).*((-
((cosd(thc(k))+cosd(thmax)).*(cosd(thc(k)).*sind(thc(k))+sind(thmax)*cos
d(thc(k))))./sind(thc(k)))+0.5*(sind(thc(k))+sind(thmax)).2); %
extensor force.
fexx(k)=(((104)*p(k).*be.2)/(8*pi*ne2)).*((-
((cosd(z(1))+cosd(thmax)).*(cosd(z(1)).*sind(z(1))+sind(thmax)*cosd(z(1)
)))./sind(z(1)))+0.5*(sind(z(1))+sind(thmax)).2); % extensor force @
alfa=90.
fexxt(k)=2*(((104)*p(k).*be.2)/(8*pi*ne2)).*((-
((cosd(z(1))+cosd(thmax)).*(cosd(z(1)).*sind(z(1))+sind(thmax)*cosd(z(1)
)))./sind(z(1)))+0.5*(sind(z(1))+sind(thmax)).2); % extensor force @
alfa=90.
end
feex=[0,0.98,2.45,3.92,5.635,7.35,8.82,10.29,11.76,13.72]
```

```

Lee=[.42,.442,.459,.47,.476,.479,.483,.488,.49,.491]; % the length of
bending extensor muscle experimental
alfaex=[50.0,110.0,180.0,270.0,340.0,360.0,370.0,375.0,380.0,380.0]
Lec=[.42,.445,.464,.474,.482,.485,.488,.493,.496,.498];
feext=[0.98,3.185,6.37,9.8,12.74,15.19,17.64,19.6,21.56,24.5]
alfapeql=[32,36,44,53,60,69,79,90,94,95]
alfapeq=[81,125,177,198,209,215,221,227,230,235];

figure(1);
hold on
plot(p,Lec,'b');
plot(p,Lee,'r');
title('pressure vs length of extensor muscle ', 'FontSize', 12,
'FontWeight', 'bold', 'Color', 'r');
xlabel('pressure (bar)', 'FontSize', 12, 'FontWeight', 'bold', 'Color',
'b');
ylabel('length of muscle (m)', 'FontSize', 12, 'FontWeight', 'bold',
'Color', 'b');
legend( 'equation', 'experimental')

figure(2);
hold on
plot(p,alfae,'b');
plot(p,alfaex,'r');
title('pressure vs extensor bending angle', 'FontSize', 12,
'FontWeight', 'bold', 'Color', 'r');
xlabel('pressure (bar)', 'FontSize', 12, 'FontWeight', 'bold', 'Color',
'b');
ylabel('bending angle (degree)', 'FontSize', 12, 'FontWeight', 'bold',
'Color', 'b');
legend( 'equation', 'experimental')

figure(3);
hold on
plot(p,fexx,'b');
plot(p,feex,'r');
title('pressure vs Force @alfa=90', 'FontSize', 12, 'FontWeight',
'bold', 'Color', 'r');
xlabel('pressure (bar)', 'FontSize', 12, 'FontWeight', 'bold', 'Color',
'b');
ylabel('Force (N)', 'FontSize', 12, 'FontWeight', 'bold', 'Color', 'b');
legend('equation', 'experimental')

figure(4);
hold on
plot(p,fexxt,'b');
plot(p,feext,'r');
title('pressure vs two parallel extensor Force @alfa=90', 'FontSize',
12, 'FontWeight', 'bold', 'Color', 'r');
xlabel('pressure (bar)', 'FontSize', 12, 'FontWeight', 'bold', 'Color',
'b');
ylabel('Force (N)', 'FontSize', 12, 'FontWeight', 'bold', 'Color', 'b');
legend('equation', 'experimental')

Lco=.3;
k=0;
for
p=[0.5*10^5,1*10^5,1.5*10^5,2*10^5,2.5*10^5,3*10^5,3.5*10^5,4*10^5,4.5*1
0^5,5*10^5]
k=k+1;
Lcc(k)=Lco-((s(1)*Lco)/(1+exp((-s(2)*(d/sr)*p)))^6.214);

```

```

end

Lcn=.3; % nominal length for contractor
Lco=.3;
bc=Lcn/cosd(thn);
nc=Lcn*tand(thn)/(pi*dn);
do=bc/(nc*pi) ; %actual bending muscle diameter.
thmin=acosd(Lco/bc);
dmin=bc*sind(thmin)/(nc*pi);
k=0;
p=0.5:0.5:5;

n= fsolve(@myfun1,r)
nn= fsolve(@myfun5,r)
for Lcc=[.271,.251,.239,.227,.222,.221,.218,.216,.213,.212]; % the
length of bending contractor muscle
    k=k+1;
    thcc(k)=acosd(Lcc/bc); %angel of braided thread for contractor
    dcc(k)=bc*(sind(thcc(k))+sind(thmin))/(2*pi*nc);
    alfac(k)=180*bc*(cosd(thmin)-cosd(thcc(k)))/(dcc(k)*pi);

fcx(k)=(((10^5)*p(k).*bc.^2)./(8*pi*nc^2)).*(((cosd(thcc(k))+cosd(thmin)
)).*(cosd(thcc(k)).*sind(thcc(k))-
sind(thmin)*cosd(thcc(k))))./sind(thcc(k)))+0.5*(sind(thcc(k))+sind(thmi
n)).^2)*2.3; % contractor force.

fcxxx(k)=(((10^5)*p(k).*bc.^2)./(8*pi*nc^2)).*(((cosd(n(1))+cosd(thmin)
)).*(cosd(n(1)).*sind(n(1))+sind(thmin)*cosd(n(1))))./sind(n(1)))-
0.5*(sind(n(1))+sind(thmin)).^2)/5; % contractor force @alfa=45.

end

%@p=2 bar
global m;
k=0;
for m=[0,.5,1,1.5,2,2.5,3,3.5,4,4.5,5];
    k=k+1;
    r=[.5 10];
    z=fsolve(@myfun3,r);
    thccp(k)=z(1);
    Lccp=bc*cosd(z(1));
end
Lccpx=[.228,.229,.23,.231,.233,.235,.237,.239,.241,.243,.245]
Lce=[.271,.253,.238,.228,.224,.222,.22,.218,.215,.213]; % the length of
bending contractor muscle experiamental
alfacx=[65.0,110.0,160.0,175.0,180.0,183.0,184.0,185.0,185.0,185.0]
Lcc=[.271,.251,.239,.227,.222,.221,.218,.216,.213,.212];
fcxxxt=[0.98,2.45,4.165,5.88,7.84,9.31,11.27,13.23,15.19,16.66] %
contractor muscle @ alfa =45
fp = fcxxx+2*fexx+5;
fpt=[10.78,17.64,24.5,30.38,34.79,40.18,45.08,49.98,54.39,59.78] %
prototype @ alfa = 90
alfapexl=[30.0,35.0,42.0,49.0,56.0,64.0,74.0,85.0,90.0,91.0]

global p;
k=0;
for p=[.5:0.5:5]
    k=k+1;
    % syms p x y ;

```

```

r=[1 90];
z=fsolve(@myfun2,r)
thcp(k)=z(1);
thccp(k)=z(2);
dcep(k)=be*(sind(z(1))+sind(thmax))/(2*pi*ne);
dccp(k)=bc*(sind(z(2))+sind(thmin))/(2*pi*nc);
alfaep(k)=180*be*(cosd(z(1))-cosd(thmax))/(dcep(k)*pi);
alfacp(k)=180*bc*(cosd(thmin)-cosd(z(2)))/(dccp(k)*pi);
end
p=0.5:0.5:5;
alfapex=[80.0,120.0,170.0,190.0,200.0,205.0,210.0,215.0,217.0,220.0];

figure(5);
hold on
plot(p,Lcc,'b');
plot(p,Lce,'r');
title('pressure vs length of contractor muscle ', 'FontSize', 12,
'FontWeight', 'bold', 'Color', 'r');
xlabel('pressure (bar)', 'FontSize', 12, 'FontWeight', 'bold', 'Color',
'b');
ylabel('length of muscle (m)', 'FontSize', 12, 'FontWeight', 'bold',
'Color', 'b');
legend('equation','experiamental')

figure(6);
hold on
plot(p,alfac,'b');
plot(p,alfacx,'r');
title('pressure vs contractor bending angle', 'FontSize', 12,
'FontWeight', 'bold', 'Color', 'r');
xlabel('pressure (bar)', 'FontSize', 12, 'FontWeight', 'bold', 'Color',
'b');
ylabel('bending angle (degree)', 'FontSize', 12, 'FontWeight', 'bold',
'Color', 'b');
legend('equation','experiamental')

figure(7);
plot(p,fcx);
title('pressure vs Force', 'FontSize', 12, 'FontWeight', 'bold',
'Color', 'r');
xlabel('pressure (bar)', 'FontSize', 12, 'FontWeight', 'bold', 'Color',
'b');
ylabel('Force (N)', 'FontSize', 12, 'FontWeight', 'bold', 'Color',
'b');

figure(8);
hold on
plot(p,fcxxx,'b');
plot(p,fcxxxr,'r');
title('pressure vs contractor Force @alfa=45', 'FontSize', 12,
'FontWeight', 'bold', 'Color', 'r');
xlabel('pressure (bar)', 'FontSize', 12, 'FontWeight', 'bold', 'Color',
'b');
ylabel('Force (N)', 'FontSize', 12, 'FontWeight', 'bold', 'Color', 'b');
legend('equation','experiamental')

figure(9);
hold on
plot(p,fp,'b');
plot(p,fpT,'r');
title('pressure vs prototype Force @alfa=90', 'FontSize', 12,
'FontWeight', 'bold', 'Color', 'r');

```

```

xlabel('pressure (bar)', 'FontSize', 12, 'FontWeight', 'bold', 'Color',
'b');
ylabel('Force (N)', 'FontSize', 12, 'FontWeight', 'bold', 'Color', 'b');
legend('equation','experimental')

figure(10);
hold on
plot(p,alfapeq,'b');
plot(p,alfapex,'r');
title('pressure vs prototype bending angle @ no load', 'FontSize', 12,
'FontWeight', 'bold', 'Color', 'r');
xlabel('pressure (bar)', 'FontSize', 12, 'FontWeight', 'bold', 'Color',
'b');
ylabel('bending angle (degree)', 'FontSize', 12, 'FontWeight', 'bold',
'Color', 'b');
legend('equation','experimental')

figure(11);
hold on
plot(p,alfapeql,'b');
plot(p,alfapexl,'r');
title('pressure vs prototype bending angle @load=1.5kg', 'FontSize', 12,
'FontWeight', 'bold', 'Color', 'r');
xlabel('pressure (bar)', 'FontSize', 12, 'FontWeight', 'bold', 'Color',
'b');
ylabel('bending angle (degree)', 'FontSize', 12, 'FontWeight', 'bold',
'Color', 'b');
legend('equation','experimental')

```

2. General code for the whole prototype

```

clc;
clear;
be=1.131370849898476;
bc=0.424264068711929;
ne=12.732395447351626;
nc=4.774648292756860;
thmax=72.511138854842100;
thmin=45.000000000000010;
% (cosd(thc)-cosd(thmax))/(sind(thc)+sind(thmax))=(cosd(thmin)-
cosd(thcc))/(sind(thmin)+sind(thcc));
% (2*(p(k).*be.^2)./(ne^2)).*((-
((cosd(thc(k))+cosd(thmax)).*(cosd(thc(k)).*sind(thc(k))+sind(thmax)*cosd(t
hc(k)))./sind(thc(k)))+0.5*(sind(thc(k))+sind(thmax)).^2)-
((p(k).*bc.^2)./(nc^2)).*((-
((cosd(thcc(k))+cosd(thmin)).*(cosd(thcc(k)).*sind(thcc(k))+sind(thmin)*cos
d(thcc(k)))./sind(thcc(k)))+0.5*(sind(thcc(k))+sind(thmin)).^2)));
global p;
k=0;
for p=[.5:0.5:5]
k=k+1;
% syms p x y ;
r=[1 90];
z=fsolve(@myfun2,r)
thc(k)=z(1);
thcc(k)=z(2);

```

```

dce(k)=be*(sind(z(1))+sind(thmax))/(2*pi*ne);
dcc(k)=bc*(sind(z(2))+sind(thmin))/(2*pi*nc);
alfae(k)=180*be*(cosd(z(1))-cosd(thmax))/(dce(k)*pi);
alfac(k)=180*bc*(cosd(thmin)-cosd(z(2)))/(dcc(k)*pi);
end
p=0.5:0.5:5;
figure(1)
alfapex=[80.0,120.0,170.0,190.0,200.0,205.0,210.0,215.0,217.0,220.0]; %
experimental Bending Angle for prototype
alfapeq=[81,125,177,198,209,215,221,227,230,235];
hold on
plot(p,alfapeq,'b');
plot(p,alfapex,'r');
title('pressure vs prototype bending angle', 'FontSize', 12, 'FontWeight',
'bold', 'Color', 'r');
xlabel('pressure (bar)', 'FontSize', 12, 'FontWeight', 'bold', 'Color',
'b');
ylabel('bending angle (degree)', 'FontSize', 12, 'FontWeight', 'bold',
'Color', 'b');
legend('equation','experimental')

figure(2)
alfapem=[30.0 ,35.0 ,42.0 ,49.0, 56.0, 64.0 ,74.0, 85.0 ,90.0 ,91.0 ]; %
experimental Bending Angle for prototype
alfapen=[30.032,34.0232,41.043,50,56.32,65.432,75.6,80.321,85.432,92];
hold on
plot(p,alfapem,'b');
plot(p,alfapen,'r');
title('pressure vs prototype bending angle( Load)', 'FontSize', 12,
'FontWeight', 'bold', 'Color', 'r');
xlabel('pressure (bar)', 'FontSize', 12, 'FontWeight', 'bold', 'Color',
'b');
ylabel('bending angle (degree)', 'FontSize', 12, 'FontWeight', 'bold',
'Color', 'b');
legend('equation','experimental')

```

3. Help Functions

```

function F=myfun(z)
x= z(1);
y= z(2);
F(1)= (-.5*pi)+(1.1314*(cosd(x)-cosd(72.5))/(y));
F(2)= -y+1.1314*(sind(x)+sind(72.5))/(2*pi*12.7324);
end

```

```

function F=myfun1(n)
x= n(1);
y= n(2);
F(1)= (-.25*pi)+(.4243*(cosd(45)-cosd(x))/(y));
F(2)= -y+.4243*(sind(45)+sind(x))/(2*pi*4.774648292756860);
end

```

```

function F=myfun2(z)
    x= z(1);
    y= z(2);
    global p
    %
    F(1)= (cosd(x)-
    cosd(72.511138854842100))/(sind(x)+sind(72.511138854842100))-
    ((cosd(45.000000000000010)-cosd(y))/(sind(45.000000000000010)+sind(y)));
    %
    F(2)= (-2*(p*1.131370849898476^2)/(12.732395447351626^2))*((-
    ((cosd(x)+cosd(72.511138854842100))*(cosd(x)*sind(x)+sind(72.51113885484210
    0)*cosd(x)))/sind(x))+0.5*(sind(x)+sind(72.511138854842100))^2)+(((p*0.4242
    64068711929^2)/(4.774648292756860^2))*(((cosd(y)+cosd(45.000000000000010))
    *(cosd(y)*sind(y)+sind(45.000000000000010)*cosd(y)))/sind(y))-
    0.5*(sind(y)+sind(45.000000000000010))^2);
    F(1)=(180*1.131370849898476*(cosd(z(1))-
    cosd(72.511138854842100))/((1.131370849898476*(sind(z(1))+sind(72.511138854
    842100))/(2*pi*12.732395447351626))*pi))-
    (180*0.424264068711929*(cosd(45.000000000000010)-
    cosd(z(2)))/((0.424264068711929*(sind(z(2))+sind(45.000000000000010))/(2*pi
    *4.774648292756860))*pi));

F(2)=2*(((10^4)*p.*1.131370849898476.^2)./(8*pi*12.732395447351626^2)).*((
-
((cosd(z(1))+cosd(72.511138854842100)).*(cosd(z(1)).*sind(z(1))+sind(72.511
138854842100)*cosd(z(1))))./sind(z(1))+0.5*(sind(z(1))+sind(72.51113885484
2100)).^2))-
(((10^5)*p.*0.424264068711929.^2)./(8*pi*4.774648292756860^2)).*((((cosd(z
(2))+cosd(45.000000000000010)).*(cosd(z(2)).*sind(z(2))+sind(45.00000000000
0010)*cosd(z(2))))./sind(z(2)))-
0.5*(sind(z(2))+sind(45.000000000000010)).^2));
end

% ???k ???
% (cosd(x)-cosd(72.511138854842100))/(sind(x)+sind(72.511138854842100))-
(cosd(45.000000000000010)-cosd(y))/(sind(45.000000000000010)+sind(y));

```

```

function F=myfun3(z)
    x= z(1);
    global m
    F(1)=(((10^5)*2.*0.424264068711929.^2)./(8*pi*4.774648292756860^2)).*((((co
sd(z(1))+cosd(45)).*(cosd(z(1)).*sind(z(1))-
sind(45)*cosd(z(1))))./sind(z(1))+0.5*(sind(z(1))+sind(45)).^2)*2.3+m.*9.8
;
end

```

```

function F=myfun4(z)
    dce= z(1);
    thc= z(2);
    global thmax be ne
    F(1)= -dce+(be*(sind(thc)+sind(thmax))/(2*pi*ne));
    F(2)= -90+(180*be*(cosd(thc)-cosd(thmax))/(dce*pi));
end

```

```
function F=myfun5(z)
    dcc= z(1);
    thcc= z(2);
    global thmax be ne bc thmin nc
    F(1)= -dcc+(bc*(sind(thcc)+sind(thmin))/(2*pi*nc));
    F(2)= -90+(180*bc*(cosd(thmin)-cosd(thcc))/(dcc*pi));
end
```

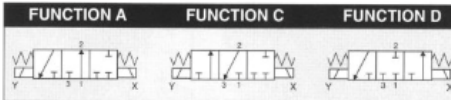
Appendix (C)

754 • 3/3

NC-NO

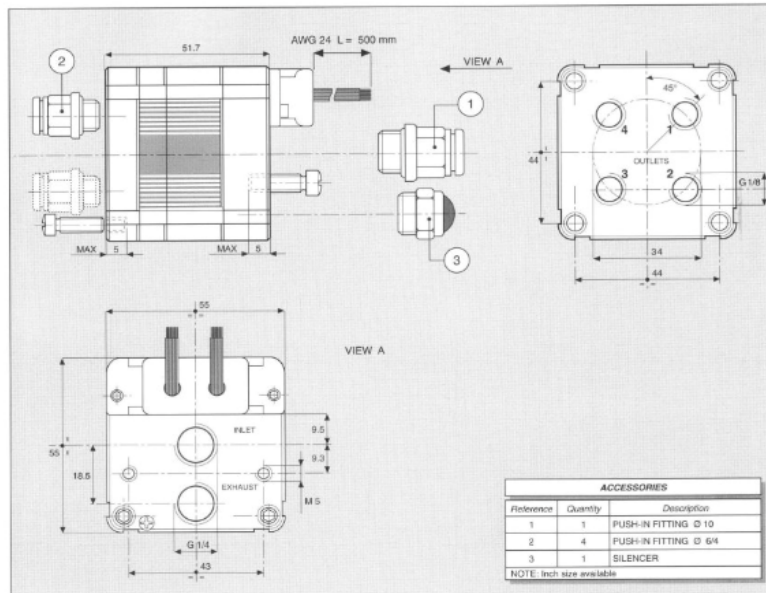


CONTROL: DIRECT PFM PNM PWM

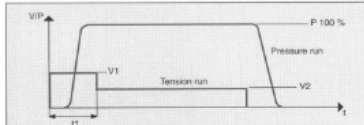


GENERAL CHARACTERISTICS

FLUID	Non-lubricated dry air, neutral gases (-10 + 50°C)		
FILTRATION RATING	Min 40 micron		
TEMPERATURE	- 10 + 50°C (Standard version)		
RESPONSE TIME IN OPENING	12 / 24 < 7 ms	JJ < 5 ms	XX / KK < 2 ms
RESPONSE TIME IN CLOSING	12 / 24 < 3 ms	JJ < 2 ms	XX / KK < 2 ms
MAXIMUM FREQUENCY	100 Hz	200 Hz	300 Hz
WEIGHT	340 g		
PRODUCT LIFE EXPECTANCY	≥ 500 M/s cycles		
IP RATING	IP 52 - IP 62 - IP 65		



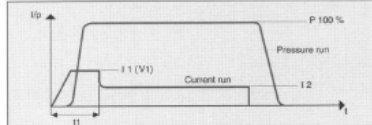
CHARACTERISTICS OF THE ELECTRICAL CONTROL - MODELS KK



N.B. KK MODELS ARE CONTROLLED IN TENSION

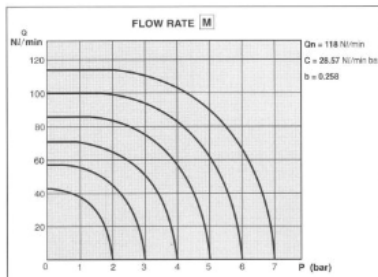
V1 = 24 VDC t1 = 2 ms V2 = 5 VDC

CHARACTERISTICS OF THE ELECTRICAL CONTROL - MODELS XX



N.B. XX MODELS ARE CONTROLLED IN CURRENT

I1 = 0.7 A I1 = 2 ms I2 = 0.3 A



ELECTRICAL PORT CONNECTION

COLOUR	S CONTROLS (OUTLET)
BLACK	COMMON
BROWN	1 (1)
RED	2 (1)
ORANGE	3 (2)
YELLOW	4 (2)
GREEN	5 (3)
BLUE	6 (3)
VIOLET	7 (4)
GREY	8 (4)

Appendix (D)

NN Training code (observed data)

```
clc;
clear all;
close all;
%% Select Database

[u,y] = refmodel_dataset;
m1 = [1:2];
m2 = [1:2];
S1 = 5;
arm = narxnet(m1,m2,S1);
arm.divideFcn = '';
arm.inputs{1}.processFcns = {};
arm.inputs{2}.processFcns = {};
arm.outputs{2}.processFcns = {};
arm.trainParam.min_grad = 1e-10;
[p,Pi,Ai,t] = preparets(arm,u,{},y);
arm = train(arm,p,t,Pi);
narx_net_closed = closeloop(arm);
view(narx_net_closed)
arm2_net = feedforwardnet([S1 1 S1]);
arm2_net.layerConnect = [0 1 0 1;1 0 0 0;0 1 0 1;0 0 1 0];
arm2_net.outputs{4}.feedbackMode = 'closed';
arm2_net.layers{2}.transferFcn = 'purelin';
arm2_net.layerWeights{3,4}.delays = 1:2;
arm2_net.layerWeights{3,2}.delays = 1:2;
arm2_net.layerWeights{3,2}.learn = 0;
arm2_net.layerWeights{3,4}.learn = 0;
arm2_net.layerWeights{4,3}.learn = 0;
arm2_net.biases{3}.learn = 0;
arm2_net.biases{4}.learn = 0;
%%
arm2_net.divideFcn = '';
arm2_net.inputs{1}.processFcns = {};
arm2_net.outputs{4}.processFcns = {};
arm2_net.name = 'Model Reference Adaptive Control Network';
arm2_net.layerWeights{1,2}.delays = 1:2;
arm2_net.layerWeights{1,4}.delays = 1:2;
arm2_net.inputWeights{1}.delays = 1:2;
%%
[refin,refout] = refmodel_dataset;
ind = 1:length(refin);
plot(ind,cell2mat(refin),ind,cell2mat(refout))
arm2_net = configure(arm2_net,refin,refout);
%%
arm2_net.LW{3,2} = narx_net_closed.IW{1};
arm2_net.LW{3,4} = narx_net_closed.LW{1,2};
arm2_net.b{3} = narx_net_closed.b{1};
arm2_net.LW{4,3} = narx_net_closed.LW{2,1};
arm2_net.b{4} = narx_net_closed.b{2};

%%
arm2_net.LW{2,1} = zeros(size(arm2_net.LW{2,1}));
arm2_net.b{2} = 0;

arm2_net.plotFcns = {'plotperform','plottrainstate',...
    'ploterrhist','plotregression','plotresponse'};
arm2_net.trainFcn = 'trainlm';
```

```

view(arm2_net)

[x_tot,xi_tot,ai_tot,t_tot] = ...
    preparets(arm2_net,refin,{},refout);
arm2_net.trainParam.epochs = 50;
arm2_net.trainParam.min_grad = 1e-10;
[arm2_net,tr] = train(arm2_net,x_tot,t_tot,xi_tot,ai_tot);

%%
testin = skyline(1000,50,200,-.7,.7);
testinseq = con2seq(testin);
testoutseq = arm2_net(testinseq);
testout = cell2mat(testoutseq);
figure
plot([testin' testout'])

```

REFERENCES

- Tsagarakis, N. G., & Caldwell, D. G. (2003). Development and Control of a 'Soft-Actuated' Exoskeleton for Use in Physiotherapy and Training. *Autonomous Robots*, 15(1), 21-33.
- Ada, L., Canning, C., & Low, L. (2003). stroke Patients have Selective Muscle weakness in Shortened Range. *126(3)*, 724-731.
- Ahn, K., & T. C. (2004). Improvement of the control performance of pneumatic artificial muscle manipulators using an intelligent switching control method. *KSME*, 18(8), 1388-1400.
- Aiello, L., & Dean, C. (2002). *An Introduction to Human Evolutionary Anatomy* (6 ed.). London, UK: Elsevier.
- Al-Fahaam, H., Davis, S., & Nefti-Meziani, S. (2018). The Design and Mathematical Modelling of novel Extensor Bending Pneumatic Artificial Muscle (EBPAMs) for Soft Exoskeletons. *Robotics and Autonomous Systems*, 99, 63-74.
- Al-Ibadi, A., Davis, S., & Nefti-meziani, S. (2018). Design, Kinematics and Controlling a Novel Soft Robot Arm with Parallel Motion. *Robotics*.
- Al-Ibadi, A., Nefti-Meziani, S., & Davis, S. (2017). Efficient Structure-Based Models for the McKibben Contraction Pneumatic Muscle Actuator: The Full Description of the Behaviour of the Contraction PMA. *Actuators*, 6(32), 1-15.
- Almurib, H. A., Al-Qrimli, H. F., & Kumar, N. (2011). Design of Human Elbow Joint Mechanism. *Australian Journal of Basic and Applied Science*, 5(7), 976-981.
- Aschemann, H., & Schindele, D. (2008). Sliding-mode control of a high-speed linear axis driven by pneumatic muscle actuators. *Industrial Electronics*, 55(11).
- Association, S. (2017). *State of the Nation, Stroke Statistics*. Stroke Association.
- Balasubramanian, S., Wei, M., Shepard, B., Koeneman, E., Koenman, J., & He, J. (2008). RUPERT: An exoskeleton Robot for Assisting Rehabilitation of Arm Functions. *Virtual Rehabilitation* (pp. 163-167). Vancouver, BC, Canada: IEEE.
- Bartlett, R. (2007). *Introduction to Sports Biomechanics: Analysing Human Movement Patterns* (2 ed.). London: Routledge.

- Basteris , A., Nijenhuis, S., Stienen, A., Buurke, J., Prange, G., & Amirabdollahian, F. (2014). Training Modelities in Robot-Mediated Upper Limb Rehabilitation in Stroke: A Framework for Classification Based on Systematic Review. *Journal of NeuroEngineering and Rehabilitation*, *11*(111).
- Bishop, L., & Stein, J. (2013). Three Upper Limb Robotic Devices for Stroke Rehabilitation: A Review and Clinical Perspective. *Neurorehabilitation*, *33*(1), 3-11.
- Bradshaw, R. (2012). Constraint Induced Movement Therapy (CIMT): A feasible Treatment Option in A Inpatient Rehabilitation Environment within the NHS. *Synapse*, 4-9.
- Burgard, C., Lum, P., Shor, P., & Loos, H. (2002). robot-assisted movement Training Compared with Conventional therapy Techniques for the Rehabilitation of Upper Limb Motor Function after Stroke. *pubMed*, *83*(7), 952-959.
- Caldwell, D., Medrano-Cerda, ,, & Goodwi, M. (1995). Control of pneumatic muscle actuators. *Control Systems Magazine*, *15*(1), 40–48.
- Caldwell, G., Medrano-Cerda, G., & Goodwin, M. (1995). Control of Pneumatic Muscle Actuators . *IEEE Control Systems Magazine* , *15*(1), 40-48.
- Carignan , C., Tang, J., & Roderick , S. (2009). Development of an Exoskeleton Haptic for Virtual Task Training. *International Conference on Intelligent Robots and Systems* (pp. 3697-3702). St. Louis, MO: IEEE.
- Cauraugh, J., Light, K., Thigpen, M., & Behrman, A. (2000). Chronic Motor Dysfunction after Stroke Recovering Wrist and Fingers Extension bu Electromyographic-Triggered Neuromuscular Simualtion. *stroke*, *6*, 31000.
- Chan, S., Lilly, J., Repperger, D., & Berlin, J. (2003). Fuzzy PD+I learning control for a pneumatic muscle,. *International Conference on Fuzzy Systems* (pp. 278–283). IEEE.
- Cheng, P.-Y., & Lai, P.-Y. (2013). Comparison of Exoskeleton Robots and End-Effector Robots on Training Methods and Gait Biomechanics. *Intelligent Robotics and Applications*, *8102*, 258-266.
- Chou, C.-P., & Hannaford, B. (1996). Measurement and modeling of McKibben pneumatic artificial muscles. *IEEE Transactions on Robotics and Automation*, *12*(1), 90-102.

- Colbrunn, R. W., Nelson, G. M., & Quinn, R. D. (2001). Modeling of braided pneumatic actuators for robotic control. *International Conference on Intelligent Robots and Systems*. . IEEE/RSJ .
- Culmer, P., Jackson , A., Richardson , R., Bhakta, B., Levesely, M., & Alastair, C. (2005). Development of a Dual Robotic System for Upper-Limb Stroke. *International Conference on Rehabilitation Robotics*, (pp. 61-65). Chicago,IL.
- Curtin , M., Molineux , M., & Supky-Mellson, J. (2009). *Occupational Therapy and Physical Dysfunction* (6 ed.). (M. Curtin, M. Molineux, & J. Supky-Mellson, Eds.) Churchill Livingston.
- Delavande , A., Hurd , M., Martorell , P., & Langa , K. (2013). Dementia and out-of-pocket spending on health care services. *Alzheimer's & Dementia*, 9(1), 19-29.
- Department of Health. (2016, October 28). *Quality and Outcomes framework (QOF) Achievement data 2015/16*. Retrieved October 15, 2017, from Department of Health: <https://www.health-ni.gov.uk/publications/quality-and-outcomes-framework-qof-achievement-data-201516>
- Dobkin, B. H. (2005). Rehabilitation after Stroke. *New England Journal of Medicine*, 352, 1677-1684.
- Dobkin, B., & Dorsch, A. (2013). New Evidence for Therapies in Stroke Rehabilitation. *Current Atherosclerosis Reports*, 15(6), 331-340.
- Doumit, M., Fahim, A., & Munro, M. (2009). Analytical Modeling and Experimental Validation of the Braided Pneumatic Muscle. *IEEE Transactions on Robotics*, 25(6), 1282-1292.
- Dzahir, M., & Yamamoto, S.-i. (2014). Recent Trends in Lower-Limb Robotic Rehabilitation Orthosis: Control Scheme and Strategy for Pneumatic Muscle Actuated Gait Trainers. *Robotics* , 3(2), 120-148.
- Fazekas, G., Hovath, M., Troznai, T., & Toth, A. (2007). Robot-Mediated Upper Limb Physiotherapy for Patients with Spastic Hemiparesis: A Preliminary Study. *Journal of Rehabilitation Medicine*, 39(7), 580-582.
- Fok, S. C., & Ong, E. K. (1999). Position Control and Repeatability of a Pneumatic Rodless Cylinder System for Continuous Positioning. *Robotics and Computer Integrated Manufacturing*, 15, 365-371.

- Freivalds, A. (2011). *Biomechanics of the Upper Limbs: Mechanics, Modeling and musculoskeletal Injuries* (2nd ed.). Boca Raton, FL: CRC Press Taylor and Francis Group.
- Gaponov, I., Popov, D., Jun Lee, S., & Hwan Ryu, J. (2016). Auxilio: A Portable Cable-driven Exosuit for Upper Extremity Assistance. *International Journal of Control, Automation and Systems*, 15(1), 73-84.
- Gaylord, R. (n.d.). *Patent No. 2844126,1958*. US.
- Godage, I. S., Branson, D. T., Guglielmino, E., & Caldwell, D. G. (2012). Pneumatic muscle actuated continuum arms: Modelling and experimental assessment. I. *IEEE International Conference on Robotics and Automation (ICRA)*, (pp. 4980-4985).
- Gopura, R., Kiguchi, K., & Horikawa, E. (2010). A Study on Human Upper-Limb Muscles Activities during Daily Upper-Limb Motions. *International Journal of Bioelectromagnetism*, 12(2), 54-61.
- Guo, Z., & Sluys, L. J. (2006). Application of a new constitutive model for the description of rubber-like materials under monotonic loading. *International Journal of Solids and Structures*, 43(9), 2799-2819.
- Hall, S. (2003). Kinematic Concepts for Analyzing Human Motion. In *Basic Biomechanics* (4 ed.). Boston, MA: McGraw-Hill.
- Hamed, S., & Hayek, R. (2008). Role of electrical stimulation for rehabilitation and regeneration after spinal cord injury: an overview. *European Spine*, 17(9), 1256–1269.
- Hannaford, B., & Winters, J. (1990). Actuator Properties and Movement Control: Biological and Technological Models. In J. M. Winters , & S. L.-y. Woo (Eds.). New-York: Springer-Verlag.
- Hoenig, H., Sanford, J., Butterfield, T., Griffiths, P., Richardson, P., & Hagraves, K. (2006). Development of a Teletechnology Protocol for in-home rehabilitation . *Rehabilitation research and development* , 43(2), 287.
- Hollerbach, J., Hunter, I., & Ballantyne, J. (1992). A Comparative Analysis of Actuator Technologies for Robotics. In O. Khatib, J. Craig, & Losano-Perez Eds (Eds.), *The Robotics Review 2* (pp. 299-342). Cambridge: MIT press.

- Huang , C., Li , Y., Wang , H., Sung, P., Wang , L., Sun, Y., . . . Tsai , K. (2016). Stroke suggests increased risk of dementia. *Current Alzheimer Research*, 12(3), 287-295.
- Huang, V., & Krakauer, J. W. (2009). Robotic Neurorehabilitation: A Computational Motor Learning Perspective. *Journal of NeuroEngineering and Rehabilitation*, 6(5).
- Huston, R. L. (2009). *Principles of Biomechanics*. Boca Raton, FL: CRC Press, Taylor and Francis Group.
- Inagaki, K. (2013). Current Concepts of Elbow-joint Disorders and their Treatment. *Journal of Orthopadeic Science*, 18(1), 1-7.
- Intercollegiate Stroke . (2017, January 2017). *Royal Collage of Physicians*. Retrieved September 2017, 2017, from Stroke Audit: <https://www.strokeaudit.org/Documents/Results/National/2016/2016-AOANationalReport.aspx>
- Jackson, A., Culmer, P., Makower, S., Levesley, M., Richardson , R., Cozens, A., . . . Bhakta, B. (2007). Initial patient testing of iPAM - a robotic system for Stroke rehabilitation. *International Conference on Rehabilitation Robotics* (pp. 250-256). Noordwijk: IEEE.
- Jackson, A., Holt, R., Culmer, R., Makower , S., Levesley, M., Richardson, R., . . . Bhakta, B. (2007). Dual robot system for upper limb rehabilitation after stroke: The design process. *Journal of Mechanical Engineering Science*, 221(7), 845-867.
- Kaitwanidvilai, S., & Parnichkun,, M. (2005). Force Control in a Pneumatic System Using Hybrid Adaptive Neuro-Fuzzy Model Reference Control. *Mechatronics* ,. 15, 23-41.
- Kiguchi, K., Esaki, R., Tsuruta, T., Watanabe, K., & Fukuda T. (2003). An Exoskeleton System for Elbow Joint Motion Rehabilitation. *International Conference on Advanced Intelligent Mechatronics (AIM)*. 2, pp. 1228-1233. Port Island, Japan: IEEE.
- Kiguchi, K., Iwami, K., Makoto, Y., & Watanabe, K. (2003). An Exoskeleton ROBOT for Human Shoulder Joint Motion Assist. *IEEE/ASME Trans on Mechatronics*, 8(1), 125-135.
- Kong, K., & Tomizuka, M. (2009). Realization of Fictitious Gain in Human: Experimental Verification on Elbow Joint. *IEEE/ ASME Internatinal Conference on Advanced*

Intelligent Mechatronics Suntec Convention and Exhibition Center, Singapore, 439-444.

- Krebs, H., Ferraro, M., Buerger, S., Newbery, M., Makiyama, A., Sandmann, M., . . . Hogan, N. (2004). Rehabilitation Robotics: Pilot trial of spatial extension for MIT-Manus. *Journal of NeuroEngineering and Rehabilitation, 1*(1), 5.
- Krebs, H., Hogan, N., Aisen, M., & Volpe, B. (1998). Robot-Aided Neurorehabilitation. *Neural Systems and Rehabilitation Engineering, 6*, 75-87.
- Kwakkel, G., Kollen, B., Van Der Grond, J., & Prevo, A. (2003). Probability of Regaining Dexterity in the Flaccid Upper limb: Impact of Severity of Paresis and Time since onset in Acute Stroke. *Stroke, PubMed, 34*(9), 2181-2186.
- Langhorne, P., Coupar, F., & Pollock, A. (2009). Motor Recovery after Stroke: A Systematic Review. *The Lancet Neurology, 8*(8), 741-754.
- Liska, O., More, M., Janacova, G., & Charvatova, H. (2013). Design of Rehabilitation Robot based on Pneumatic Artificial Muscle. *World Scientific and Engineering Academy and Society.*
- Liu, S., & Bobrow, J. E. (1998). An Analysis of a Pneumatic Servo System and Its Application to a Computer-Controlled Robot. *ASME Journal of Dynamic Systems, 110*, 228-235.
- Liu, W., & Rahn, C. R. (2004). Fiber-Reinforced Membrane Models of McKibben Actuators. *Journal of Applied Mechanics, 70*(6), 853-859.
- Lo, H., & Xie, S. (2012). Exoskeleton robots for upper-limb rehabilitation: State of the art and future prospects. *Medical Engineering & Physics, 34*(3), 261-268.
- Loureiro, R., Amirabdollahian, F., Topping, M., Driessen, B., & Harwin, W. (2003). Upper Limb Robot Mediate Stroke Therapy- GENTLE/s Approach. *Autonomous Robots, 15*(1), 35-51.
- Lum, P. S., Burgar, C. G., Van der Loos, M., Shor, P. C., Majmundar, M., & Yap, R. (2006). MIME Robotics device for Upper Limb Neurorehabilitation in Subacute Stroke Subjects: A Follow-Up Study. *Journal of Rehabilitation Research and Development, 43*(5), 631-642.

- Lum, P., Reinkensmeyer, D., Mahoney, R., Rymer, W., & Burgar, C. (2002). Robotic Devices for Movement Therapy after Stroke: Current Status and Challenges to Clinical Acceptance. *Stroke Rehabilitation*, 8(4), 40-53.
- Maciejasz, P., Eschweiler, J., Gerlach-Hahn, K., Jansen-Troy, A., & Leonhardt, S. (2014). A Survey on Robotic Devices for Upper Limb Rehabilitation. *NeuroEngineering and Rehabilitation*, 11(3).
- Mansouri, M., & Darijani, H. (2014). Constitutive modeling of isotropic hyperelastic materials in an exponential framework using a self-contained approach. *International Journal of Solids and Structures*, 51, 4316-4326.
- Manuello Bertetto, A., & Ruggiu, M. (2014). Characterization and modeling of air muscles. *Mechanics Research Communications*, 31, 185-194.
- Marchel-Crespo, L., & Reinkensmeyer, D. (2009). Review of Control Strategies for Robotic Movement Training after Neurologic Injury. *Journal of NeuroEngineering Rehabilitation*, 6(20).
- McMahan, W., Chitrakaran, V., Csencsits, M., Dawson, D., Walker, I. D., Jones, B. A., . . . Rahn, C. D. (2006). Field Trials and Testing of the OctArm Continuum Manipulator. *International Conference on Robotics and Automation*, (pp. 2336-2341). Orlando, Florida.
- Mechatronics, M. (n.d.). 750 Series compact solenoid multi-valve | 3/3. Italy: matrix.to.it.
- Micera, S., Carrozza, M., Guglielmelli, E., Cappiello, G., Zaccone, F., Freschi, C., . . . Pisano, F. (2005). A simple robotic system for neurorehabilitation. *Autonomous Robots*, 19(3), 271-284.
- Mingrui, L., & Zhan, F. (2000). The finite deformation theory for beam, plate and shell. Part IV. The Fe formulation of Mindlin plate and shell based on Green-Lagrangian strain. *Computer Methods in Applied Mechanics and Engineering*, 182(1-2), 187-203.
- Mizakova, J., Pitel, J., & Tothava, M. (2014). Pneumatic Artificial Muscle as Actuator in Mechatronics system. *Applied Mechanics and Materials*, 460, 81-90.
- Mizrahi, J. (2015). Mechanical Impedance and Its Relations to Motor Control, Limb Dynamics, and Motion Biomechanics. *Journal of Medical and Biological Engineering*, 35(1), 1-20.

- Muratori, L., Lamberg, E., Quinn, L., & Duff, S. (2013). Applying Principles of Motor Learning and Control to Upper Extremity Rehabilitation. *Journal of Hand Therapy*, 26(2), 94-103.
- National Institute for Health and Clinical Excellence. (2010). *NICE Cost Impact and Commissioning assesment: Quality Standard for Stroke*. Department of Health, NHS,UK Government. Retrieved from <https://www.gov.uk/government/publications/national-quality-board-nice-quality-standards>
- Nef, T., Guidali, M., Klamroth-Marganska, V., & Riener, R. (2009). Effects of Arm Training with the Tobic Device ARMin 1 in Chronic Stroke: Three Single Cases. In D. Schlegel (Ed.), *World Congress on Medical Physics and Biomedical Engineering*. 25, pp. 127-130. Munich, Germany: Springer.
- Nickel, V., Perry, J., & Garrett, A. (1963). Development of Useful Function in the Severely Paralyzed Hand. *Journal of Bone and Joint Surgery*, 45A(5), 933-952.
- Nikolova, G. S. (2010). Anthropometric Measurements and Model Evaluation of Mass-Inertial Parameters of the Human Upper and Lower Extremities. *XII Mediterranean Conference on Medical and Biological Engineering and Computing*. 29, pp. 574- 577. IFMBE Proceedings - Springer.
- Patel, S., Park, H., Bonato, P., Chan, L., & Rodgers, M. (2012). A review of Wearable Sensors and Systems with Application in Rehabilitation. *Journal of NeuroEngineering and Rehabilitation*, 9(21).
- Pignolo, L. (2009). Robotics in Neuro-Rehabilitation. *Journal of Rehabilitation and Medicine*, 41(12), 955-960.
- Poli, P., Morone, G., Rosati, G., & Masiero, S. (2013). Robotic Technologies and Rehbilitation: New Tools for Patient's Therapy. *BioMed Research International* , 8.
- Polygerinos, P., Correll, N., Morin, S. A., Mosadegh, B., Onal, C. D., Petersen, K., . . . Shepherd, R. F. (2017). Soft Robotics: Review of Fluid-Driven Intrinsically Soft Devices;Manufacturing, Sensing, Control, and Applications in Human-Robot Interaction. *Advanced Engineering Materials* (12), 201700016.

- Pujana-arrese, A., Martinez-esnaola, A., & Land, J. (2007). Modelling in Modelica of a pneumatic muscle: application to model an experimental set-up. *21st European conference on modelling and simulation*. ECMS.
- Qiang, S., & Fang, L. (2006). Improved control of a pneumatic actuator pulsed with PWM. *IEEE*.
- Rahman, T., Sample, W., & Seliktar, R. (2004). Design and Testing of WREX. In: *Bien ZZ, Stefanov D, eds. Advances in Rehabilitation Robotics*. (pp. 243-250). Berlin: Springer-Verlag.
- Rao, Z., & Bone, G. M. (2008). Nonlinear Modeling and Control of Servo Pneumatic Actuators. *Control Systems Technology*, 16(3), 562-569.
- Ren, Y., Park, H.-S., & Zhang, L.-Q. (2009). Developing a Whole-arm Exoskeleton Robot with Hand Opening and Closing Mechanism for Upper Limb Stroke Rehabilitation. *International Conference on Rehabilitation Robotics* (pp. 761-765). Kyoto: IEEE.
- Repperger, D., Phillips, C., & Krier, M. (1999). Controller design involving gain scheduling for a large scale pneumatic muscle actuator. *International Conference on Control Applications* (pp. 285–290). IEEE.
- Rietman, J., Prange, G., Stienen, A., & Burke, P. (2011). An Arm Support Training Device for Stroke Patients; From Development to Implementation. *Journal of Rehabilitation and Medicine*, 5, 52.
- Rosen, J., Brand, M., Fuchs, M., & Arcan, M. (2001). A Myosignal-Based Powered Exoskeleton System. *IEEE Trans Sys, Man and Cybernet, Part A*, 31(3), 210-222.
- Rosen, J., Pery, J., Manning N., & Burns, S. (2005). The Human Arm Kinematics and Dynamics during Dially Activities- Toward a 7 DOF Upeer Limb Powered Exoskeleton. *12th International Conference on Adanced Robotics* (pp. 532-539). Seattle, WA: IEEE.
- Rus, D., & Tolley, M. T. (2015). Design, fabrication and control of soft robots. *Nature*, 521, 467-475.
- Saka, R. O., MCGuire, A., & Wolfe, C. D. (n.d.). *Economic Burden of Stroke in England*. University of London, Health and Social Care, London.

- Sale, P., Franceschini, M., Mazzoleni, S., Palma, E., Agosto, M., & Poteraro, F. (2014). Effects of Upper Limb Robot-assisted Therapy on Motor Recovery in Subacute Stroke Patients. *Journal of NeuroEngineering and Rehabilitation*, *11*(104).
- Sanchez, R., Reinkensmeyer, D., Shah, P., Smith, R., Cramer, S., Rahman, T., & Bobrow, J. (2004). Monitoring Functional Arm Movement for Home-Based Therapy after Stroke. *International Conference on Medicine and Biology Society*, *7*, pp. 4787-4790. San Francisco : IEEE.
- Scott, S., & Dukelow, S. (2011). Potential of Robots as Next-Generation Technology for Clinical Assessment of Neurological Disorders and Upper-Limb Therapy. *Journal of Rehabilitation Research & Development*, *48*(4), 335-354.
- Serres, J. L. (2008). Dynamic Characterization of a Pneumatic Muscle Actuator and Its Application to a Resistive Training Device. *Doctor of Philosophy in Engineering Dissertation*, 2008. Wright State University, Dayton, OH.
- Serres, J., Reynolds, D., Phillips, C., Rogers, D., & Repperger, D. (2010, Feb.). Characterisation of a Pneumatic Muscle Test Station with Two Dynamic Plants in Cascade. *Computer Methods in Biomechanics and Biomedical Engineering*, *13*(1).
- Seung, H. (2009). Trajectory tracking control of a pneumatic c-y table using neural network based PID control”, *International Journal of Precision Engineering and Manufacturing*, *10*(5), 37-44.
- Shahzad, M., Kamran, A., Zeeshan Siddiqu, M., & Farhan, M. (2015). Mechanical Characterization and FE Modelling of a Hyperelastic Material. *Ibero-American Journal of Material*, *18*(5), 919-924.
- Song, R., Tong, K.-Y., Hu, X., & Li, L. (2008). Assistive Control System Using Continuous Myoelectric Signal on Robot- Aided Arm Training for Patients after Stroke. *Neural systems and Rehabilitation*, *16*(4), 371-379.
- Starr, C., Evers, C., & Starr, L. (2010). *Biology: A Human Emphasis* (8 ed.). Delmont, CA: Cengage Learning.
- Stefanovic, M., & Safonov, M. (2008). Safe Adaptive Switching Control: Stability and Convergence. *Automatic Control*, *53*(9), 2012-2021.
- Stroke Association. (2013, June). *Physical effects of stroke*. Retrieved from Stroke Association: <https://www.stroke.org.uk/resources/physical-effects-stroke>

- Stroke Association. (2017, January). *State of Nation: Stroke Statistics*. Retrieved from Stroke Association: <https://www.stroke.org.uk/resources/state-nation-stroke-statistics>
- Suzler, J., Peshkin, M., & Patton, J. (2007). Design of A Mobile, Inexpensive Device for Upper Extremity Rehabilitation at Home. *International Conference on Rehabilitation Robotics (ICORR)* (pp. 933-937). Noordwijk, Netherlands: IEEE.
- Takosoglu, J. E., Laski, P. A., Blasiak, S., Bracha, G., & Pietrala, D. (2016). Determining the static characteristics of pneumatic muscles. *Meas. Control*, *49*, 62-71.
- Taylor, N., Dodd, K., & Damiano, D. (2005). Progressive Resistance Exercise in Physical Therapy: A Summary of Systematic Reviews. *Physical Therapy*, *85*(11), 1208-1223.
- Tondu, B., & Lopez, P. (2000). Modeling and control of McKibben artificial muscle robot actuators. *IEEE Control Systems*, *20*(2), 15-38.
- Tothava, M., Pitel, J., & Borzikova, J. (2013). Operating Modes of Pneumatic Artificial Muscles. *Applied Mechanics and Materials*, *308*, 39-44.
- Tsagarakis, N., Kousidou, S., & Caldwell, D. (2008). Case Study: Soft Actuated Excoskeleton for the use in physiotherapy and training. In J. L. Pons, *Wearable Robots: Biomechatronics Excoskeletons* (pp. 269-278). Chichester: John Wiley and Sons Ltd. .
- Tur, M., Albelda, J., Manuel, J., & Ji, N. (2015). A modified perturbed Lagrangian formulation for contact problems. *Springer*, *55*(4), 737-754.
- Wang, J., Wang, D. J., Moore, P. R., & Pu, J. S. (2001). Modelling Study, Analysis, and Robust Servocontrol of Pneumatic Cylinder Actuator Systems. . *IEEE Process Control Theory and Applications*, 35-42.
- Wickramatunge, K., & Leephakpreeda, T. (2010). Study on Mechanical Behaviours of Pneumatic Artificial Muscle. *International Journal of Engineering Science*, *48*(2), 188-189.
- Winter, D. A. (2009). *Biomechanics and Motor Control of Human Movement* (4th ed.). New Jersey: John Wiley & Sons.
- Wolf, S., Blanton, S., Baer H., Breshears J., & Butler, A. (2002). Repetitive Task Practice: A Critical Review of Constraint-induced Movement Therapy in Stroke. *The Neurologist, PubMed*, *8*(6), 325-338.

- Xiang, F., & Wikander, J. (2004). Block-oriented approximate feedback linearization for control of pneumatic actuator system. *UKACC Conference Control*, 12 (4), pp. 387-399.
- Xing, K., Huang, J., Wang, Y., Wu, J., Xu, Q., & He, J. (2010). Tracking control of pneumatic artificial muscle actuators based on sliding mode and non-linear disturbance observer. *IET Control Theory and Applications*, 4(10), 2058-2070.
- Zhang , H., Balasubramanian, S., Wei, R., Austin, H., Bunchan, S., Herman, R., & He, J. (2010). RUPERT closed loop control design. Conference Proceedings : ... Annual International Conference of the Ieee Engineering in Medicine and Biology Society. *IEEE Engineering in Medicine and Biology Society*, (pp. 3686-3689).
- Zhang, J. F., Chen, Y., Zhang, Y., & Dong, Y. M. (2008). Modelling and Control of a Curved Pneumatic Muscle Actuator for Wearable Elbow Exoskeleton . *Mechatronics*, 448-457.
- Zhang, J., Yang, C., Chen, Y., Zhang, Y., & Dong, Y. (2008). Modeling and Control of a Curved Pneumatic Muscle Actuator for Wearable Elbow Exoskeleton. *Mechatronics*, 18(8), 448-457.
- Zhiguo, Y., Zhizhong, W., & Hongbo, X. (2008). Joint Application of Rough Set-Based Feature Reduction and Fuzzy LS-SVM Classifier in Motion Classification. *MedicalAbiological Engineering & Computing*, 46(6), 519-527.